From accelerometric records to the dynamic behavior of existing buildings

Guillermo Wenceslao Fernández Lorenzo

UNIVERSITÉ CÔTE D'AZUR

École Doctorale de Sciences Fondamentales et Appliquées

Unité de recherche : Géoazur / LJAD

Thèse de doctorat

Présentée en vue de l'obtention du

grade de docteur en sciences pour l'ingénieur

de

l'UNIVERSITE COTE D'AZUR

par

Guillermo Wenceslao FERNÁNDEZ LORENZO

From accelerometric records to the dynamic behavior of existing buildings

Des données accélérométriques au comportement dynamique des bâtiments existants

Dirigée par Anne DESCHAMPS et Maria Paola SANTISI D'AVILA

Soutenue le 17 Octobre 2016

Devant le jury composé de :

Etienne BERTRAND	Chargé de recherche, CEREMA	Conseiller d'étude
Françoise COURBOULEX	Directeur de recherche, CNRS	Président du jury
Anne DESCHAMPS	Directeur de recherche, CNRS	Directeur de thèse
Philippe GUÉGUEN	Directeur de recherche, IFSTTAR	Rapporteur
Luca LENTI	Chargé de recherche, IFSTTAR	Examinateur
E. Diego MERCERAT	Chargé de recherche, CEREMA	Examinateur
Maria Paola SANTISI D'AVILA	Maître de conférence, UNS	Directeur de thèse
Jean-François SEMBLAT	Directeur de recherche, IFSTTAR	Rapporteur

Earthquakes don't kill people,
collapsed buildings do...
— UNOPS

To my parents

Acknowledgements

I start by saying *merci* to Fred. You supported me during all this time and without you I would probably not be here. *Je t'aime*.

Thanks to Paola, Anne, my supervisors, for your patience, encouragement and guidance throughout these years.

Thanks to the members of my doctoral committee, to my *rapporteurs* Jean Francois and Philippe and *examinateurs* Luca and Francoise for having accepted to take the time to read and comment my thesis work. Specially to Philippe for having received me at Grenoble.

A special thank to Diego and Etienne for your unofficial guidance, advice, and for keeping me motivated when the work became harder. Thank to Julie and the rest of the CEREMA team (Nathalie, Simon, David, etc.) for all the coffee discussions we shared.

Thanks to everyone at Geoazur, researchers, students and technical staff. A special mention to Maelle, Edouard, companions of adventures and parties, respectively, and the rest of the doctorants team (Mathilde, Stephen, Sadrac, Alex, Sargis, Chloé, etc.) for making the lab a great place to pass by.

Thanks to the participants of the JDPN and their organizers. The seminar 'from *doctorants* to *doctorants*' where scientific research, fun and friendship can always be found. Thanks to the members of the *group jeunes de l'AFPS* (Cedric, Celine, etc.), a great starting point to get into the para-seismic community.

Thanks to Piero, who initiated me to earthquake engineering and who encouraged me to pursue this thesis in Nice.

I wish to express my deep gratitude to the *Provence Alpes Côte d'Azur* region, that has founded this thesis trough a 3-year doctoral contract as a result of a strong interaction with the CEREMA partner.

Finally, thanks to my mother Margarita, and my brothers, Alfonso and Santiago, my closer family, who always supported me, in as many ways as possible.

Nice, 17 October 2016 G. W. F. L.

Abstract

The aim of this thesis is to simulate the time history response of a high rise building under seismic excitation and provide simplified methodologies that properly reproduce such response. Firstly, a detailed three-dimensional finite element model is produced to validate its reliability to simulate the real behavior of the building during ground motions, recorded using accelerometers. It is proposed to improve the accuracy of the numerical model by imposing multiple excitations, considering rocking effect and spatial variability on the input motion. The finite element model provides excellent results when dynamic parameters are calibrated to match the service condition of the structure.

The use of empirical Green's functions is proposed to simulate the seismic response directly from past event records, without the need of construction drawings and mechanical parameters calibration. A stochastic summation scheme, already used to predict ground motions, is adopted to generate synthetic signals at different heights of the building, extending the wave propagation path from the ground to the structure. The procedure shows good agreement with numerical signals provided by the finite element model.

A simplified representation of the building as a homogeneous Timoshenko beam is proposed to simulate the seismic response directly from ambient vibration records. Equivalent mechanical parameters are identified using deconvolution interferometry in terms of wave dispersion, natural frequencies, and shear to compressional wave velocities in the medium. Response simulation of lower modes, up to the fifth natural frequency, is properly reproduced by the equivalent model.

Both proposed techniques provide alternatives to finite element modeling, when in-situ records (either seismic or ambient noise) are available, to avoid difficulties related with the lack of data about structure and materials and computing time.

Keywords: *seismic response simulation, high rise building, operational modal analysis, finite element modeling, empirical Green's function, deconvolution interferometry*

Contents

List of Figures

List of Tables

1 General introduction

Population in seismic zones increases and, despite the continuous scientific and engineering advances, continues to suffer damages. Some dramatic recent scenarios such as Sumatra (2004), Sichuan (2008), Haiti (2010), Tohoku (2011), Nepal (2015), Ecuador (2016), remind us too often the unpredictable nature and destructive power of these natural events.

The main cause of losses during seismic events is related to the effect that earthquakes have on civil structures. This may seem obvious, but explains the reasons which often lead to catastrophe: underestimated hazard, unappropriated structural dimmensioning, lack of disposed resources, inadequate execution, etc.

Nowadays, seismic codes provide guidelines to follow in order to protect property and life in buildings in case of earthquakes. Such provisions do not exist since a long time. The first prescriptive rules for buildings are issued after the 1755 Lisbon earthquake. Events in Messina (1908) and Kanto (1923) lead to guidelines for engineers to design buildings in such regions. Modern codes are heavily influenced by California seismic regulations, which started to appear after the Santa Barbara earthquake (1925). In France, the first technical document related to paraseismic construction is issued for North Africa (PS55) after the 1954 Orleansville event. The arrival of seismic rules for metropolitan France does not take place until 1969 (PS69), pushed by the occurrence of Arette 1967 earthquake, being such guidelines non-mandatory. In 1977 such rules become obligatory for public buildings, and in 1983 for all new constructions (Lestuzzi, 2008). Such provisions are notably improved in 1995 (PS92) and with the begining of Eurocode 8 publication (in 2005) that harmonises construction norms across Europe. Most of the building park in French cities dates from before seismic code and have not followed any type of anti-seismic measures.

In such a context, knowing how an existing structure will react against ground motion produced by an earthquake becomes important. But, do we really know how to model the real response of an structure to an earthquake? We do not often have the possibility to validate the reliability of the seismic response prediction obtained using numerical models. The instrumentation of structures enables to record the real response of buildings during seismic motions and provides measures to validate numerical simulations. During a strong event, the building response to earthquakes is highly nonlinear (due to material rheology and effects as soil structure interaction), and most actual research efforts intend to reproduce such behavior during the ground shake.

Metropolitan France is characterized by a moderate seismicity and a town such as Nice (in the South of France) is aware of destructive earthquakes (1565 and 1887, with MSK intensities of VIII and X at their epicenters, respectively). Consequently, the anti-seismic approach is different than in higher seismic risk areas and research efforts should be adapted to fit specific needs (lower hazard and lower available resources). This study focus on what can be learned from the instrumentation of the Nice prefecture building. The building has been instrumented in 2010, and no damage has been identified since sensors have been placed.

The purpose of this research is to evaluate how well we can reproduce the behavior of the building during earthquakes using numerical modeling techniques and propose alternative simplified techniques to simulate the response of the building to be used when construction plans and material properties are not easily available. For such purpose the following questions will be developed:

1. Can we reproduce the actual state of the structure starting from structural plans and adopted design conditions?

2. Can we obtain reliable numerical models to simulate the seismic response?

3. Can we simulate the response to stronger earthquakes using past seismic records?

4. Can we simulate building seismic response using a simplified model and ambient vibration records?

Numerical simulation using finite elements requires modeling, computing time, knowledge of building structure and material properties. This approach could be replaced, specially in the case of a city model, by simplified methods. In this context, the instrumentation of structures

offers new possibilities to evaluate building dynamic properties and reproduce its operating response to an earthquake.

In order to answer such questions, the following research has been developed and presented in different Chapters:

- **Structural identification** (Chapter 3): We use measurements from in-situ records to extract the dynamic properties of the building. The influence of material properties on structural dynamic behavior is highlighted. A detailed three-dimensional finite element model of the building is created from structural plans. It is presented how empirical measures can be used to calibrate a numerical model to match the life service condition and to validate modeling hypothesis. The variability of the structural condition with external factors (notably temperature) is discussed.

- **Finite elements response** (Chapter 4): The created model is used to reproduce the recorded time-history responses, at different levels of the structure, by imposing the ground motion of past earthquakes. The intention is to evaluate if a numerical model is able to reproduce the seismic response of the building. A fixed base is initially considered (as usually done for buildings) and a triaxial seismic load is imposed. However, transitional variations of the natural frequencies of buildings are observed during strong ground motions (Udwadia and Trifunac, 1973b). Todorovska (2009b) assotiates these changes to the contribution of the soil structure interaction, as a result of rocking effects during the motion. These transitient drops in natural frequencies exist and can be considerable (Todorovska 2009b quantified a 18% contribution to drop in a rigid body rocking frequency), but are they relevant to the response of a building? Trifunac (2009b) is concerned about this common simplification, showing that neglecting the rotational motion component near faults can lead to a story drift underestimation by a factor of two in shear buildings. A fixed-base model is unable to reproduce base rotation and such effects are traditionally neglected for simplification. Multiple recorded sources of excitation, adding spatial variability on input motion, are imposed to relevant parts of the base of the structure to reproduce such rocking behavior (if present). The comparison of the response given by both models with records enables to quantify the importance of rocking effects on the response of a building.

- **Empirical Green's funtion** (Chapter 5): Analysis of wave propagation for structural response prediction to earthquakes date from 1930s with the works of Sezawa and Kanai (1935, 1936). In 1963, Kanai and Yoshizawa (1963) proposed a simple formula to approximate the response at the base of the building from records at the roof level, based on seeing the response of a

structure as a superposition of propagating waves. Hence, the response at the base resulted on a superposition of two time shifts of the roof response. Such concept is considered as the predecessor of the impulse response method (Snieder and Safak, 2006; Todorovska, 2009a). Kanai-Yoshizawa formulation has been recently revisited and generalized to any level (Ebrahimian et al., 2016), which shows to approximate well the response of tall and very tall buildings for both weak and strong motions. Such formulation can approximate motions at different floors by only disposing a single earthquake recording at the roof level. But, can we use these records to predict the motion generated by a larger earthquake? The prediction of ground motions stronger than the available records is very usual for risk and structural vulnerability assessment. The seismic load can be simulated by using a numerical model of the source rupture and wave propagation path (deterministic approach), or defined among a set of selected records (empirical approach). The use of small earthquake records to generate synthetic signals of large earthquakes is proposed by Hartzell (1978). According to this semi-empirical approach, each record represents the propagation effect between the source and the receiver and is considered as an empirical Green's function. The main advantage of such methods is that they naturally incorporates both regional propagation path features and local site effects (which are difficult to model if the mechanical properties of the medium are not known or if 3D effects are present). We propose a stochastic summation procedure (Kohrs-Sansorny et al., 2005), already used to simulate ground motion, to simulate the response of a building to a given earthquake from records. The original technique is developed to propose realistic strong motions on free field where only intermediate magnitude event are recorded for larger magnitude characteristic events. It is based on the knowledge of the modification suffered by the waves trough the propagating medium, from the earthquake source to the soil where the response is to be reproduced. The response of a building to an earthquake can be seen in a similar way. The building transforms the content of the input waves trough the propagation across the structure, according to its frequency content. Hence, it would make sense to extend the propagation path from the bottom to the top of the structure. Such implementation does not require knowledge of material properties and structure dimensions neither long computing time. A single record of the structural response during an earthquake is sufficient.

- **Deconvolution interferometry** (Chapter 6): Interferometry is another extremely interesting field of seismology. The first observations of seismic ambient noise date from the end of the XIX century (Bertelli, 1872). The development of the acquisition material improved the comprehension of seismic noise and the information that it contains. New techniques with networks of sensors, measuring the propagation lag between different stations, enable the

obtention of soil velocity profiles based on surface wave dispersion properties. Two different methodologies are distinguished by the analysis of frequency-wavenumber (FK) domain (Capon et al., 1967; Capon, 1969), and the signal correlation (Aki, 1957, 1965). It enables to follow the propagations of different waves trough the earth, making possible to determine their velocities, and hence the rigidity of the soils trough which they propagate, enabling non invasive prospections of layers underneath the surface. If we consider that the response of a building is the result of a propagating wave, it also make sense to use such developments to follow the wave propagation across the structure. Snieder et al. (2006) show how wave propagation can be followed across the structure, and dynamic properties of the building can be obtained from interferograms. A few principles of interferometry are used to find equivalent mechanical parameters of the Nice prefecture building in order to model it as a Timoshenko beam. Mechanical parameters can be obtained analyzing structural response records under ambient vibration excitation, without the need of detailed knowledge of the structural element arrangement.

2 Basis concepts of structural dynamics and background of building instrumentation

Contents

This Chapter refreshes a list of concepts considered as important for the global understanding of the rest of the manuscript. Fundamentals of structural dynamics are introduced in Section 2.1. The evolution of building instrumentation for seismic monitoring is summarized in Section 2.2.

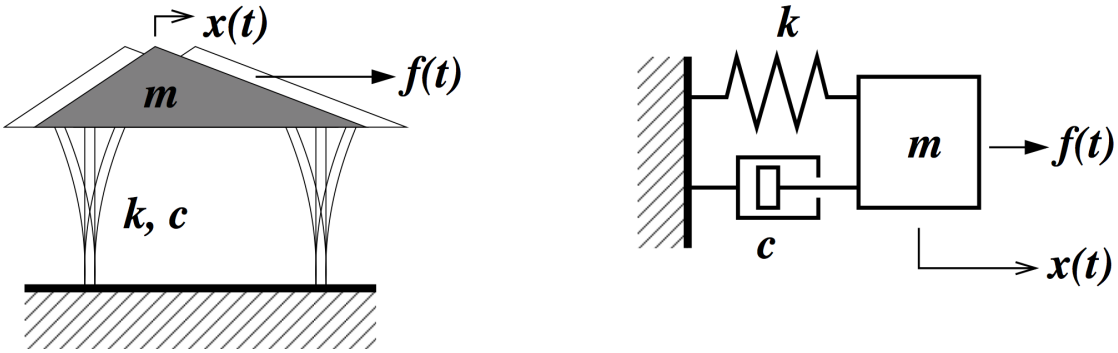

Figure 2.1 – Representation of a single degree of freedom oscillator (from Gavin, 2014).

2.1 Structural dynamics

A brief selection of structural dynamics principles is introduced, please refer to the abundant existing literature (e.g. Chopra, 2012; Clough and Penzien, 2003; Datta, 2010; Kramer, 1996) for a detailed development of these subjects.

2.1.1 Equation of motion

The simplest representation of the dynamic behavior of a building is a single degree of freedom (SDOF) oscillator. It consists of a spring-mass-damper system where the lumped mass moves in only one direction. Such model is specially convenient to reproduce the horizontal vibrations of a single-story building (Figure 2.1).

The dynamic equilibrium is obtained by balancing the inertia, damping and elastic forces, f_I, f_D and f_S, respectively

$$f_I + f_D + f_S = f(t) \tag{2.1}$$

$$f_I = m\ddot{u}(t) \tag{2.2}$$

$$f_D = c\dot{u}(t) \tag{2.3}$$

$$f_S = ku(t) \tag{2.4}$$

with the external excitation force $f(t)$, where $u(t)$ is the displacement of the center of mass of the moving object, m is the mass of the moving object, c is the linear viscous damping coefficient and k is the linear elastic stiffness.

The following equation of motion is obtained by substitution of expressions 2.2, 2.3 and 2.4 in

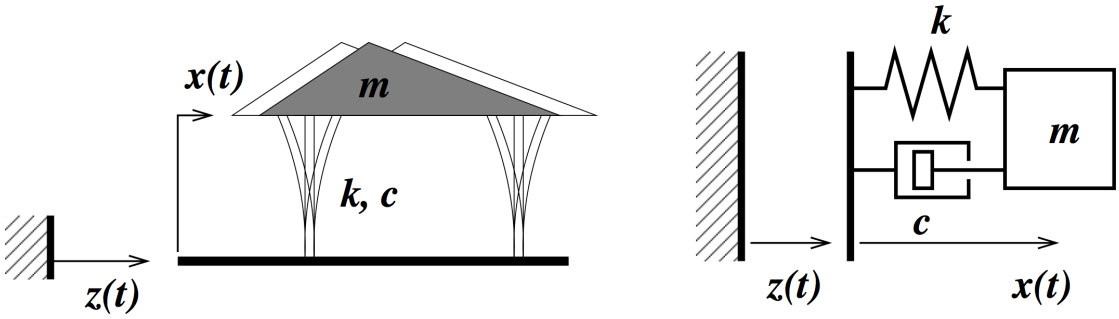

Figure 2.2 – Representation of a single degree of freedom oscillator subjected to ground motion (from Gavin, 2014).

equation 2.1:

$$m\ddot{u}(t) + c\dot{u}(t) + ku(t) = f(t) \tag{2.5}$$

The principal concern for structural engineers in earthquake prone regions is the behavior under seismic induced motion at the base of the structure (Figure 2.2). The solicitation on the structure is caused by the inertial force to resist the ground acceleration $\ddot{u}_g(t)$

$$f(t) = -m\ddot{u}_g(t) \tag{2.6}$$

Referring to equation 2.6, the equation of motion 2.5 may be rewritten as

$$m\ddot{u}(t) + c\dot{u}(t) + ku(t) = -m\ddot{u}_g(t) \tag{2.7}$$

2.1.2 Free vibration

Free vibration is characterised by a null external excitation $f(t)$, where the disturbance is initiated by an imposed initial displacement d_0 and velocity v_0 to the mass. By imposing such conditions, equation 2.5 is modified as

$$m\ddot{u}(t) + c\dot{u}(t) + ku(t) = 0 \tag{2.8}$$

$$d_0 = u(0) \tag{2.9}$$

$$v_0 = \dot{u}(0) \tag{2.10}$$

Undamped vibration

In the undamped case, for $c = 0$, the response is an oscillation, $u(t)$, of given amplitude and frequency, which can be described by sinusoidal functions. The differential equation governing the free vibration of undamped systems corresponds to

$$m\ddot{u}(t) + ku(t) = 0 \tag{2.11}$$

the solution of this homogeneous differential equation 2.11 taking into account the initial conditions 2.9 and 2.10 is a simple harmonic motion in the form

$$u(t) = d_0 \cos(\omega_n t) + \frac{v_0}{\omega_n} \sin(\omega_n t) \tag{2.12}$$

where ω_n is the *natural angular frequency* of the system

$$\omega_n = \sqrt{k/m} \tag{2.13}$$

Note that ω_n has units of radians per second and is independent of the initial conditions or external solicitations. The time required to complete an oscillation cycle, T_n is called *natural period* of the system, measured in seconds, and is related to ω_n. The *natural cyclic frequency* of the system, f_n, measured in Hertz, represents the number of cycles executed in one second

$$f_n = \frac{1}{T_n} = \frac{\omega_n}{2\pi} \tag{2.14}$$

Viscously damped vibration

In the general case of damped systems the dynamic response decays with time. The simplest representation of such decrement is the linear viscous damping, proportional to the velocity (see equation 2.3). A division of the dynamic equilibrium equation 2.8 by the mass, m, gives

$$\ddot{u}(t) + 2\xi\omega_n \dot{u}(t) + \omega_n^2 u(t) = 0 \tag{2.15}$$

where ξ is the, dimensionless *damping ratio*

$$\xi = \frac{c}{2m\omega_n} = \frac{c}{c_r} \tag{2.16}$$

where c_{cr} is the *critical damping coefficient*

$$c_{cr} = 2m\omega_n = 2\sqrt{km} = \frac{k}{\omega_n} \tag{2.17}$$

Note that the damping coefficient c is a measure of the dissipated energy during a cycle of forced harmonic vibration, while the damping ratio ξ is a property of the system dependent of its mass and stiffness.

The form of the solution of equation 2.15, corresponding to the response of the structure, is dependent of the amount of damping present in the system. The types of motion, caused by an initial displacement x_0, are classified as (see Figure 2.3):

- *Undamped* : if $c = 0$ or $\xi = 0$, the system response does not decay.
- *Critically damped* : if $c = c_{cr}$ or $\xi = 1$, the system returns to equilibrium without oscillating.
- *Overdamped* : $c > c_{cr}$ or $\xi > 1$, the system returns to equilibrium without oscillating and with a slower rate than in the critically damped situation.
- *Underdamped* : $0 < c < c_{cr}$ or $0 < \xi < 1$, the system oscillates decreasing its amplitude around the equilibrium position.

Civil engineering structures (such as buildings, bridges, nuclear power plants, dams, etc.) have typically damping ratios lower than 0.1 (Chopra, 2012). Hence, only the underdamped situation is treated on this manuscript.

The solution of equation 2.15 for underdamped systems, taking into account the initial conditions 2.9 and 2.10, is

$$u(t) = exp(-\xi\omega_D t)(d_0 \cos\omega_D t) + \frac{v_0 + \xi\omega_D t}{\omega_D} \sin(\omega_D t) \tag{2.18}$$

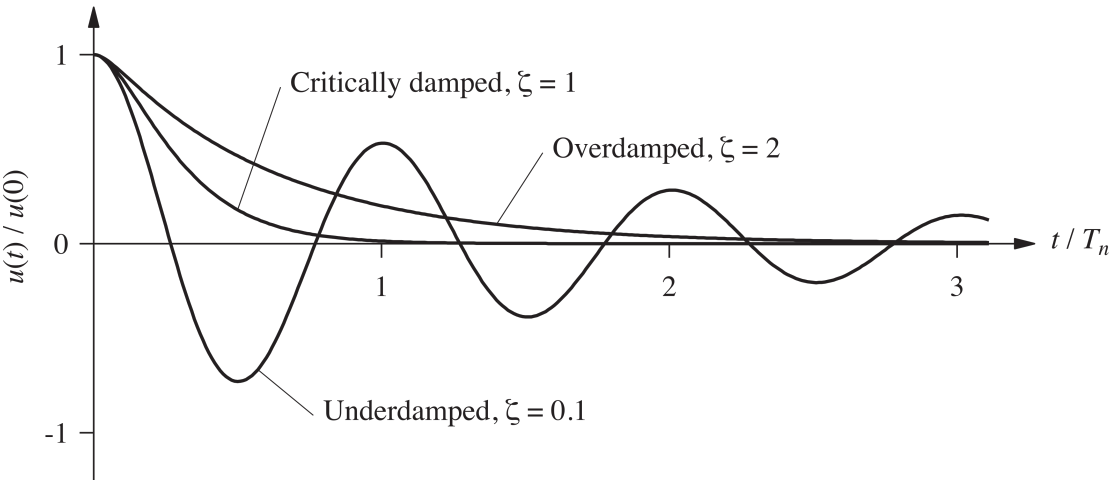

Figure 2.3 – Free vibration of underdamped ($\xi < 1$), critically damped ($\xi = 1$) and overdamped ($\xi > 1$) systems (from Chopra, 2012).

where ω_D corresponds to the damped angular frequency of vibration

$$\omega_D = \omega_n \sqrt{1 - \xi^2} \tag{2.19}$$

2.1.3 Harmonic excitation

The system is subject to a sinusoidal force of the form $p(t) = p_0 \sin(\omega t)$, where p_0 is the *amplitude* and ω is the *exciting frequency*. The dynamic equilibrium equation governing the movement is

$$m\ddot{u}(t) + c\dot{u}(t) + ku(t) = p_0 \sin(\omega t) \tag{2.20}$$

The solution is in the form

$$u_p(t) = C \sin(\omega t) + D \cos(\omega t) \tag{2.21}$$

where

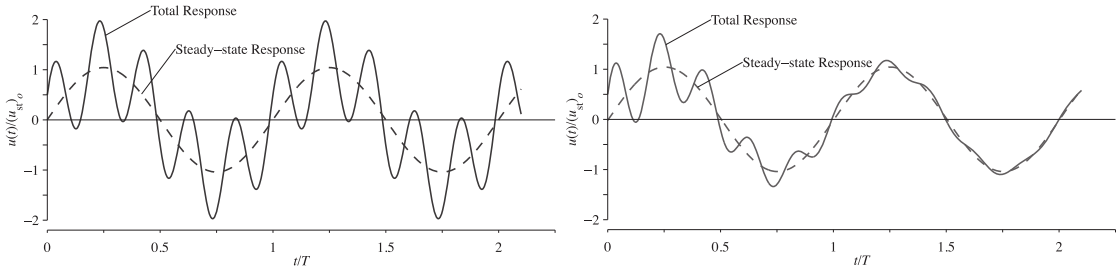

Figure 2.4 – Response of undamped (a) and damped ($\xi = 0.05$) (b) systems to harmonic force $\omega/\omega_n = 0.2$, with $u(0) = 0$ and $\dot{u}(0) = \omega_n p_0/k$ (from Chopra, 2012).

$$C = \frac{p_0}{k} \frac{1-(\omega/\omega_n)^2}{(1-(\omega/\omega_n)^2)^2 + (2\xi(\omega/\omega_n)^2)^2} \tag{2.22}$$

$$D = \frac{p_0}{k} \frac{-2\xi\omega/\omega_n}{(1-(\omega/\omega_n)^2)^2 + (2\xi(\omega/\omega_n)^2)^2} \tag{2.23}$$

The solution is composed of a transitory and a steady state part:

$$u(t) = \overbrace{exp(-\xi\omega_n t)(A\cos\omega_D t + B\sin\omega_D t)}^{Transitient} + \overbrace{C\sin\omega t + D\cos\omega t}^{Steady\ state} \tag{2.24}$$

where

$$A = d_0 \tag{2.25}$$

$$B = \frac{v_0}{\omega_n} - \frac{p_0}{k}\frac{\omega/\omega_n}{1-(\omega/\omega_n)^2} \tag{2.26}$$

The presence of damping reduces the transitory component amplitude across time, tending to the permanent response (Figures 2.4 and 2.5).

When the load frequency corresponds to the natural frequency of the system $\omega = \omega_n$, the system enters into *resonance*. Each cycle of excitation is in *phase* with the structure displacement, increasing the response. The amplitude of the steady-state deformation and the rate at which such state is attained are strongly dependent of damping. In the ideal case of an undamped structure, the deformation amplitude would grow indefinitely with time (Figure 2.5).

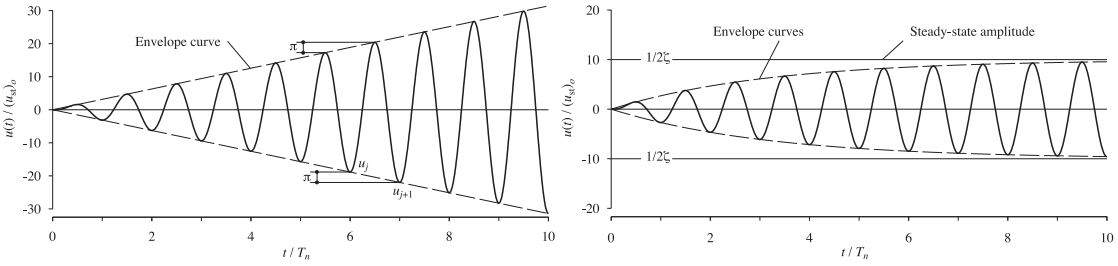

Figure 2.5 – Response of undamped (a) and damped ($\xi = 0.05$) (b) systems to sinusoidal force of frequency $\omega = \omega_n$, with $u(0) = 0$ and $\dot{u}(0) = 0$ (from Chopra, 2012).

The steady-state deformation caused by an harmonic force can be expressed as

$$u(t) = u_0 \sin(\omega t - \phi) = (u_{st})_0 R_d \sin(\omega t - \phi) \tag{2.27}$$

where $u_0 = \sqrt{C^2 + D^2}$ and $\phi = \tan^{-1}(-D/C)$. The deformation response factor, R_d, is the ratio of the dynamic deformation amplitude , u_0, to the static deformation $(u_{st})_0$. It determines the amplification between dynamic and static response and phase angle, ϕ , that gives the time lag between the excitation and the response are identified as

$$R_d = \frac{u_0}{(u_{st})_0} = \frac{1}{\sqrt{(1-(\omega/\omega_n)^2)^2 + (2\xi(\omega/\omega_n))^2}} \tag{2.28}$$

$$\phi = \tan^{-1}\left(\frac{2\xi(\omega/\omega_n)}{1-(\omega/\omega_n)^2}\right) \tag{2.29}$$

The variation of the deformation amplification and phase angle versus frequency ratio ω/ω_n, for different values of damping, is shown in Figure 2.6. The following behaviors are highlighted:

- If $\omega/\omega_n << 1$: the phase angle is close to 0^o, hence the displacement is in phase with the applied force and amplification R_d is slightly larger that 1.
- If $\omega/\omega_n >> 1$ the phase angle is close to 180^o, hence the displacement is out phase with the applied force and the amplification R_d tends to zero.
- If $\omega/\omega_n \approx 1$ the phase angle is close to 90^o, hence the forcing frequency is close to the resonant frequency of the system and the amplification R_d is very sensitive to damping. For small values of damping the dynamic response can be much larger than the static deformation.

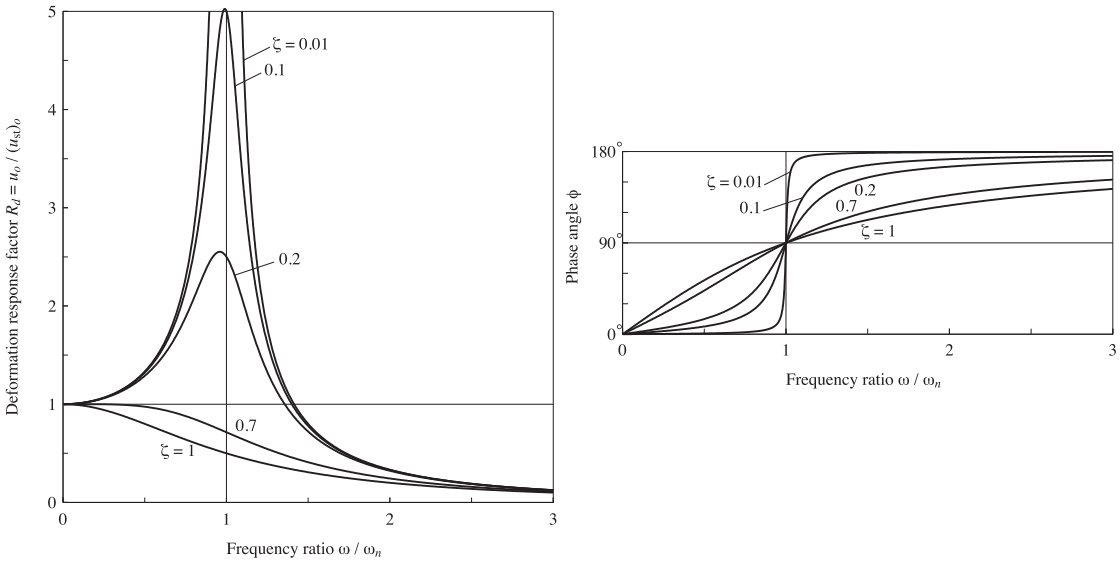

Figure 2.6 – Deformation response factor and phase angle for a damped system excited by harmonic force (from Chopra, 2012).

In the case $\omega = \omega_n$ the response is controlled by the damping properties of the system, and equation 2.27 results in $u_0 = (u_{st})_0/(2\xi)$. Note that R_d is also referred to as quality factor, Q, in the literature (Knopoff, 1964). The civil engineering community usually refers to damping ratio ξ, while geophysicists to Q, beeing the relationship between both

$$Q = 1/(2\xi) \tag{2.30}$$

2.1.4 Seismic response

The time variation of ground acceleration $\ddot{u}_g(t)$ is the most usual representation of the earthquake shaking in civil engineering. The first strong motion accelerogram was recorded in 1933, during the Long Beach earthquake (Chopra, 2012). Figure 2.7 shows the acceleration recorded during different significant earthquakes of the XX century. Real earthquakes are far from being sinusoidal mono-frequencial signals. As seen in Figure 2.7, the ground motion varies with time in a highly irregular manner and the earthquake signature can be very different depending of their nature (signal length, amplitude, strong motion duration, etc.).

The equation of motion of a SDOF system subject to ground motion is expressed as

$$\ddot{u}(t) + 2\xi\omega_n\dot{u}(t) + \omega_n^2 u(t) = -\ddot{u}_g(t) = F(t) \tag{2.31}$$

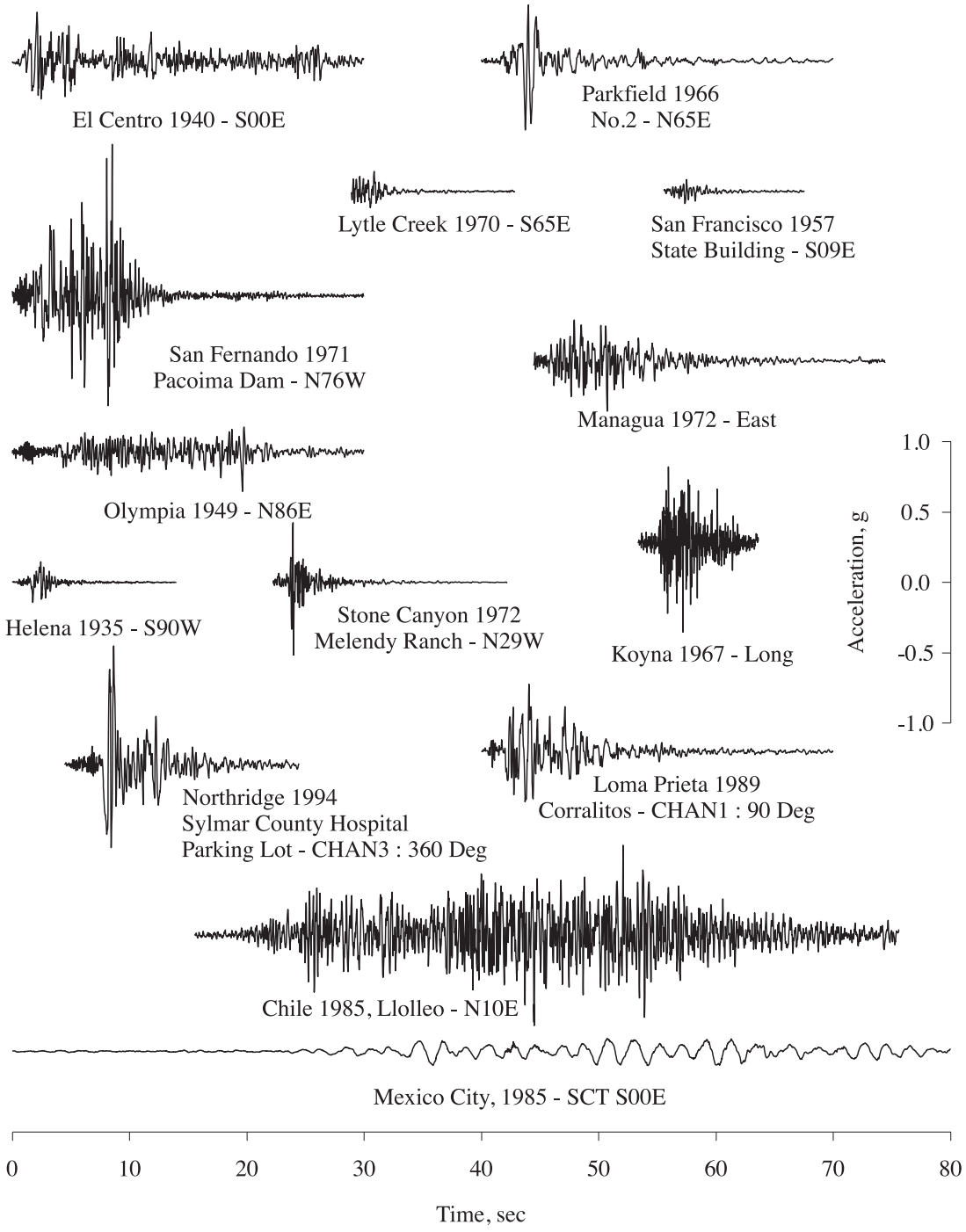

Figure 2.7 – Ground motions recorded during several earthquakes (from Chopra, 2012).

According to equation 2.31, different SDOF systems with identical natural frequency, ω_n, and damping ratio, ξ, sollicited by the same ground motion have the same dynamic behavior, even though they have different masses or rigidity.

The analytical solution of the equation of motion of a system under seismic loading is known at each time instant. Starting from at-rest condition, $u(0) = 0$ and $\dot{u}(0) = 0$, the SDOF deformation time history, $u(t)$ is obtained as

$$\mathbf{y}_k = \theta(\Delta t)\mathbf{y}_{k-1} + \gamma_0(\Delta t)\mathbf{v}F_{k-1} + \gamma_1(\Delta t)\mathbf{v}F_k \tag{2.32}$$

$$\dot{\mathbf{y}}_k = \mathbf{D}\mathbf{y}_k + \mathbf{v}F_k \tag{2.33}$$

where the subscript k is the iteration step and

$$\mathbf{y}_k = \begin{bmatrix} u(t_k) \\ \dot{u}(t_k) \end{bmatrix} \tag{2.34}$$

$$\theta(\Delta t) = \begin{bmatrix} -\omega_n^2 g(\Delta t) & h(\Delta t) \\ -\omega_n^2 h(\Delta t) & \dot{h}(\Delta t) \end{bmatrix} \tag{2.35}$$

$$\mathbf{D} = \begin{bmatrix} 0 & 1 \\ -\omega_n^2 & -2\xi\omega_n \end{bmatrix} \tag{2.36}$$

$$\gamma_0(\Delta t) = \left(\theta(\Delta t) - \frac{1}{\Delta t}\mathbf{L}(\Delta t)\right)\mathbf{D}^{-1} \tag{2.37}$$

$$\gamma_1(\Delta t) = \left(\frac{1}{\Delta t}\mathbf{L}(\Delta t) - \mathbf{I}\right)\mathbf{D}^{-1} \tag{2.38}$$

$$\mathbf{L}(\Delta t) = (\theta(\Delta t) - \mathbf{I})\,\mathbf{D}^{-1} \tag{2.39}$$

$$\mathbf{v} = \begin{bmatrix} 0 & 1 \end{bmatrix}^T \tag{2.40}$$

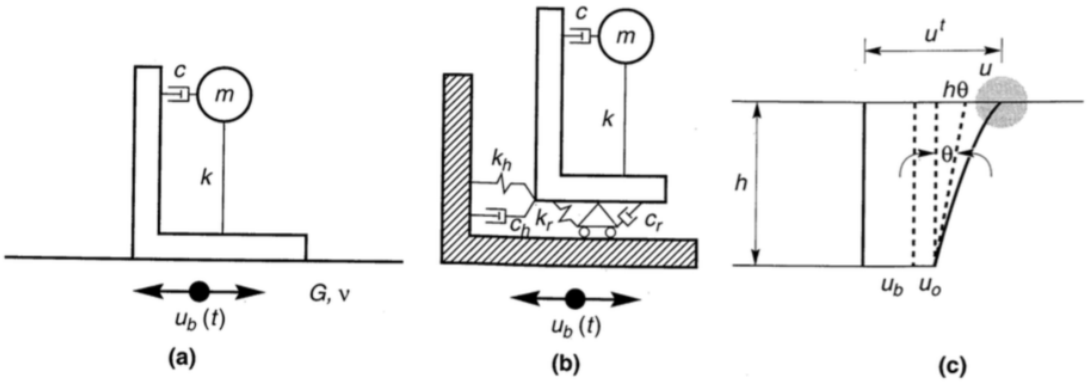

Figure 2.8 – One degree of freedom base model for: (a) system on a elastic soil, (b) discrete system where base compliance is represented by springs and dashpots, (c) components of motion of base and mass (from Kramer, 1996).

$$g(\Delta t) = -\frac{1}{\omega_n^2} e^{-\xi\omega_n\Delta t}\left(cos(\omega_D\Delta t) + \frac{\xi\omega_n}{\omega_D} sin(\omega_D\Delta t)\right) \tag{2.41}$$

$$h(\Delta t) = \dot{g}(\Delta t) = \frac{1}{\omega_D} e^{-\xi\omega_n\Delta t} sin(\omega_D\Delta t) \tag{2.42}$$

$$\dot{h}(\Delta t) = e^{-\xi\omega_n\Delta t}\left(cos(\omega_D\Delta t) - \frac{\xi\omega_n}{\omega_D} sin(\omega_D\Delta t)\right) \tag{2.43}$$

where ω_D is defined in 2.19. Matrices in equations 2.32 and 2.33 are constant during the time history.

2.1.5 Effects of SSI on natural frequencies

To illustrate the most important effects of soil-structure interaction, the case of a SDOF system mounted on a rigid, massless, L-shape foundation supported on an elastic soil (Figure 2.8a) is adopted (Wolf, 1985). Being the structure characterized by its mass, m, stiffness, k, and damping coefficient c, the fixed-base natural frequency, ω_n, and hysteretic damping ratio, ξ, are, respectively (as described in Section 2.1.2):

$$\omega_n = \sqrt{k/m} \tag{2.44}$$

$$\xi = \frac{c\omega_n}{2k} \tag{2.45}$$

However, if the supporting material is compliant with the structure, the foundation can rotate and translate. The compliant soil-foundation system is shown in Figure 2.8b, where stiffness

and damping characteristics are represented by springs and dashpots. Two sources of damping are represented: material damping (caused by the inelastic behavior of the foundation) and radiation damping (caused by the soil deformation due to dynamic forces in the structure). Radiation damping is often much greater than material damping for typical foundations (Kramer, 1996). The total displacement of the base and the structural mass can be separated in individual components (see Figure 2.8b). Then, the natural frequency of the equivalent model, ω_e, can be obtained as a combination of: the natural frequency of the fixed-base system, ω_n, the natural frequency for translational vibration, ω_h and the natural frequency for rocking, ω_r.

$$\frac{1}{\omega_e^2} = \frac{1}{\omega_n^2} + \frac{1}{\omega_h^2} + \frac{1}{\omega_r^2} \tag{2.46}$$

$$\omega_e = \frac{\omega_n}{\sqrt{1 + k/k_h + kh^2/k_r}} \tag{2.47}$$

Equation 2.47 shows that the natural frequency of a system considering soil-structure interaction always decreases with respect to the fixed-base structure. Hence, the greater the importance of the soil-structure interaction, the greater the reduction of the natural frequency.

2.1.6 MDOF systems

Modal analysis

Vibrational approach for the estimation of seismic response of multi-degree-of-freedom (MDOF) systems in earthquake engineering comes from the general theory of transitient response by Biot (1932).

The dynamic response of a structure can be represented by a SDOF model in the case of one story buildings or structures with a single lumped mass at their head (water towers, airport control towers, etc.).

The equation 2.7 for structures with MDOF becomes

$$\mathbf{M}\ddot{\mathbf{u}}(t) + \mathbf{C}\dot{\mathbf{u}}(t) + \mathbf{K}\mathbf{u}(t) = -\mathbf{M}\tau\,\ddot{u}_g(t) \tag{2.48}$$

The modal transformation

$$\mathbf{u} = \Phi\mathbf{q} \tag{2.49}$$

is adopted to diagonalize the matrices in equation 2.48. Φ is the modal matrix, which columns are the eigenvectors obtained solving the following eigenproblem 2.50:

$$\mathbf{K}\Phi = \mathbf{M}\Phi\Omega^2 \tag{2.50}$$

Imposing the condition

$$|\mathbf{K} - \lambda\mathbf{M}| = 0 \tag{2.51}$$

the eigenvalues λ_i can be deduced, with $i = 1,...,n$, where n is the number of degrees of freedom of the MDOF system. They correspond to the squared angular frequencies ω_i^2 of the structure, with $\omega_1 < \omega_2 < ... < \omega_n$. If the modal matrix is orthonormal with respect to the mass matrix **M**, equation 2.48 becomes

$$\ddot{\mathbf{q}}(t) + \Xi\dot{\mathbf{q}}(t) + \Omega^2\mathbf{q}(t) = -\Phi^T\mathbf{M}\tau\ddot{u}_g(t) \tag{2.52}$$

where $\Xi = diag\{2\xi\omega_i\}$ and $\Omega^2 = diag\{\omega_i^2\}$. Thanks to modal transformation 2.52 is a system of independent equations where each one is the dynamic equilibrium equation of a SDOF system, which analytical solution is known at each time step.

Once evaluated the modal displacement vector **q**, the modal transformation 2.49 provides nodal displacement vector **u** of the MDOF system. The same relationship is adopted for velocity and acceleration

$$\dot{\mathbf{u}} = \Phi\dot{\mathbf{q}} \tag{2.53}$$

$$\ddot{\mathbf{u}} = \Phi\ddot{\mathbf{q}} \tag{2.54}$$

This procedure avoids numerical time integration schemes and reduces computational time.

Modal transformation is possible according to the superposition principle and is only valid for linear behavior of materials.

Further works facilitate the application of the theory (Biot, 1933, 1934) introducing the actually known as response spectrum method. Nowadays, such approach is commonly used by earthquake engineers after 80 years without many changes (Trifunac, 2008a). The response spectrum method proposes to use the maximum expected acceleration for the analyzed seismic zone (depending on the building period) instead of a reference acceleration time-history.

Direct integration dynamic analysis

The differential equation 2.48 can be directly solved using an implicit algorithm as a Newmark process. It can be written in incremental form as

$$\mathbf{M}\Delta\ddot{\mathbf{u}}_k + \mathbf{C}\Delta\dot{\mathbf{u}}_k + \mathbf{K}\Delta\mathbf{u}_k = -\mathbf{M}\tau\Delta\ddot{u}_{gk} = \Delta\mathbf{F}_k \tag{2.55}$$

where $\mathbf{u}_k = \mathbf{u}(t_k)$. The solution is obtained by defining displacement and velocity as function of acceleration, according to the following expressions:

$$\dot{u}_{k+1} = \dot{u}_k + (1-\gamma)\Delta t\ddot{u}_k + \gamma\Delta t\ddot{u}_{k+1} \tag{2.56}$$

$$u_{k+1} = u_k + (\Delta t)\dot{u}_k + (0.5-\beta)(\Delta t)^2\ddot{u}_k + \beta(\Delta t)^2\ddot{u}_{k+1} \tag{2.57}$$

Parameters β and γ define the variation of acceleration over a time step, characterising the accuracy and stability of the method. If they are assumed according to $2\beta \geq \gamma \geq 1/2$, unconditional stability of the method is assured.

Hilbert, Hughes and Taylor (Hughes, 1987) introduce the α-method as improvement of Newmark process. The time discrete equation of motion is modifies as follows:

$$\mathbf{M}\Delta\ddot{\mathbf{u}}_{k+1} + (1+\alpha)\mathbf{C}\Delta\dot{\mathbf{u}}_{k+1} - \alpha\mathbf{C}\Delta\dot{\mathbf{u}}_k + (1+\alpha)\mathbf{K}\Delta\mathbf{u}_{k+1} - \alpha\mathbf{K}\Delta\mathbf{u}_k = (1+\alpha)\Delta\mathbf{F}_k - \alpha\Delta\mathbf{F}_{k-1} \tag{2.58}$$

If $\alpha = 0$ equation 2.58 reduces to the Newmark method. If the parameters are selected such that $\alpha \in [-1/3, 0]$, $\gamma = (1-2\alpha)/2$, and $\beta = (1-\alpha)^2/4$, an unconditionally stable, second-order

accurate scheme results. At $\alpha = 0$, the trapezoidal rule is obtained. Decreasing α increases the amount of numerical dissipation.

The damping matrix in equation 2.48 can be assumed dependent on mass and stiffness matrices, and expressed according to the Rayleigh approach

$$\mathbf{C}_k = a\mathbf{M} + b\mathbf{K}_k \tag{2.59}$$

The coefficients are estimated as function of the first and second natural angular frequency ω_1 and ω_2, respectively:

$$a = 2\xi\frac{\omega_1\omega_2}{\omega_1 + \omega_2} \tag{2.60}$$

$$b = 2\xi\frac{1}{\omega_1 + \omega_2} \tag{2.61}$$

2.1.7 Euler–Bernoulli beam

Structures with one predominant dimension in relation to the other two can be modeled as beam elements with rigidity and mass homogeneously distributed along the element axis. The Euler–Bernoulli beam theory (Timoshenko, 1953) describes the behavior of a beam under bending deformation under the assumption of negligible axial and shear strain. Consequently, the beam cross-section remains orthogonal to the beam axis during deformation. The beam movement is described by the following equation (Clough and Penzien, 2003):

$$\frac{\partial^4 u(x,t)}{\partial x^4} + \frac{m}{EI}\frac{\partial^2 u(x,t)}{\partial t^2} = 0 \tag{2.62}$$

where $u(x,t)$ is the displacement, m is the mass, E is the elasticity modulus in compression and I is the moment of inertia. The solution of the differential equation 2.62 is achieved by modal decomposition of time, t, and space, x, variables:

$$u(x,t) = \phi(x)U(t) \tag{2.63}$$

where $\phi(x)$ is function of the modal shape and $U(t)$ represents the amplitude for a given time. By applying the decomposition, equation 2.62 results:

$$\frac{\partial^2 U(t)}{\partial t^2} + \omega_0^2 U(t) = 0 \tag{2.64}$$

$$\frac{\partial^4 \phi(x)}{\partial x^4} + \alpha^4 \phi(x) = 0 \tag{2.65}$$

where $\alpha^4 = (m\omega_0^2)/(EI)$ and ω_0 is the fundamental angular frequency of the beam. The solutions of equations 2.64 and 2.65 are respectively:

$$U(t) = A\cos(\omega_0 t) + B\sin(\omega_0 t) \tag{2.66}$$

$$\phi(x) = C1\sin(\alpha x) + C2\cos(\alpha x) + C3\sinh(\alpha x) + C4\cosh(\alpha x) \tag{2.67}$$

where A and B are constants related to the initial displacement, U_0, and velocity, V_0. Constants $C1$, $C2$, $C3$ and $C4$ are related to the boundary conditions of the beam. For the specific case of a cantilever beam (fixed at the base and free at the top), rotations and displacements are null at the base, while shear, V, and moment, M, are null at the top:

$$u(0,t) = 0 \rightarrow \phi(0) = 0 \rightarrow C4 = -C2 \tag{2.68}$$

$$\frac{\partial u(t)}{\partial x} = 0 \rightarrow \frac{\partial \phi(0)}{\partial x} = 0 \rightarrow C3 = -C1 \tag{2.69}$$

$$M(H,t) = 0 \rightarrow EI\frac{\partial^2 \phi(H)}{\partial^2 x} = 0 \rightarrow$$
$$C1(\sin(\alpha H) + \sinh(\alpha H)) + C2(\cos(\alpha H) + \cosh(\alpha H)) = 0 \tag{2.70}$$

$$Q(H,t) = 0 \rightarrow EI\frac{\partial^3 \phi(H)}{\partial^3 x} = 0 \rightarrow$$
$$C1(\cos(\alpha H) + \cosh(\alpha H)) + C2(-\sin(\alpha H) + \sinh(\alpha H)) = 0 \tag{2.71}$$

The solutions of the system can be obtained numerically trough the following equation:

$$1 + \cos(\alpha H)\cosh(\alpha H) = 0 \tag{2.72}$$

which are used to obtain the natural frequencies of the cantilever bending beam:

$$f_1 = \frac{0.5596}{H^2}\sqrt{\frac{EI}{m}} \tag{2.73}$$

$$\frac{f_n}{f_1} = 0.7(2n-1)^2 \qquad \forall n > 1 \tag{2.74}$$

which leads to frequencies ratios characteristics of a beam with bending behavior: $f_2/f_1 = 6.3$, $f_3/f_1 = 17.5$, $f_4/f_1 = 34.3$, etc.

2.1.8 Timoshenko beam

Timoshenko beam theory (Timoshenko, 1921, 1922) considers a non negligible shear strain of the beam under shear effort. Consequently, orthogonality of the beam cross-section to the beam axis is not imposed, as in the Euler-Bernoulli beam theory. The difference between both, Euler-Bernoulli and Timoshenko, beam theories lies on their assumptions. The contribution of shear strain leads to the equation of motion (Dunand, 2005)

$$\frac{\partial^2 u(x,t)}{\partial x^2} + \frac{m}{GS}\frac{\partial^2 u(x,t)}{\partial t^2} = 0 \tag{2.75}$$

where S is the cross section area and G is the shear modulus. Equation 2.75, using modal decomposition (equation 2.63), becomes

$$\frac{\partial^2 U(t)}{\partial t^2} + \omega_0^2 U(t) = 0 \tag{2.76}$$

$$\frac{\partial^2 \phi(x)}{\partial x^2} + \alpha^2 \phi(x) = 0 \tag{2.77}$$

where $\alpha^2 = (m\omega_0^2)/(GS)$ and ω_0 is the fundamental angular frequency of the beam. The solutions of equations 2.76 and 2.77 are respectively

$$U(t) = A\cos(\omega_0 t) + B\sin(\omega_0 t) \tag{2.78}$$

$$\phi(x) = C1\cos(\alpha x) + C2\sin(\alpha x) \tag{2.79}$$

where A and B are constants related to the initial displacement, U_0, and velocity, V_0. $C1$ and $C2$ are related to the boundary conditions of the beam. For the case of a cantilever beam:

$$u(0,t) = 0 \rightarrow \phi(0) = 0 \rightarrow C1 = 0 \tag{2.80}$$

$$Q(H,t) = 0 \rightarrow \cosh(\alpha H) = 0 \tag{2.81}$$

The natural frequencies can be obtained from the solutions of equation 2.81:

$$f_n = \frac{n-0.5}{2H}\sqrt{\frac{GS}{m}} \tag{2.82}$$

$$\frac{f_n}{f_1} = (2n-1) \qquad \forall n > 1 \tag{2.83}$$

which leads to the frequency ratios that are characteristics of a beam with not negligible shear strain: $f_2/f_1 = 3$, $f_3/f_1 = 5$, $f_4/f_1 = 7$, etc.

The equation defining the movement in the modal base (after variable separation of equation 2.63) is (Hans, 2002)

$$EI\frac{\partial^4\phi(x)}{\partial x^4} + \frac{EI}{K}m\omega^2\frac{\partial^2\phi(x)}{\partial x^2} - m\omega^2\phi(x) = 0 \tag{2.84}$$

where K is a shear parameter according to $V(x) = -K\gamma(x)$, where γ is the shear strain and V the associated shear force. The behavior of an Euler-Bernouilli beam is stiffer than a Timoshenko beam, in the case of slender enough structures the error for both models is relatively small. In the case of structures with smaller length to thickness ratios, the Timoshenko beam is a more appropriate choice (as shear effects are more relevant).

A beam with predominant bending behavior is sometimes referred as *bending beam*, and to a beam with predominant shear behavior as *shear beam*. A dimensionless parameter of a beam (Michel, 2007)

$$C = \frac{EI\pi^2}{4KH^2} \tag{2.85}$$

related to the structural behavior, is useful to inform if the bending type behavior is predominant or rather the shear one. A structure is considered to behave in bending for values of $C < 0.05$, and in shear for values of $C > 5$ (Boutin et al., 2005). Figure 2.9 shows the variation of frequency ratios with the parameter C, it is observed that the case values of pure bending

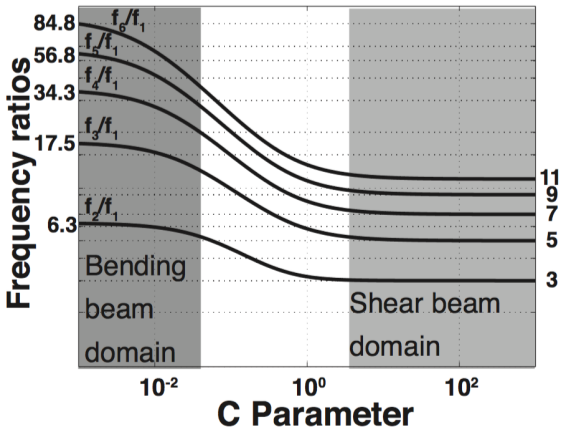

Figure 2.9 – Variation of frequency ratios f_n / f_1 for modes above the fundamental frequency with the dimensionless parameter C, for a continuous Timoshenko beam. Grey areas represent the limit for bending and shear beam behavior (Michel, 2007).

beam are found for $C \to 0$, while pure shear are found for $C \to \infty$.

Additional details about Timoshenko beam theory are discussed in Section 6.3.2

2.2 Instrumentation of buildings

2.2.1 Vibrational analysis of buildings

Recordings of vibrations in civil engineering structures are undertaken at the beginning of the XX century by the seismologist Fusakichi Omori in Japan. He records earthquakes on masonry between 1900 and 1908, with the aim to observe structures to increase seismic resistance (Davison, 1924). Omori takes records during the construction of buildings, after seismic damage and after rehabilitation (Omori, 1922). After him, researchers in Japon (Ishimoto and Takahasi, 1929) and the United States (Byerly et al., 1931) continued to further investigate this topic.

The earthquakes of Santa Barbara in 1925 (6.8 magnitude, 13 deaths and 8$ millions in damages) and Long Beach in 1933 (6.4 magnitude, 115 deaths and 40$ millions in damages) encouraged the implementation of the program *US Coast and Geodetic Survey*. Leaded by Dean Carder, 336 buildings were instrumented and their fundamental periods were obtained. The study establishes the first empirical relationship between building height and period (Carder, 1936), which settles the principles afterward used in the para-seismic codes (Housner and Brady, 1963).

Several studies about vibrations in structures are developed in Japon in the following years, specially regarding the use of forced vibrations (Kanai et al., 1949; Kanai and Tanaka, 1951; Kanai and Yoshizawa, 1952). Hisada and Nakagawa (1956) used forced vibrations in buildings up to failure.

An extended program arises in the 1960s at the United States, which objective is to observe building behavior under strong seismic motion. It allows better understanding of: soil effects on the structure response (Housner, 1957), building shape modes (Blume, 1972), and its nonlinear response (Safak and Celebi, 1991).

The California strong motion instrumentation program (CSMIP) is established after the San Fernando earthquake in 1971. The goal of the program is collecting the necessary data to improve anti-seismic conception criteria and design codes. Nowadays more than 900 stations are placed, including 650 ground-response stations, 170 buildings, 20 dams and 60 bridges. Buildings in California have been typically instrumented installing between 12 to 15 sensors per building (Huang and Shakal, 2012). A non-exhaustive list of permanently instrumented buildings by the USGS is provided in Table 2.1. A detailed list of all structural and geotechnical arrays managed by the U.S. Geological Survey (USGS), withing the National Strong-Motion Project (NSMP), can be found in the USGS website (USGS, 2016).

In Japan, the building research institute (BRI) operates about 70 stations on buildings, distributed in major cities of the country. For example , on the 11 March 2011, the M_w9 earthquake has triggered 60 of those stations. Analysis of records shows that at least four buildings have suffered damage (Kashima et al., 2012).

In France, the French accelerometric network (RAP) starts to permanently instrument buildings in 2004. Nowadays, the national building array program (NBAP) continuously monitors 5 buildings and data are of public access via internet through the French seismological and geodetic network (RESIF, 1995):

- The Town Hall of Grenoble
- The Earth Discovery Center in Martinique
- The Ophite Tower of Lourdes
- The Tower of Nice Prefecture
- The College of Basse Pointe in Martinique

Table 2.1 – List of selected USGS extensively instrumented buildings (adapted from Dunand et al., 2004).

Building Name	Stories	Image	Instrumentation
LA Public Works Headquarters	13		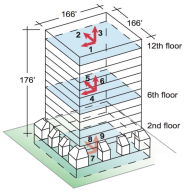
Whittier Lutheran Towers	10		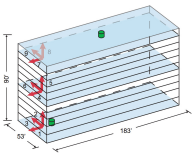
Former Great Western Savings	13		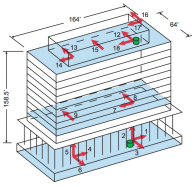
Transamerica Pyramid	49		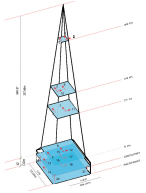
Pacific Park Plaza	30		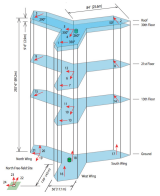
Long Beach VA Hospital	11		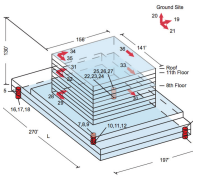
Brinderson Towers #2	13		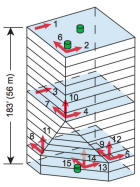
Millikan Library	9		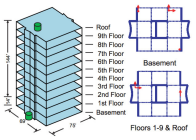

As observed, the instrumentation of civil structures using strong motion sensors has been extensively carried out in seismic regions to understand their dynamic behavior, see Erdik et al. (2001) for a review. Another tendency is to undertake temporary campaigns. The city of Grenoble has been objective of several instrumentation programs. For example, a campaign performed over RC buildings (having shear resisting frame structure) has been carried out by Farsi and Bard (1998). In Nice, a campaign of ambient noise recording in 54 buildings have been carried out in the framework of the project GEMGEP (Bard et al., 2005). Recently, the city of Beirut (Lebanon) has been widely instrumented (Salameh, 2016; Salameh et al., 2016), having performed ambient vibration records on 330 RC buildings for urban scale risk and vulnerability assessment.

The charaterization of dynamic properties of buildings using ambient vibration recordings starts in the 70s by Stubbs and MacLamore (1973) and Udwadia and Trifunac (1973a). Structures are continuously exposed to low amplitude ambient noise (such as wind, rain, traffic, etc.). Such excitation exists everywhere and reveals their dynamic characteristics without the need of external excitation. The identification of dynamic features using low amplitude loading is representative of the elastic state of the structure under small deformations. Values obtained from ambient vibration are comparable to those obtained from artificially induced sollicitations (Boutin et al., 1999; Hans, 2002) or small earthquakes (Dunand et al., 2004).

The study of ambient vibrations starts with seismological studies and the application to civil engineering structures happens much later. Hence, a brief chronology of interesting developments in Earth observation is presented.

2.2.2 Seismic ambient noise

Observations of seismic ambient noise date back to the end of the XIX century. In 1872, Bertelli observed the correlation between microearthquakes and atmospheric perturbations on the movement of a pendulum (Bertelli, 1872). Since then, several studies have been carried out to identify the origins and nature of this phenomena (Table 2.2). During the first half of the XX century, quantitative studies associate the source microseismicity to oceanic waves and meteorological conditions (Gutenberg, 1911; Bernard, 1941). In 1924, Banerji observe variations on noise seismograms which enable him to predict the beginning of the monsoon a few weeks in advance (Banerji, 1925).

Between 1950 and 1970, the development of the acquisition material encourages the employment of seismic noise and and increases the understanding of its richness. Developments

Table 2.2 – Summary of ambient noise sources according to frequency. Summary established after studies by Gutenberg (1958), Asten (1978) and Asten and Henstridge (1984) (modified from Bonnefoy-Claudet et al. (2006)).

	Gutenberg (1958)	Asten (1978,1984)
Oceanic waves striking along the coasts	0.05–0.1 Hz	0.5–1.2 Hz
Monsoon/Large meteorological perturbations	0.1–0.25 Hz	0.16–0.5 Hz
Cyclones over the oceans	0.3–1 Hz	0.5–3 Hz
Local scale meteorological conditions	1.4–5 Hz	
Volcanic tremor	2–10 Hz	
Urban	1–100 Hz	1.4–30 Hz

of new techniques with networks of sensors, measuring the propagation lag between different stations, enable the obtention of soil velocity profiles based on surface wave dispersion properties. Two different methodologies appear to analyze seismic signals by looking at the frequency-wavenumber (FK) domain (Capon et al., 1967; Capon, 1969), and the signal correlation (Aki, 1957, 1965), which are later used with noise records.

After 1970, the number of publications increases continuously bringing new applications. The most extended use is to characterize sites by seismic microzonation, for which the site-reference spectral ratio, and the H/V ratio (Nogoshi and Igarashi, 1971; Nakamura, 1989, 1996) are used. Later developments inverse the H/V curve to estimate the wave velocity profile of S waves (Tokimatsu et al., 1998; Fäh et al., 2001; Arai and Tokimatsu, 2004).

2.2.3 Ambient vibrations in buildings

Seismic background noise that seems useful to characterize soils contains valuable information about engineering structures. In civil engineering, sources of excitation are classified in two groups, depending on if they are natural of human. Natural sources are mainly related to tidal waves or wind, while human vibrations are caused by traffic, people walking on structures, rotating machinery, etc. (Bonnefoy-Claudet et al., 2006).

In an urban environment, such sources are characteristic of a particular frequency content. A first approximation is to consider that frequencies below 1 Hz are natural, while those above 1 Hz are related to human activities (Nasser-Barakat, 2015):

- f < 1 Hz: Large scale oceanic waves are normally around 0.2 Hz. The interaction of sea waves with coasts happens at about 0.5 Hz. Atmospheric conditions produce ambient vibrations at frequencies lower than 0.1 Hz (normally out of interest for seismologists

and engineers).

- f ≃ 1 Hz: Local weather, wind, rain and water flows are associated to such frequency range.
- f > 1 Hz: Sources mainly located at the surface of the earth. Human activities are the main responsible and they suffer from a high amplitude variability (day/night, work day/weekend, etc.)

Amplitude of ambient vibrations is generally low, typically in the range of 10^{-5} - 10^{-6} m/s, depending on the distance and nature of noise sources (Bonnefoy-Claudet, 2004). Velocities estimated using noise vibrations are independent of building nonlinear behavior because the level of excitation remains far below the threshold of nonlinearity. The analysis of ambient vibrations in structures usually consider the input motion as unknown, assuming these vibrations to be stationary and modeling them as white Gaussian noise.

3 Structural identification: the Nice prefecture building

Contents

Analysis of ambient vibration records enables to identify the dynamic properties of a structure. This study uses an original set of deformation records of a 22-story reinforced concrete (RC)

building in Nice (France), where no remarkable damages have been detected since it was instrumented.

Section 3.2 provides a detailed presentation of the case study: description of the structure, monitoring instrumentation, geotechnical context and seismic activity.

An introduction to operational modal analysis (OMA) techniques is provided in Section 3.3, being applied to the building. The main goal is to extract dynamic parameters (natural frequencies, mode shapes and damping) of the structure using different techniques: basic frequency domain (BFD), frequency domain decomposition (FDD) and random decrement (RD). In-situ signals acquired using accelerometers and velocimeters are compared in different frequency ranges to verify the reliability of accelerometric records.

A three-dimensional finite element (FE) model of the resistant structure is presented in Section 3.4, using the available constructions plans of the building. Information deduced from records is used to optimize the model and reproduce the service state of the building. The influence of a non-structural filler of a seismic joint on the dynamic behavior of the structure is studied by comparison of natural frequencies obtained using the numerical model and record analysis.

The variability of dynamic properties of the building during a year of monitoring is shown in Section 3.5. The correlation of such observations with environmental parameters (such as temperature variations), is discussed in time and frequency domains.

3.1 Introduction

The empirical identification of structural dynamic properties is traditionally done using experimental modal analysis, that demands the application of an external load. Such techniques have gradually been replaced by the operational modal analysis (OMA) (Zhang and Brincker, 2005), that uses ambient vibration as source of excitation (such as traffic, wind and microseismicity). This is extremely convenient as it is usually expensive, hard and undesired to induce artificial loading to existing buildings. The empirical approach for the identification of dynamic properties strongly depends on complete seismic record databases. In France, the construction of such database is the main objective of the French accelerometric network (RAP) promoted since the end of 90's (Pequegnat et al., 2008).

OMA algorithms can be divided in two types, whether if they operate in the frequency domain (BFD, FDD, etc.) or in the time domain (RD, stochastic subspace, etc.). Such methods have been object of multiple comparisons (Brincker et al., 2001b; Peeters and De Roeck, 2001).

Reproducing the dynamic response of structures using numerical modeling is a widely adopted approach during conception to asses the limit state of the structure and design it to resist a given load. The operating service state condition of a structure is different than design conditions assumed in the conception phase (existing loads, real material properties, change of properties with ageing, construction defects, non-structural elements, safety factors, etc.). Instead, finite element model requires assumptions concerning boundary conditions, material rheology and structural element behavior.

Unknown parameters are deduced by trial and error procedure, so that numerical results fit empirical data (Friswell and Mottershead, 1995). Model assumption can be optimized thanks to the comparison of simulations and observations, so as to highlight the physical behavior of structures.

3.2 Case study of the Nice prefecture

3.2.1 Description of the structure

This research focuses on the 67.5 m height building of Nice prefecture, in France, having 22 storys (Figure 3.1a). It has been built in 1979, according to the French PS69 seismic code. The building has a non-regular reinforced concrete bearing wall structure according to the Eurocode 8 regularity criteria (European Committee for Standardisation, 2004b) regularity criteria. It is composed of two symmetric parts separated by a 10 centimeters joint designed to make independent the dynamic response of both sides during strong motions. Each part is made up of a reinforced concrete cage (containing lifts and stairs) that support RC slabs. These are loaded by a glass facade and inter-storey thin columns placed to limit inflection, that are not connected to foundation but laid on a box girder at the first floor above ground (Figure 3.1a,b). The building has deep foundations consisting of piles, not rigidly connected to the pile cap. The prefecture integrity during earthquakes is of vital importance for civil protection (importance class IV of Eurocode 8, European Committee for Standardisation, 2004b).

The building has been classified as having *low vulnerability* according to the French method of seismic vulnerability assessment VULNERALP (2007) (which considers six criteria: construction materials, irregularity in elevation, irregularity in plan, roof shape, year of construction and nature of the foundation). A previous study of the dynamic behavior of the building (GEMGEP, 2005) has determined that the shells of the ground floor may suffer important solicitations in the case of a strong motion.

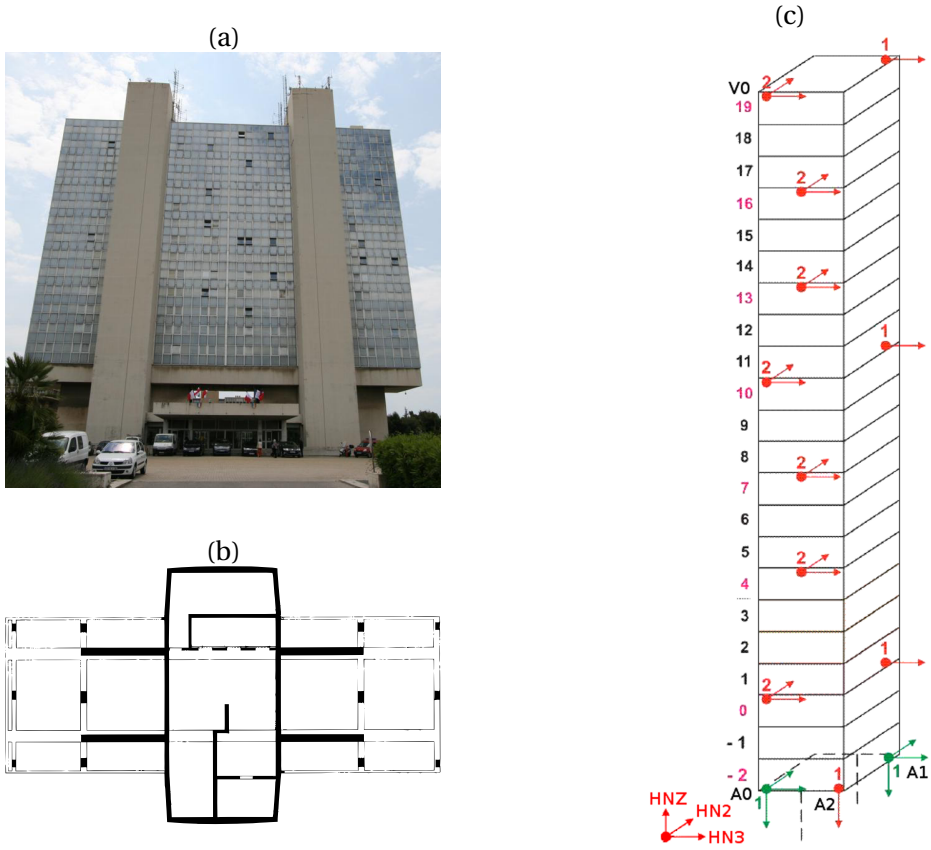

Figure 3.1 – (a) Front view of the Nice prefecture building (CETE, 2010). (b) Horizontal section of the RC tower to which RC shells are connected at each floor and of vertical columns (from structural plans). (c) Distribution of sensors along the instrumented tower. Red and green arrows represent monoaxial and triaxial accelerometers, respectively (CETE, 2010).

The foundation of the building is composed by 30 centimeter thick RC slab and a set of 141 piles having a diameter of 73 centimeters diameter and a length of 3 meters. Slab and piles are not fixed together.

3.2.2 Recording instrumentation

The building is included in a French national building array program for response analysis and vulnerability assessment and it is continuously monitored since June 2010 through 24 accelerometric sensors, operated by the RAP (Pequegnat et al., 2008). The location of different sensors all along the building is detailed in Figure 3.1c. Only one tower is instrumented due to their similarity. The recording station is a Kephren 24 channels 124 dB, which is disposed in the second underground level of the building. The network is composed of 18 monoaxial Episensor FBA ES-U2 accelerometers, placed at different levels, and 2 triaxial Episensor FBA EST accelerometers at the basement, The sensors are configured to a sensibility of ±1 g. Recordings are performed at a sampling frequency of 125 Hz and synchronized in time by the use of a GPS Garmin 16. The installation process and network characteristics are detailed in the technical report of the instrumentation(CETE, 2010; Brunel and Bertrand, 2010).

3.2.3 Geotechnical context

The Nice prefecture is located in the Var river delta (Figure 3.2), that is an alluvial area with soft soil, subject to ground motion amplifications produced by the sedimentary basin located underneath. Geotechnical surveys have been carried out to characterize the zone (Dubar, 2003). The soil column consists of a 40 to 60 m thick quaternary alluvial sediment over a pliocene conglomerate considered as bedrock. The average value of S-wave velocity in the upper 30 m of the soil profile is estimated as $v_{s,30}$ = 235 m/s, which corresponds to a soil type C, according to Eurocode 8 (European Committee for Standardisation, 2004b).

Geotechnical explorations show a high heterogeneity in the alluvial deposits under the building (located in the Var valley). This basin geological configuration produces local amplification effects on seismic waves exciting the structure. A succession of ambient vibration studies, carried out between 2000 and 2007, estimate the fundamental frequency of the soil profile as 2.7 Hz (CETE, 2007). In the same context, $1^s t$ and $2^n d$ natural frequencies (which correspondent mode shapes are translations in transverse and longitudinal direction) are estimated as 1.20 Hz and 1.22 Hz, respectively.

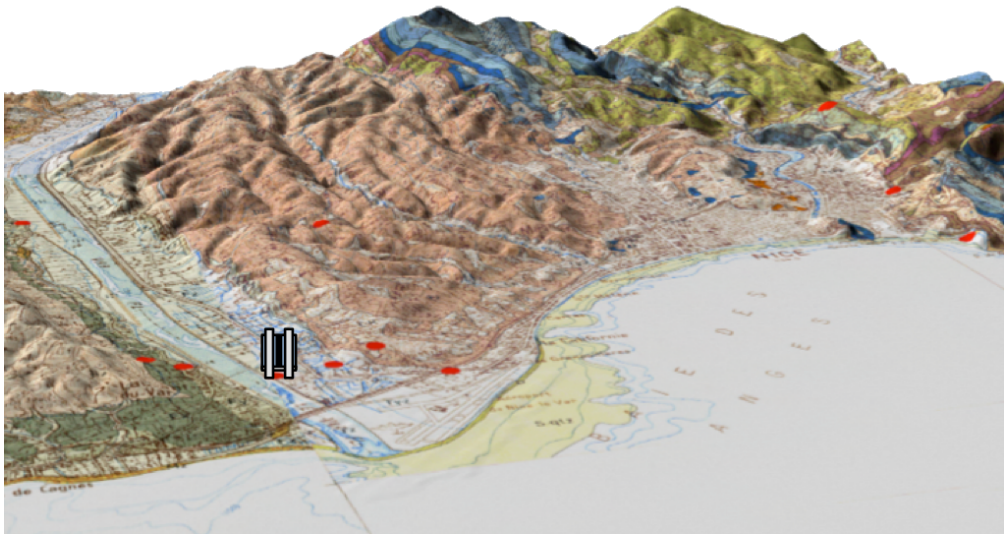

Figure 3.2 – Location of the building in the Var valley. Building is not to scale (adapted from Bertrand et al. 2014).

3.2.4 Regional and national seismicity

The building is located in a moderate hazard zone (reference peak ground acceleration on rock ground a_{gR} = 0.16 g) according to the 2010 French seismic zonation (Figure 3.3).

Southeastern France is situated at the junction between the Alps massif and the Ligurian basin, therefore is one of the most active seismic region in western Europe (Larroque et al., 2001) as can be seen in Figure 3.4. Nowadays, it is characterized by a moderate seismic activity, well recorded by the permanent broadband seismic networks used to build the French national seismicity catalogue (Cara et al., 2015). Between 1920 and 2015 around 80 events with a magnitude range from 4 to 6 (Larroque et al., 2001) occurred in the area. The spatial distribution is diffuse and most of the seismicity is concentrated below the Argentera massif and along the northern Ligurian margin. The reference event for seismic risk assessment is the Ligurian earthquake that occurred offshore in 1887 (Larroque et al., 2012) and had a magnitude estimated between 6.5 and 6.9. It caused many damages and fatalities from Imperia (Italy) to Nice. According to probabilistic seismic hazard assessment studies, the peak ground acceleration associated to a return period of 475 years in Nice is between 0.15 and 0.20 g (Dominique et al., 1998; Martin et al., 2002).

The city of Nice and its surroundings includes about 350.000 inhabitants and the whole French Rivera almost 1 million. Some areas of the city are well known to be prone to site effects that amplify seismic waves (Semblat et al., 2000). For all these reasons, seismic risk is a

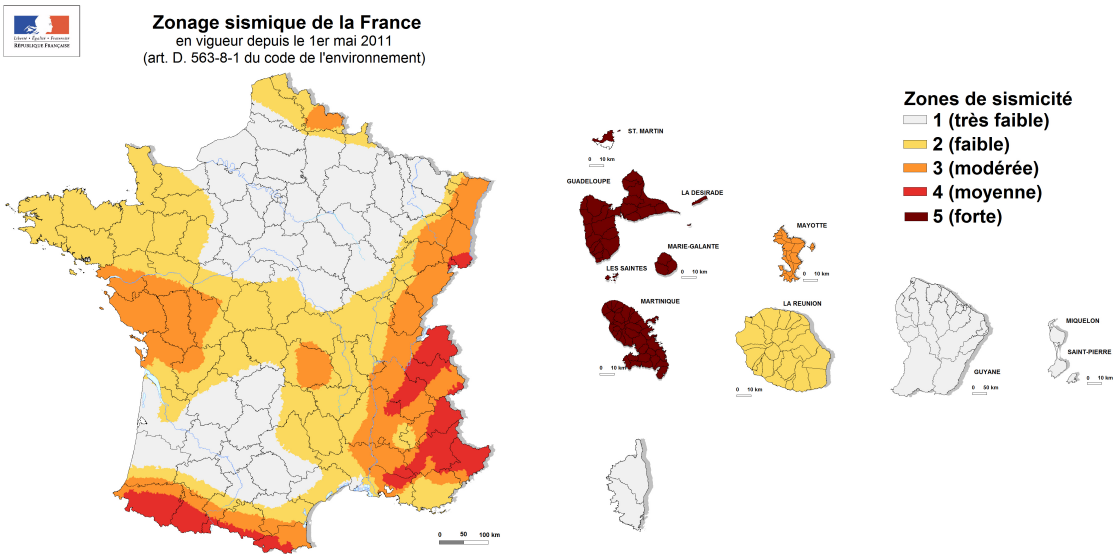

Figure 3.3 – 2010 French seismic zonation map (modified from LEGIFRANCE, 2010).

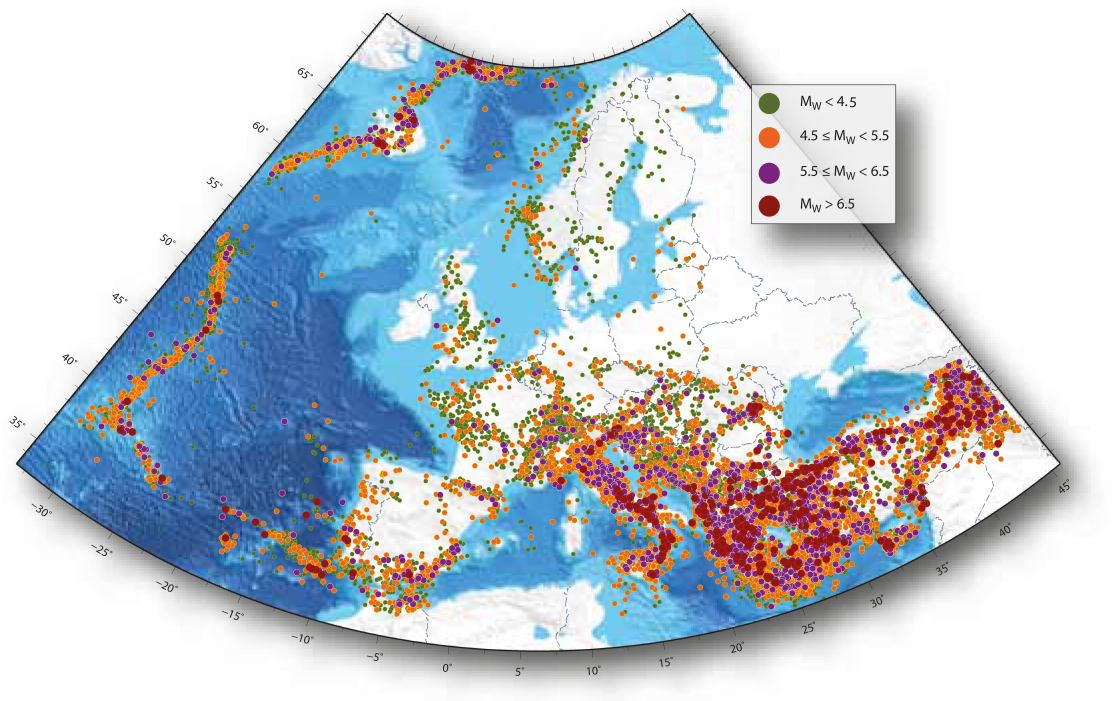

Figure 3.4 – Europe earthquakes in the SHARE European Earthquake Catalog (SHEEC) between years 1000 - 2007 with moment magnitudes $M_W \leq 3.5$ (from Cameelbeeck et al., 2013).

preoccupation in this region. Nice has been selected for a pilot program concerning a seismic hazard and vulnerability assessment operation (Mouroux and Brun, 2006). Meneroud et al. (2000) propose as reference earthquakes a magnitude 5.7 at 17 km from the northwest of Nice (beneath the village of Bouyon) and a magnitude 6.3 at 30 km from the south of the city (related to the seismic activity along the Ligurian margin).

3.3 Identification of dynamic properties from records

3.3.1 Comparison of accelerometric and velocimetric data

Sensors used to record building response to ambient vibrations should provide low noise and be sensible enough to record weak excitations in the frequency range of interest (from 0.4 to 25 Hz for conventional buildings, according to Michel, 2007).

Velocimeters are commonly used in traditional broad-band seismology, which are very sensible for a large frequency range and small amplitudes. Earthquake engineering however, is more interested in strong motions; accelerometers are then more appropriate as they are less sensible to wide band excitation and do not suffer from saturation. Both velocimeters and accelerometers have been widely used to record ambient vibrations in structures. Being the first more sensible, but the last more compact and portable.

A number of sensors are evaluated to register ambient noise (based on the signal characteristics and sensors specifications) in the context of the project SESAME (Atakan, 2002). A comparison of signals registered at the same location by two different sensors is proposed in this study to corroborate the validity of the present accelerometric network for noise recording (questioning the specifications given by the manufacturers).

The sensibility of $\pm$1g of the employed accelerometer (155dB), is selected to be able to record the signal considering the frequency content and amplitude of the signal expected at the building.

In January 2014, a triaxial velocimeter CGM40 (Figure 3.5, b) is disposed at the base of the structure, next to an existing tri-axial accelerometer Episensor FBA EST (Figure 3.5, a), to compare the records of the two types of instruments. It is decided to locate them at the base of the building to record the lowest amplitudes (avoiding signal amplifications at the building storeys) and hence show higher distortion of the records.

Cross correlation between time-histories of both instruments, disposed next to each other,

a) b)

Figure 3.5 – Episensor FBA EST tri-axial accelerometer (a) and CGM40 tri-axial velocimeter (b) used for the comparison.

is computed. Cross-correlation is used in signal processing to measure the similarity of two given waveforms. For given continuous functions f and g its cross-correlation, $f \star g$, can be defined as:

$$(f \star g)(\tau) = \int_{-\infty}^{+\infty} f^*(t)\, g(t+\tau)\, dt \tag{3.1}$$

where $*$ denotes the complex conjugate and τ is the time lag.

Time windows of 1000 s of ambient noise are considered. A passband filter is applied to the signals, varying the low-cut and high-cut frequencies from 0.1 Hz to 100 Hz with a frequency step of 0.01 Hz. Instrumental correction using poles and zeros is applied to obtain acceleration, velocity and displacement seismograms from both type of instruments. Signals are demeaned, linearly detrended, and filtered using a fourth order Butterworth filter.

Figure 3.6 shows the results of the analysis for an horizontal component of motion recorded by an accelerometer (channel HN2) and a velocimeter (channel HH2) at the basement of the building (location A1 in Figure 3.1). The time window is arbitrary chosen starting the 1^{st} February 2014 at 12:00 a.m. Values of cross correlation coefficient are higher than 97% (for acceleration and velocity) for the 0.4-25 Hz frequency range suitable for conventional buildings (red in Figure 3.6). Better results are found in the case of adapting the filter to the natural frequency content of the building. For example, a filter between 1-10 Hz provides the principal modes of the structure and increase the cross correlation coefficients values to more than 99% and 98% (respectively for acceleration and velocity, shown in green in Figure 3.6). Such results confirm that records from velocimeter and accelerometer are very well correlated (in the frequency band of interest) and confirms that we can use with confidence the accelerometers of the instrumentation to analyze ambient noise records.

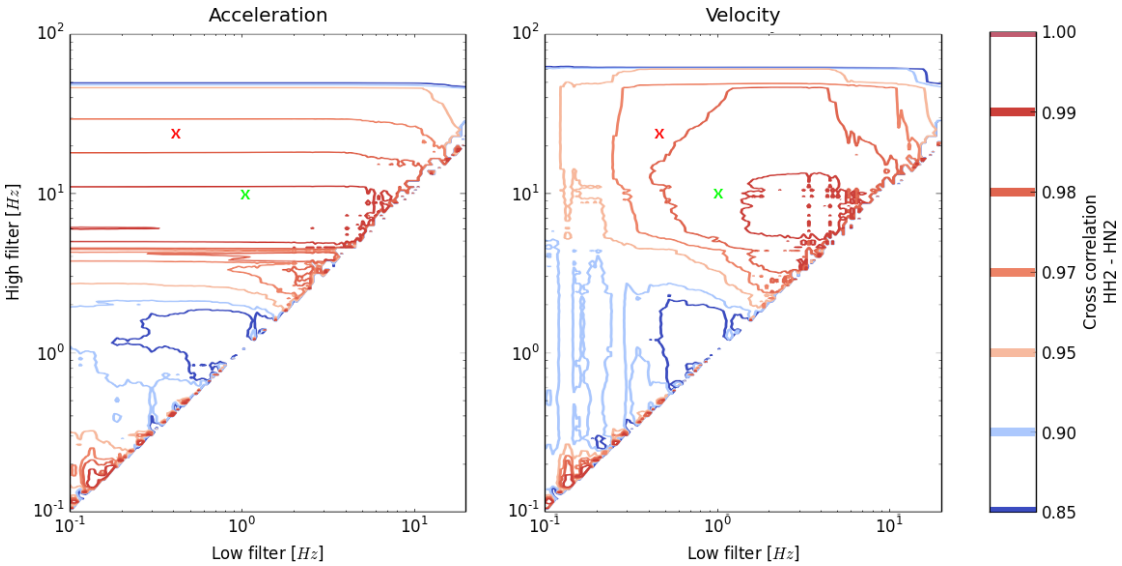

Figure 3.6 – Contour plots of cross correlation coefficient between accelerometer and velocimeter recordings for different passband cutting frequencies. Red and green crosses highlight values for 0.4-25 Hz and 1-10 Hz passband filters respectively

3.3.2 Basic frequency domain

The basic frequency domain (BFD) technique (also called Peak Picking method) is a simple way to estimate modal parameters from output-only data (Maia and Silva, 1997). The method is presented by Bendat and Piersol (1993). It is based on the transformation of the time-recorded signal to the frequency domain by using a Fourier transform.

The following conditions have to be met to obtain reliable estimates of modal frequencies using this technique (Felber, 1993):

- The structure should behave as a linear system
- Structural modes of interest should be significantly excited
- Modes of interest should be well separated and lightly damped (less than 5% of critical damping)
- Classically damped structure (therefore only having real modes)

The method can lead to erroneous results if assumptions of low damping or well separated modes are not fulfilled (Rainieri et al., 2007).

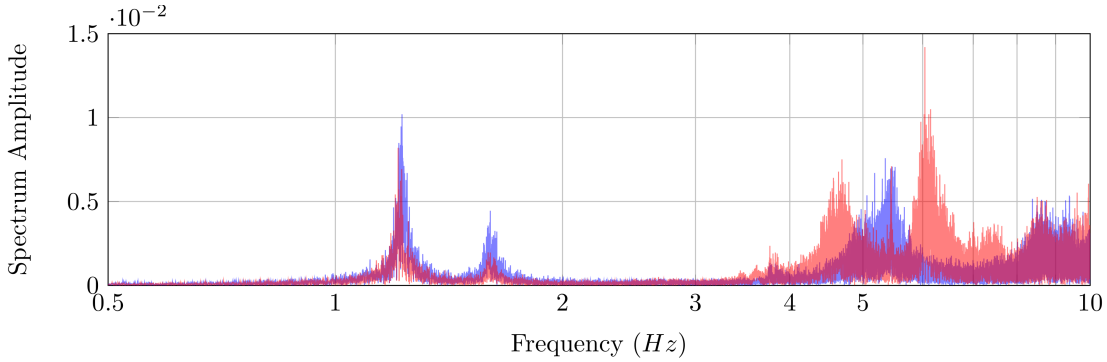

Figure 3.7 – Amplitude of the frequency spectrum for the HN2 (blue) and HN3 (red) components of acceleration recorded at the top of the building (V0)

Figure 3.7 shows the Fourier transform, of the longitudinal (HN2) and transversal (HN3) components of acceleration, recorded under ambient vibration, at the top of the building (V0 in Figure 3.1), for a given time window. Resonant frequencies are observed for both motion directions around 1.2Hz and 1.6Hz and represented in Figure 3.7. The proximity of the values for the two components suggests either the existence of two different modes, or a single one that affects both directions.

3.3.3 Frequency domain decomposition

The method of frequency domain decomposition (FDD), also known as complex mode indicator function (CMIF) (Peeters and De Roeck, 2001), is a non-parametric frequency domain technique for modal identification of dynamic features from structural deformation (classified as output-only systems as the input is considered unknown).

It is based on the decomposition of the power spectral density (PSD) matrix of the recorded signals into a set of single degree of freedom systems. The separation is done trough the singular value decomposition (SVD) method (Prevosto, 1982). Mainly, the process decomposes the spectral densities in the contribution of the different modes to the system response at selected frequency values.

Shih et al. (1988) apply this decomposition to the spatial domain parameter estimation. They identify physical modes of complex systems, calling the process CMIF. It is shown in their study that the method is able to identify modal parameters, such as mode shapes, damped natural frequencies and modal participation vectors. The application to the civil engineering field is first proposed by Brincker et al. (2001a). The technique is named FDD and is implemented in commercial software, for a wider practical application.

The method is based on the assumption of a broad-band excitation (ideally white noise), low damping and geometrically orthogonal modes. It is a multi-input/multi-output (MIMO) technique, and the relationship between the unknown input $x(t)$ and the measured response $y(t)$ is based on the PSD relationship for stochastic processes (Bendat and Piersol, 1986)

$$G_{yy}(j\omega) = H^*(j\omega)G_{xx}(j\omega)H(j\omega)^T \tag{3.2}$$

where $G_{xx}(j\omega)$ is the input PSD matrix, $G_{yy}(j\omega)$ is the output PSD matrix and $H(j\omega)$ is the frequency response function (FRF) matrix. The FRF can be expressed in partial fractions form

$$H(j\omega) = \sum_{k=1}^{n} \frac{R_k}{jw - \lambda_k} + \frac{R_k^*}{j\omega - \lambda_k^*} \tag{3.3}$$

where n is the number of nodes, λ_k are the poles and R_k is the residue

$$R_k = \phi_k \Gamma_k^T \tag{3.4}$$

where ϕ_k is the mode shape vector and Γ_k is the modal participation vector. Under the assumption of having a white noise process, the input PSD $G_{xx}(j\omega)$ is constant. Hence, the modal decomposition can be derived as

$$G_{yy}(j\omega) = \sum_{k=1}^{n} \left(\frac{A_k}{j\omega - \lambda_k} + \frac{A_k^H}{-j\omega - \lambda_k^*} + \frac{A_k^*}{j\omega - \lambda_k^*} + \frac{A_k^T}{-j\omega - \lambda_k} \right) \tag{3.5}$$

where A_k is the k^{th} residue matrix of G_{yy}, that is a Hermitian matrix

$$A_k = R_k C \left(\sum_{s=1}^{n} \frac{R_s^{T*}}{-\lambda_k - \lambda_s^*} + \frac{R_s^{T*}}{-\lambda_k - \lambda_s^*} \right) \tag{3.6}$$

The implementation of a FDD algorithm starts with the estimation at discrete frequencies ω_l of the output PSD matrix. This is done by calculating the cross power spectral density (CPSD) function (Welch, 1967) between the different input signals. Then the SVD of G_{yy} is calculted

according to

$$G_{yy}(j\omega_l) = U_l S_l U_l^H \tag{3.7}$$

where U_l is an unitary matrix containing the singular vectors u_{lm} and S_l is a diagonal matrix holding the singular values s_{lm}. In the case of a k^{th} mode dominating at a given frequency ω_k, the PSD matrix can be approximated as being formed by a single term (Bendat and Piersol, 1986), as follows:

$$\underset{\omega_l \to \omega_k}{G_{yy}(j\omega_l)} = s_l u_{l1} u_{l1}^H \tag{3.8}$$

Hence, the first singular vector u_{k1} at the k^{th} resonance is an estimation of the mode shape $\widehat{\phi}_k = u_{k1}$. Then the modal frequencies can be identified as the peaks in the singular value function. The estimation of mode shape $\widehat{\phi}_k$ is compared with the singular vectors at frequencies surrounding the peak. The similarity between the two deformations determines if the singular value belongs or not to the mode, by comparing the modal shapes. This can be made trough the modal assurance criteria (MAC) (Allemang and Brown, 1982)

$$MAC\left(\phi_1, \phi_2\right) = \frac{\left|\phi_1^H \phi_2\right|^2}{[\phi_1^H \phi_1][\phi_2^H \phi_2]} \tag{3.9}$$

All available components (a total of 23 channels) are provided as input to the FDD to extract the singular values (SV). First, second and third SV for the selected time window are shown in Figure 3.8, which show the participation of the predominant modes for a given frequency.

Principal frequency values are identified at the maximum amplitude of the SV of PSD crests. Average values and confidence interval provided by the ten studied time windows are indicated in Table 3.1. Modal shapes extracted using FDD can be seen in Figure 3.9.

The case of two close modes is observed around 1.2 Hz. The existence of a torsional mode is seen around 1.5 Hz, which influences both longitudinal and transverse motion (channels HN2 and HN3) as seen in Figure 3.7. This technique provides a clearer modal identification and interpretation compared with BFD. Two subsequent modes can be detected around 3.7 Hz and 3.8 Hz.

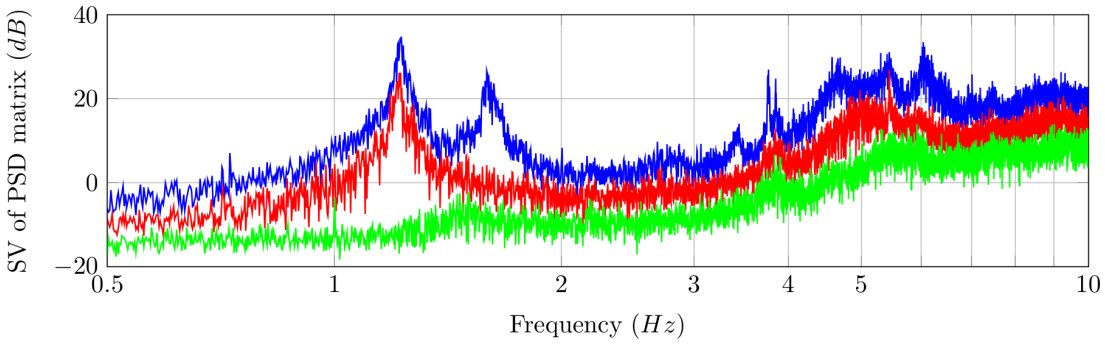

Figure 3.8 – 1^{st} (blue), 2^{nd} (red) and 3^{rd} (green) Singular Values of the of the PSD matrix from FDD technique

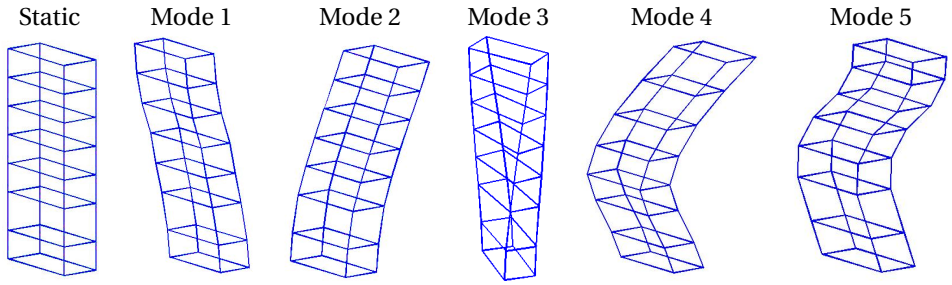

Figure 3.9 – Mode shapes of the instrumented tower, for the first five natural modes, using FDD.

3.3.4 Random decrement

Random decrement (RD) is a time domain technique originally proposed by Cole (1973) where structural responses are transformed into a RD function, sometimes called *randomdec* signature. It is based on the concept that the response of a system to random input loads is composed by the response to an initial displacement, an initial velocity and the random loads. Hence, by averaging time segments with identical initial conditions, the random component tends to disappear while the response of the structure is revealed. This provides an estimate of its free-vibration decay, $y(\tau)$, which can be obtained as:

$$y(\tau) = \sum_{l=1}^{N} s(t_l + \tau) \tag{3.10}$$

where N is the number of windows with fixed initial conditions, s is the ambient vibration window of duration τ, and t_l is the time verifying the initial conditions. Details on the theory can be found in Vandiver et al. (1982). The RD technique can be faster than a FFT algorithm (Rodrigues and Brincker, 2005), which makes it suitable for continuous monitoring of frequencies.

Null displacement and positive velocity triggering conditions are used as proposed by Cole (1973). A minimum of windows N =500 is necessary for the stabilization of damping values associated with a mode as suggested by Jeary (1986) and Dunand (2005). A segment length window of a duration τ =15s is used, considering that it is at least 10 times the fundamental period of the building (Roux et al., 2014), to assure a complete decrement of the signal for modal damping estimation. Signals are pre-processed using a Butterworth passband filter, centred in the principal frequencies f_n (previously identified), between $0.9 f_n$Hz and $1.1 f_n$Hz (Mikael et al., 2013). Damping is obtained by fitting a logarithmic decrement function $e^{-\xi\omega t}$, where ξ is the modal damping and ω is the angular frequency (related to the signal frequency by $\omega = 2\pi f$). The calculation of a RD signature of the fundamental mode of the building, to obtain frequency and damping, is illustrated in Figure 3.10.

3.3.5 Natural frequencies and mode shapes of the building

Natural frequencies of the structure are extracted from 10 arbitrary 1000-second windows of ambient vibration records, that are contiguous to minimize the temporal variability of natural frequencies (Mikael et al., 2013). Mean values of the first five natural frequencies of the building, estimated using BFD, FDD and RD, are shown in Table 3.1, using one standard

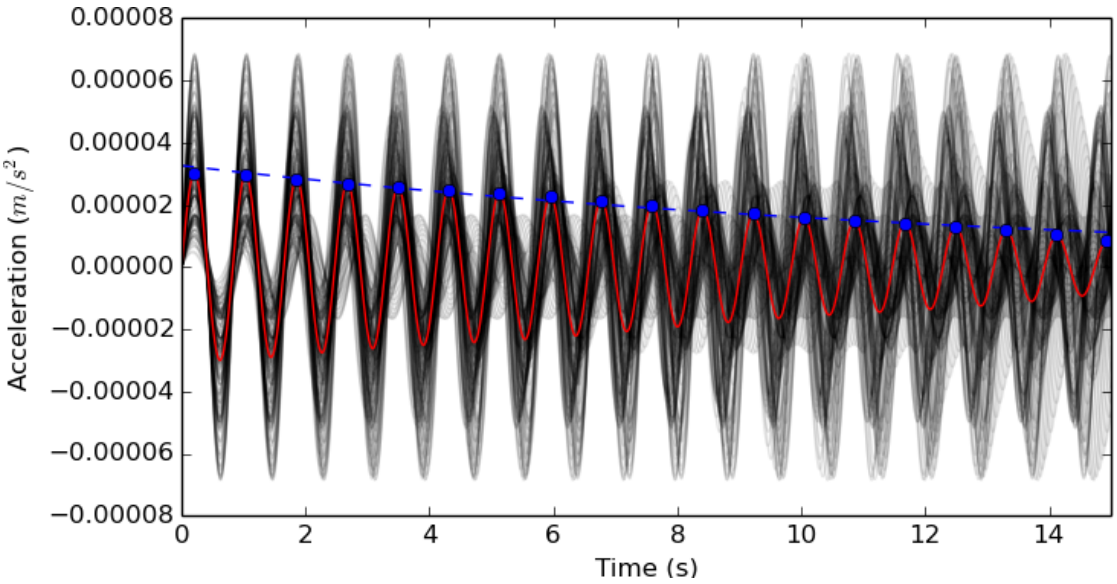

Figure 3.10 – Records of the Nice prefecture (filtered around the fundamental mode) that satisfy the null displacement and positive velocity initial conditions (black) are averaged to obtain the random decrement signature (red). Damping is obtained by fitting a logarithmic function to the envelop of the signature (blue).

deviation as confidence interval. The corresponding mode shapes of the instrumented tower (calculated by FDD) are shown in Figure 3.9. Values of modal damping, ξ, obtained using RD over building recordings of noise excitation are shown in Table 3.2.

Table 3.1 – Natural frequencies of the building identified using BFD, FDD and RD.

Mode	Frequency [Hz]		
	BFD	FDD	RD
1	1.216 ± 0.009	1.218 ± 0.007	1.209 ± 0.002
2	1.228 ± 0.006	1.224 ± 0.006	1.219 ± 0.002
3	1.602 ± 0.011	1.604 ± 0.011	1.600 ± 0.003
4	3.762 ± 0.006	3.758 ± 0.005	3.759 ± 0.002
5	3.850 ± 0.004	3.853 ± 0.005	3.851 ± 0.002

Natural frequencies are clearly identified by the three methodologies and the differences are below 1%. The frequencies given by the RD are the least dispersed. The first, second, fourth and fifth peaks correspond to translational motion in perpendicular directions (HN2 and HN3 in Figure 3.1c), the third mode is a torsional motion. Five different frequency bands are proposed in Table 3.3 to study the broadband response and isolate some vibration modes. The different bands are illustrated over the SV of the PSD matrix from FDD technique in Figure 3.11. The first and second modes are in frequency band B2, nevertheless each mode can be isolated

Table 3.2 – Modal damping under noise excitation using RD.

Mode	Damping [%]
1	0.512 ± 0.093
2	0.424 ± 0.061
3	0.458 ± 0.078
4	0.098 ± 0.051
5	0.287 ± 0.013

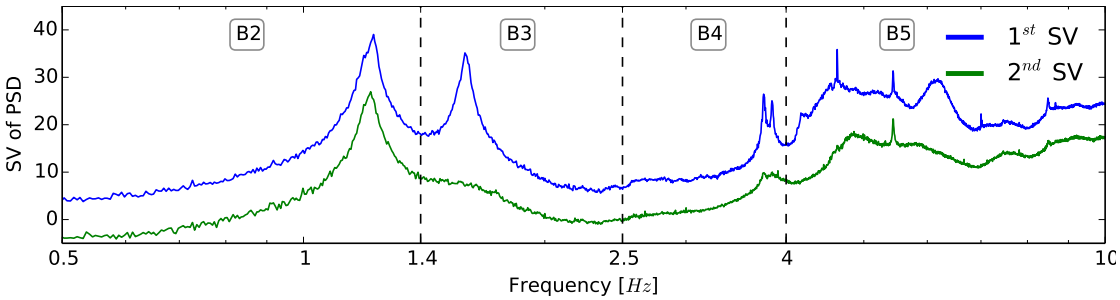

Figure 3.11 – 1^{st} and 2^{nd} Singular Values (SV) of the Power Spectral Density (PSD) matrix using FDD. Proposed frequency bands (B2, B3, B4, B5) to individually study isolated natural frequencies.

because accelerometers are placed in the two orthogonal directions of the building and each one allows capturing only mode shapes whose deformation occurs along its recording axis.

Table 3.3 – Frequency bands that allows to individually observe the frequency content of each mode in the case study.

Band	Frequency limits [Hz]
B1	0.5 - 10.0
B2	0.5 - 1.4
B3	1.4 - 2.5
B4	2.5 - 4.0
B5	4.0 - 10.0

3.4 Finite element model of the building

A finite element model of the structure is adopted in this research. In a first step, independent dynamic behavior of both towers is assumed (FEM1), due to the indication of a seismic joint in structural drawings. Accordingly, only the instrumented tower is modeled.

3.4.1 Creation of a model of an existing structure

The first attempt to model the in-situ response of a building consists on following the structural details provided in the conception project. The assumptions taken during the design phase (such as design loads, material properties, etc.) aim to provide a safe building under a design load, and may not correspond to the actual situation at the building.

Structural damping is affected not only by the material properties, but all dissipation mechanisms present on the structure. Typical values of modal damping ratio could be chosen for reinforced concrete structures in the elastic range where no damage, or minor cracking only, is observed (Hsu and Mo, 2010). However, choosing a deterministic value may be a strong assumption and result on introducing considerable differences with reality.

A number of parameters can be modified in order to fit the in-situ condition of the structure. For example, both the modulus of elasticity of the material can be decreased or the non-structural load can be increased to obtain a reduction in the fundamental frequency. It is a decision of the engineer to consider the choice that agrees with the real condition of the structure.

It should be remarked that non-structural elements play as well a very important role on the dynamic behavior of the structure, and their modelization requires careful detailing.

For our case study (a building without existing structural damage) the following procedure is used to optimize the FEM and fit simulations to in-situ recordings:

1. It has been chosen not to make assumptions about the degradation (mainly due to ageing or non-conformance of fabric materials) of the reinforced concrete.

2. The optimization of the fundamental frequency is done by considering an uniform distributed load (UDL) acting on each floor of the building (to fit the one measured from in-situ records).

3. Detailed modeling of not structural elements (considering different hypothesis) is used to match the ratio between different modal frequencies.

4. Modal damping is adopted as obtained from records. It is taken as in Table 3.2 for ambient vibrations and measured again for earthquake excitation.

3.4.2 Structural modeling from construction plans

The building mesh is created according to construction design plans. Timoshenko beam elements are used to model the columns. Four-node doubly curved general-purpose shell elements with reduced integration are used for the RC tower and horizontal shells at each floor. Mesh refinement is optimized to provide accurate results (a node spacing no longer than 1 meter is assumed).

Inclusion of details such as interior walls, floors, and holes in shear resisting walls significantly influences the rigidity of the structure. Such detailing directly affect the natural frequencies of the model and, consequently, requires careful attention.

A linear elastic behavior is adopted considering that low strains are attained under the applied seismic loading. In fact, the recorded peak ground acceleration, since the building is instrumented, is 0.036 m/s^2 (during the 2014 M_w 4.9 Barcelonnette earthquake, discussed in Section 4.2). The material mechanical properties are assumed equal to those specified in the structural design report. Density and Poisson's ratio are taken as typical properties for reinforced concrete (Meschke et al., 2006). The elastic modulus of concrete $E = 5700\sqrt{R_{ck}}$ is estimated as function of the uniaxial compressive strength of concrete cubes R_{ck}, using an empirical equation proposed by the Eurocode 2 (European Committee for Standardisation, 2004a), where both E and R_{ck} are expressed in MPa. Adopted values can be found in Table 3.4.

Table 3.4 – Adopted values of density (ρ), Young modulus (E), Poisson's ratio (ν) for the reinforced concrete material.

ρ [kg/m^3]	E [GPa]	ν
2500	30	0.2

3.4.3 Model optimization using operational modal analysis

The unknown non-structural mass in the building significantly influences natural frequencies of the structure. As observed by Liu et al. (2005), when studying the dynamic properties of a 14-story building, changing the location and quantity of non-structural mass is the most effective way to improve the accuracy of a FE model for structural dynamic analyses. An uniformly distributed load (UDL) is imposed on the floor at each level. Through model updating (Venture et al., 2001), the value of the UDL is adjusted by trial and error, starting from the value imposed by the Eurocode for structural design, to match the fundamental frequency of the building obtained from ambient vibration records. The adopted value of non-structural load for the

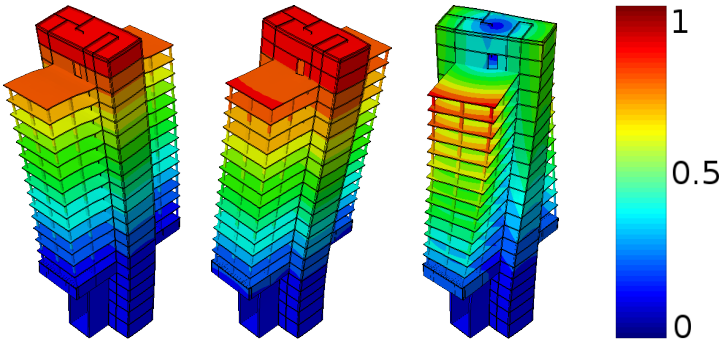

Figure 3.12 – First three mode shapes obtained by the finite element model considering independent dynamic behavior of the two towers (FEM1). Colormap show the normalized displacement of nodes.

case of half building model, named FEM1, is $q = 250$ kg/m^2.

Dynamic properties are reproduced using the finite element model and a modal decomposition. The comparison of natural frequencies, for the first three modes, obtained by OMA and FEM, is shown in Table 3.5. The third natural frequency is not well reproduced by the FEM1 model; it exhibits an error of 46.9%. The building has a complex resistant structure, where direct load paths are not clearly identified. The numerical mode shapes are represented in Figure 3.12a. The third mode, that is not well reproduced by FEM1, corresponds to a torsional deformation.

Table 3.5 – First three natural frequencies f obtained by records (REC) and by the finite element model for both independent behavior between towers (FEM1). Relative error ϵ between FEM and REC.

Mode	REC	FEM1	
	$f[Hz]$	$f[Hz]$	ϵ[%]
1	1.21	1.22	0.8
2	1.22	1.24	1.6
3	1.60	2.35	46.9

3.4.4 Effects of seismic joint on dynamic properties

The possibility of the seismic joint not correctly isolating both towers is considered, trying to numerically reproduce the 3^{rd} natural frequency associated to a torsional motion.An updated model (FEM2) with a rigid connection between the two symmetrical parts of the building (ignoring the seismic joint) is used. Non-structural load is updated to $q = 300$ kg/m^2 for

the new model in order to match the natural frequencies identified from ambient vibration records.

The comparison of natural frequencies for the first three modes obtained by OMA and FEM, in the case of whole building model (FEM2), is shown in Table 3.6. Natural frequencies obtained considering a rigid connection between towers (FEM2) are much closer than assuming independent dynamic behavior (FEM1) to those obtained applying OMA. The error, on the third natural frequency, is reduced from almost 50% in FEM1 (Table 3.5) to less than 1% in FEM2 (Table 3.6), when compared to the values obtained using OMA.

The 10 cm seismic joint provides a constraint between both towers (at least in the case of small excitation). Such constraint has a limited influence on translational modes, but it has a significant influence on the torsional mode. The first three mode shapes of the building model, considering a rigid connection between towers (FEM2), are shown in Figure 3.13.

The observed constraint is then provided, either because the joint was not properly executed, which will reduce the seismic resistance of the building or because the filling material provides constraint only under small excitation. Both towers should behave as isolated during a major event, but some natural frequencies may suffer modifications. Anyway, the seismic joint is not isolating both towers as expected and consequently the whole building model (FEM2) is considered in the following analysis.

Table 3.6 – First three natural frequencies f obtained by records (REC) and by the finite element model considering a rigid connection between towers (FEM2). Relative error ϵ between FEM2 and REC.

Mode	REC	FEM2	
	$f[Hz]$	$f[Hz]$	$\epsilon[\%]$
1	1.21	1.20	0.8
2	1.22	1.24	1.6
3	1.60	1.59	0.6

3.5 Variation of dynamic parameters with environmental conditions

Natural frequencies presented in Section 3.4.2 are issued from the numerical model of the structure and from records of building deformation. Such values represent an actual state of the building during its service life and surely not its design condition. However, the structure changes during its lifetime due to degradation, and hence also its dynamic response (mostly

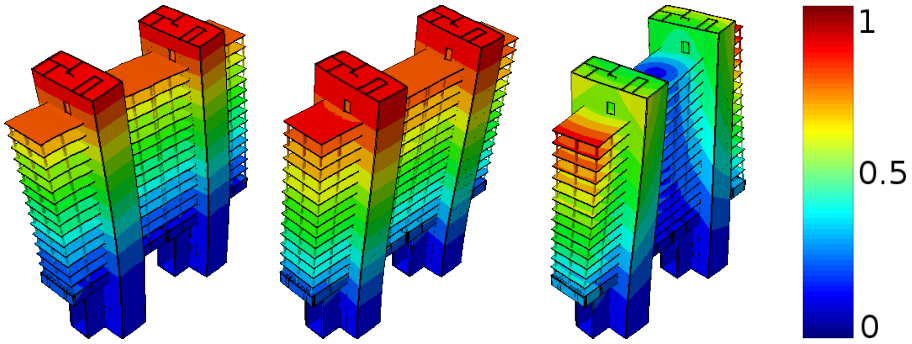

Figure 3.13 – First three mode shapes obtained by the finite element model considering a rigid connection between towers (FEM2). Colormap shows the normalized displacement of nodes.

controlled by frequency and damping values).

It should be distinguished between permanent and transitory variations. On one hand, the causes of permanent variations are associated with changes on the structure condition: material aging (i.e. reduction of the elasticity modulus of concrete with time), load variation (i.e. addition of mass to the building, such as books to a library), structural damage (i.e. strong ground motion). On the other hand, transitory variations are often caused by mass change and stiffness fluctuation (or modification of boundary conditions) due to external factors as environmental conditions: temperature, wind, humidity, amplitude of vibrations (before reaching material nonlinearity). The identification of effects caused by environmental factors is important for structural health monitoring in order to ignore transitory variations and identify those caused by natural aging or damage. The difficulty of filtering out the transitory variations (data cleansing and normalization, according to Farrar et al. 2005) is a common problem for damage identification and prognosis in civil engineering structures.

Such variation of dynamic properties with external factors, on civil engineering structures, has become a recent topic of research (Xia et al., 2012; Guéguen et al., 2014; Guillier et al., 2016). The RD technique has proved to be an effective solution to track frequency and damping variation for long term monitoring. Mikael et al. (2013) states that a proper application of RD approach provides sufficient accuracy to monitor very small variations ($\simeq$ 0.1 %).

Stiffness fluctuations are mostly controlled by the outside temperature. Clinton et al. (2006) and Herak and Herak (2010) show that modal frequencies suffer a positive correlation with temperature variation. However, Mikael et al. (2013) show a few years later that frequency and temperature trends are dependent on the type of building (some buildings show positive correlation, others negative). Variations due to changes on boundary conditions or input ground motions are also observed on buildings.

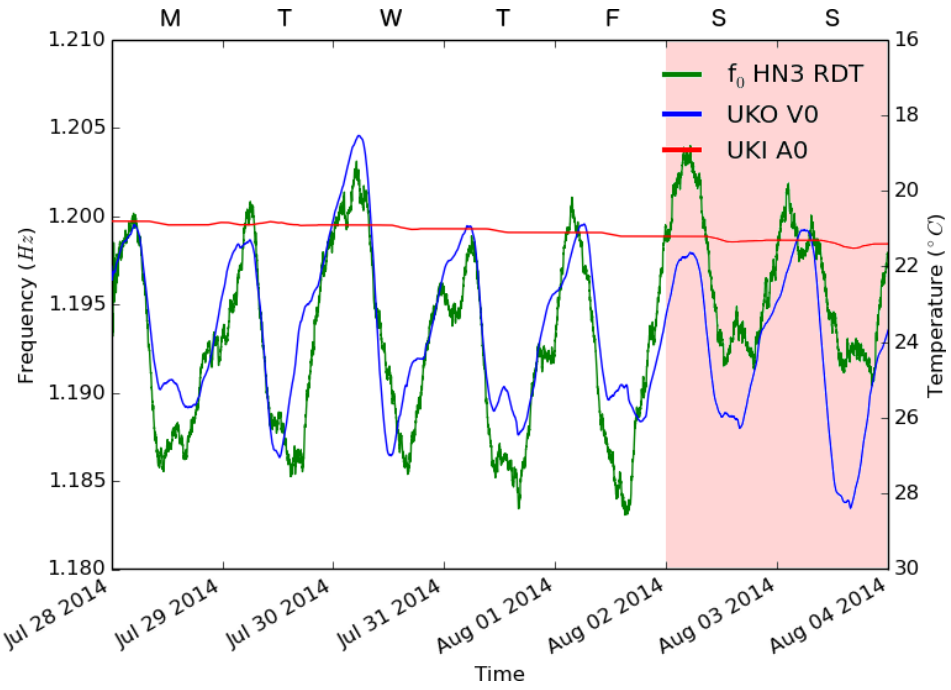

Figure 3.14 – Variation of fundamental frequency (f_0 HN3 RD) and temperature during one week at the outside (UKO V0) and the inside (UKI A0) of the building. Temperature axis is inverted to highlight the negative correlation of fundamental frequency and outer temperature. Days of the week are specified and the weekend is highlighted with a light red.

In order to study frequency variations with temperature in the Nice prefecture building, a meteorological station (including temperature and wind sensors) has been disposed in the building on April 2014. The evolution of the fundamental frequency during one week is shown on Figure 3.14. A clear negative correlation with temperature is observed in this building (note the inverted temperature axis), which explains a great part of the frequency variability. It can also be observed the lower decrease of the fundamental frequency during the weekends, associated with a lower daily mass increase compared with the work days when workers enter the building.

The same analysis during longer periods shows a similar pattern. Fundamental frequency variations are mainly controlled by temperature variations. Across a year (Figure 3.15), variations of about 4% have been observed in the studied building (between winter and summer). The yearly variations are a bit less well correlated than when comparing a week of recordings. This may be caused due to seasonal changes, other than temperature, that also affect the fundamental frequency (such as saturation of the soil, boundary conditions, etc.)

The FFT transforms of one year of data recorded in the Nice prefecture building are shown in

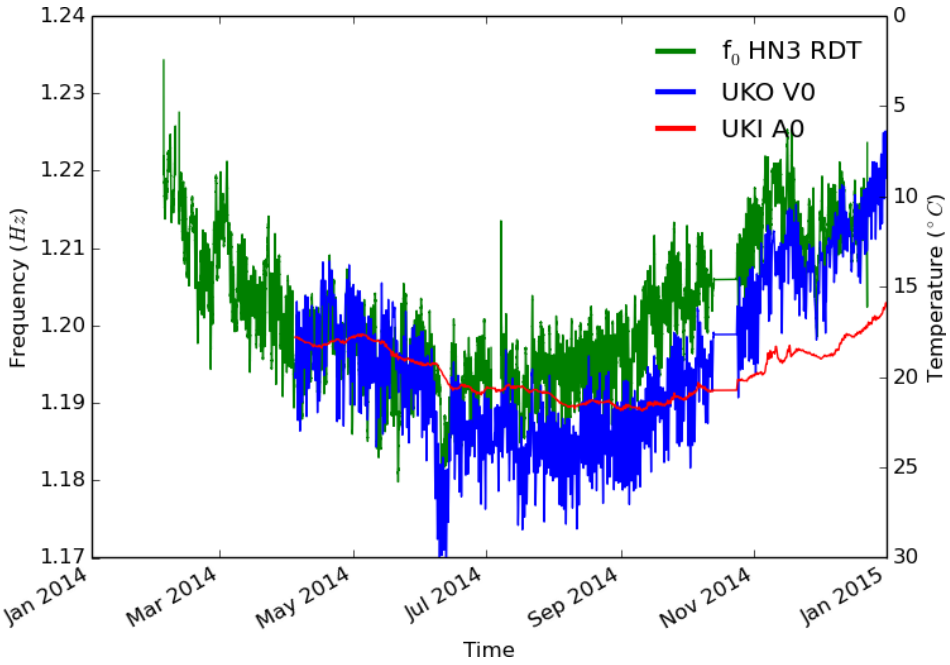

Figure 3.15 – Variation of fundamental frequency (f_0 HN3 RD) and temperature during one year at the outside (UKO V0) and the inside (UKI A0) of the building. Temperature axis is inverted to highlight the negative correlation of fundamental frequency and outer temperature.

Figure 3.16. A clear peak is observed at a period of 1 day in both frequency and temperature, which corroborates the marked daily variation.

The fundamental frequency with temperature since 2012 is shown in Figure 3.17 (the instrumentation is in place since 2010, but earlier data are not available). The meteorological station has been placed in the building in 2014. Temperature data for previous years are provided by the LFMN meteorological station (located at the Nice airport, at a distance of less than 1km to the building). Daily average values of METAR temperature data (format for reporting weather information in aviation) are obtained from the Weather Underground website (WU, 2016). The smoothed plot of the fundamental frequency in Figure 3.17 clearly shows the seasonal variations during these years. The existence of daily oscilations can be observed in terms of standard deviation. Again, a huge negative correlation between the variation of the fundamental frequency and temperature is observed. A very slight decreasing tendency trough the years can be observed in the value of fundamental frequency (not present in the temperature), which may correspond to the building aging. The FFT transforms of the four years of data are shown in Figure 3.18. An amplitude peak is observed for a period of 365 days, due to changes in temperature caused by the Earth revolution trough its orbit. Another peak is observed for a period of 1 day, due to the changes in temperature caused by the Earth rotation.

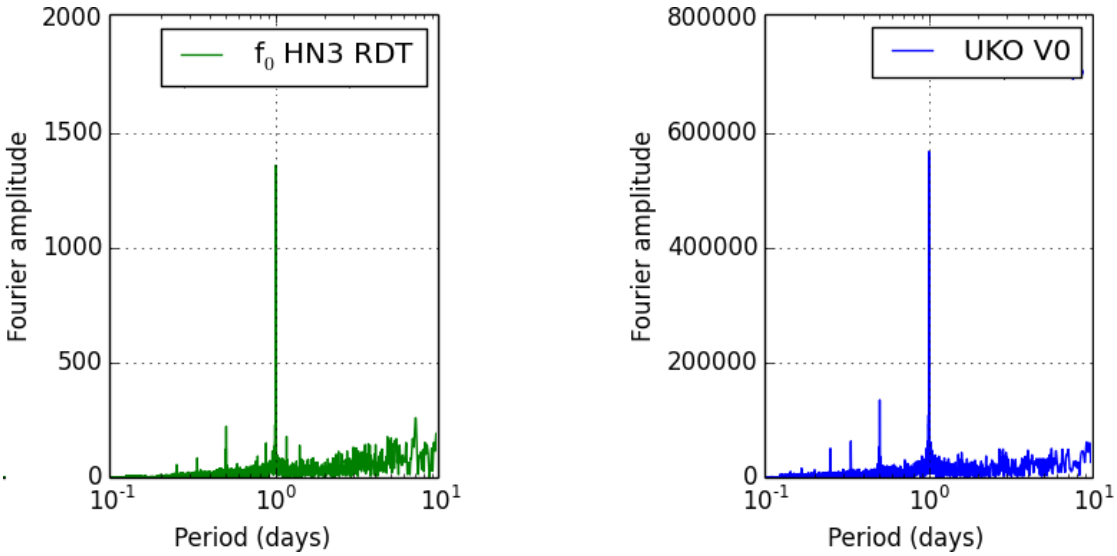

Figure 3.16 – Fourier transform of one year of measures of the fundamental frequency, f_0, using RD (left) and ambient temperature at the top of the building (right). Remark that the abscissa axis is shown in terms of period (inverse of frequency).

The yearly variation represents a peak with a much greater amplitude than the daily variation.

3.6 Conclusions

The Nice prefecture building is a RC building conceived using French design methods dating back to the 60s, that do not correspond to the anti-seismic conception criteria of actual seismic codes. The regularity in plan and in elevation according to the EC8 is not verified. Floor shells are fixed in the RC towers and inter-storey inflection is limited by columns having reduced cross-section that do not lie on the foundation. Records obtained using accelerometers show a very strong correlation with those provided by a velocimeter in the frequency range of interest for the building (a cross correlation coefficient of 99% is obtained in acceleration). Ambient vibration records have been employed to deduce dynamic properties (modal frequencies, deformed shapes and damping) of the building. Parameters extracted from three different techniques (BFD, FDD and RD) show good agreement between each other.

Comparison of results obtained from the ambient noise measurements and numerical models put in evidence the influence of a seismic joint on the dynamic properties of the building. An error of almost 50% is identified on the first torsional frequency of the building by modeling the towers as dynamically isolated. Such error is reduced to less than 1% when considering that the seismic filling material provides a rigid connection between both parts of the building

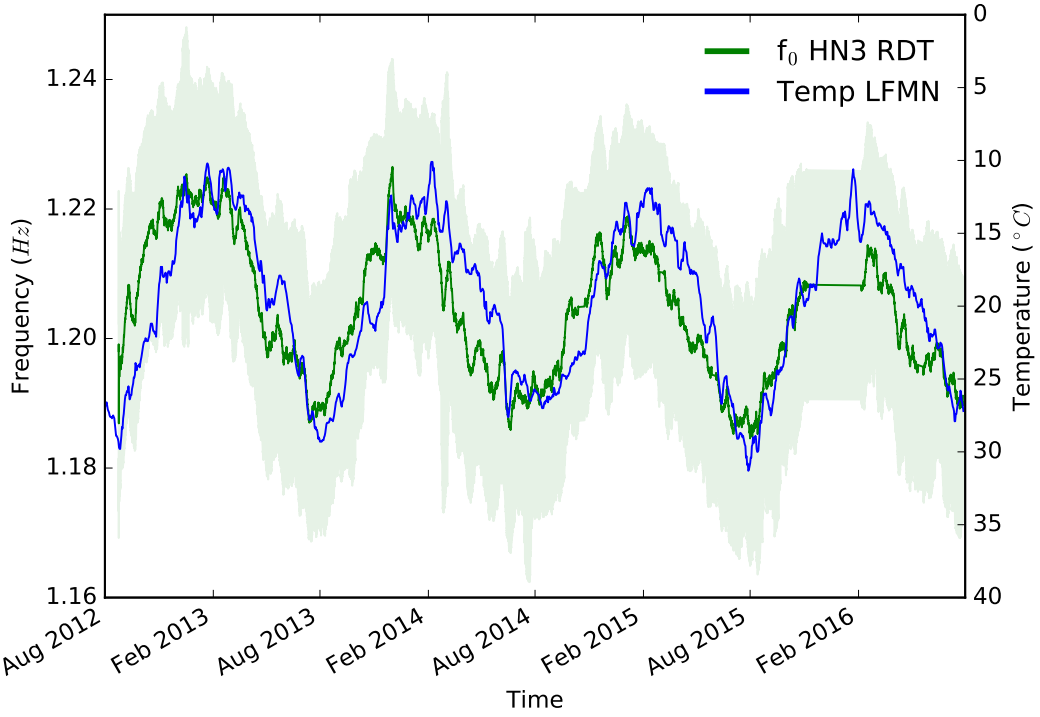

Figure 3.17 – Smoothed variation of fundamental frequency (f_0 HN3 RD) and temperature at the LFMN meteorological station (less than 1km to the building) since 2012. One standard deviation of measures is represented with a lighter color.

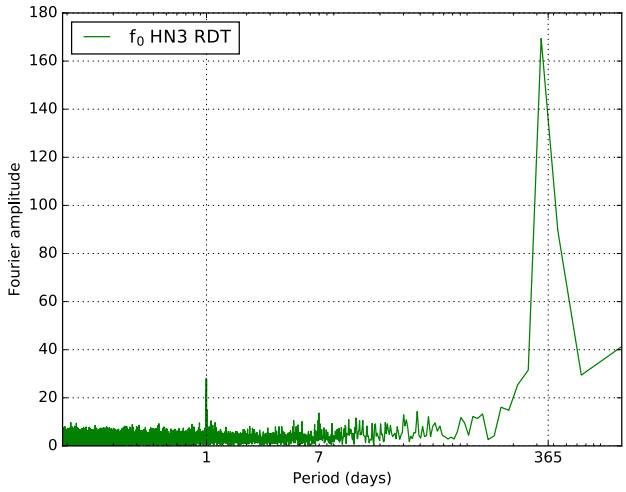

Figure 3.18 – Fourier transform of four years of measures of the fundamental frequency, f_0, using RD. Remark that the abscissa axis is shown in terms of period (inverse of frequency).

structure. The combined use of numerical modeling and empirical methods enabled to identify that the seismic joint, present in the structural plans of the building, is not working as expected.

The finite element model is able to accurately reproduce the observed frequencies and mode shapes of the building. Existence of records enable to optimize the numerical model to match the service condition of the structure (different from the design condition). Such possibility enables to have a suitable model that is able to reproduce reproduce the seismic response of the building to past and reference ground motions.

The estimation of dynamic feature variability in a long time period shows that the fundamental frequency of the building is highly negatively correlated with variations of external temperature. Fundamental frequency shows variations of up to 4% between the winter and summer of the same year. Monitoring shows strong variability patterns in a daily (related to day-night) and yearly (related to winter-summer) basis, being the yearly variation considerably more important.

4 Response simulation using finite elements: relevance of the spatial variability of the input motion

Contents

In this Chapter, the finite element model of the Nice prefecture building, presented in Chapter 3, is employed to simulate the response of the building to earthquakes and to obtain acceleration time histories at different storys. Simulations are compared with records. Signals registered during the recent Barcelonnette earthquakes of February 2012 (M_w = 4.2) and April 2014 (M_w = 4.9) are used as excitation. Instead of doing three independent simulations using a one-component loading, a three-component motion is imposed at the base of the building. However, the limitations of neglecting soil-structure interaction are highlighted. An advantage of using in-situ records is that soil-structure effects are already present in the input motion. The spatial variability of input motion, due to rotations at the foundation level, is taken into account by imposing different loading in different points at the base of the building. A quantitative comparison of goodness of fit (GoF) of numerical simulations is carried out using Anderson's criteria. The improvement obtained considering multiple input motions as source of excitation at the base of the numerical model is estimated.

4.1 Introduction

The numerical simulation of the dynamic behavior of buildings is important to better understand and predict their seismic response and anticipate the consequences of earthquakes for structures.

Instrumentation using seismological sensors provides motion records at different points of a structure. The existence of permanent installations (five buildings are continuously monitored in France), enables to record the building response during seismic motions. These records can be used to provide seismic loading and structural deformation to validate numerical models. Validated numerical models can be used to simulate the building response to reference events.

Numerical modeling of a structure is influenced by the selection of mechanical models that simulate the constitutive behavior of materials and mechanical behavior of structural elements.

Generally, rotational motion are assumed negligible in structural design. Under such favorable conditions, associated rotational motions are small and can be neglected. Trifunac (2009b) reviews the influence of the rotational motion component in near-fault cases and concludes that ignoring the rotational contribution of could lead to underestimated story drifts by a factor of up to two in shear buildings. In order to validate the numerical model of the Nice prefecture building with records, the evaluation of the contribution of imposing multiple motions is considered.

4.2 Recorded earthquakes

In the Nice prefecture building, events of magnitude between M_w 3.5 and M_w 4.5, with epicentral distance between 50 and 150 km are regularly recorded (Figure 4.1).

The sample period of the signals considered in this study is very small compared to geological times. The signal associated with a characteristic earthquake of the region for construction purposes cannot be found in the existing records. This study focuses on signals recorded at 100 km, but earthquakes of M_w 6 or more can happen at a short distance from the Nice area.

4.2.1 2012 and 2014 Barcelonnette earthquakes

The strongest ground motions is recorded by the sensor network deployed in the building during the 7 April 2014 M_w 4.9 Barcelonnette earthquake, that occurred at around 100 km

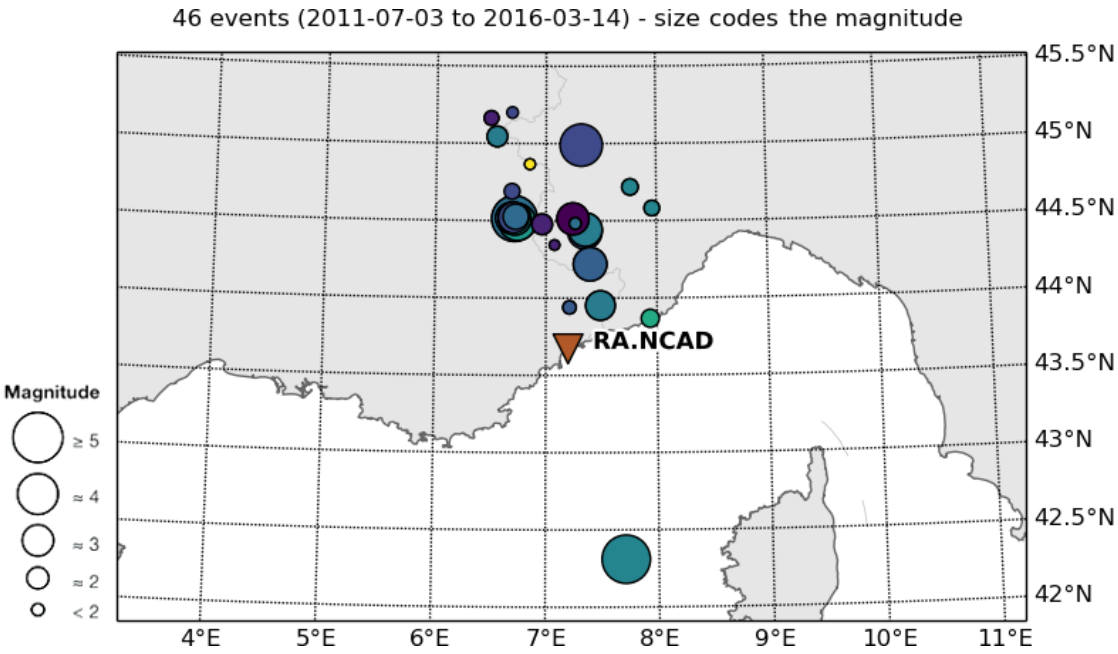

Figure 4.1 – Catalog of events properly recorded at the Prefecture building since it was instrumented (according to the RENASS catalog). Evaluation of recorded signal quality is carried out using a STA/LTA trigger.

in the north of Nice. The 26 February 2012 M_w 4.2 Barcelonnette earthquake has also been recorded (Courboulex et al., 2013). Both events have the same location and focal mechanism. The acceleration time histories recorded at the base of the building, corresponding to these events, are shown in Figure 4.2. The peak ground acceleration (sensor A0, component HN3 in Figure 3.1c) is 0.036 m/s^2 for the 2014 earthquake. A similar value of 0.034 m/s^2 is registered for the 2012 event, despite its lower magnitude. This close peak ground acceleration is due to the fact that 2012 earthquake is characterized by a strong directivity effect towards Nice, as discussed by Courboulex et al. (2014), whereas the 2014 did not exhibit such effect.

The Figure 4.3 shows the macroseismic intensity of both events. It is observed a directivity effect in the direction of Nice. Even if the events are quite different (M_w 4.2 and M_w 4.9), the effects on the city of Nice (in the directive direction) are similar and reach the same intensity in the EMS98 scale.

4.2.2 Variation of building frequencies during ground motion

Transitory and rapid variations of the fundamental frequency of a building have been observed during seismic ground shaking, being associated to a nonlinear soil-structure behavior (Todorovska and Trifunac, 2008b) or to the opening and closing of micro cracks inside reinforced

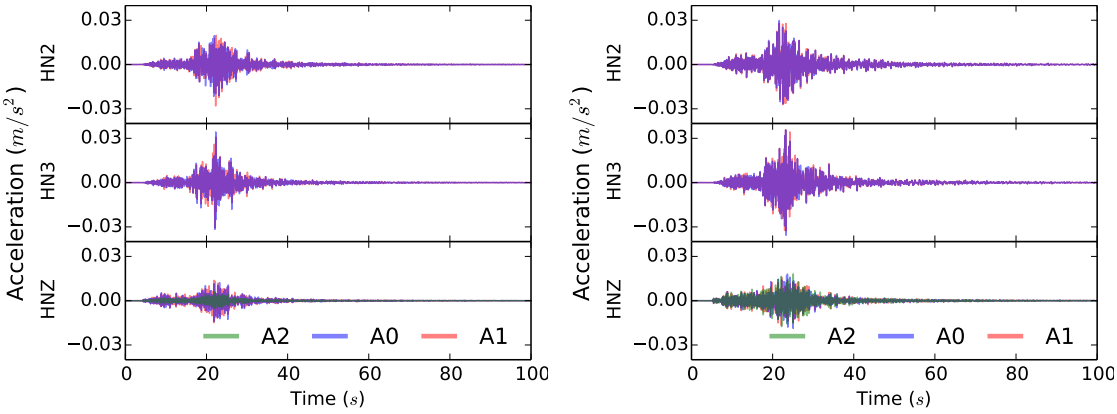

Figure 4.2 – Recorded accelerograms at different locations (A0, A1, A2) at the base of the building, for the two horizontal (HN2, HN3) and vertical (HNZ) components, during the 2012 M_w 4.2 (left) and 2014 M_w 4.9 (right) Barcelonnette earthquakes.

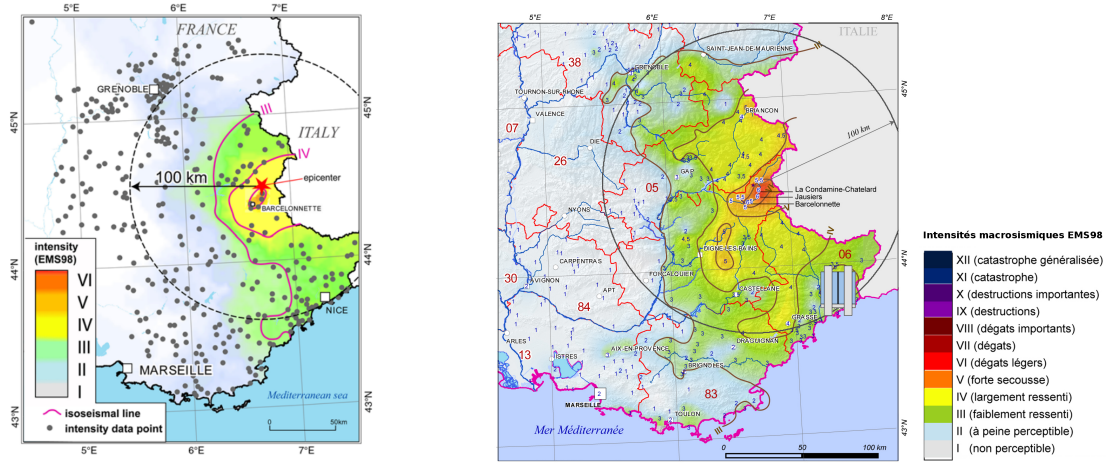

Figure 4.3 – Macrosismic intensity (EMS98) of the 26 February 2012 (left) and 7 April 2014 (right) Barcelonnette earthquakes. Modified from BCSF Sira et al. (2012, 2014).

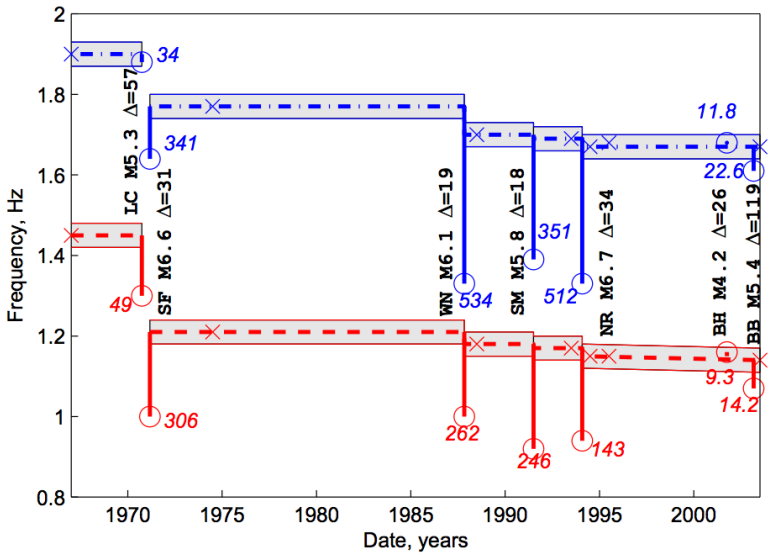

Figure 4.4 – Variation of fundamental modes in the Millikan library. Dashed lines represent the natural frequencies associated to the traslational shape mode in E-W direction and the dashed-dotted lines represent the natural frequencies associated to the translational shape mode in N-S direction. Shaded area is the likely range of natural frequencies taking into consideration errors in measurement due to various factors - weight configuration in the shaker, weather conditions at the time of the test, and experimental error. Crosses indicate actual time forced test was made. Circles indicate natural frequency estimates from the strong motion record during earthquake events, and numbers in italics are peak acceleration recorded for the event (cm/s^2). [Earthquake Abbreviations: LC: Lytle Creek, SF: San Fernando, WN: Whittier Narrows, SM: Santa Monica, NR: Northridge, BH: Beverly Hills, BB: Big Bear] (adapted from Clinton 2004).

concrete elements (Michel and Guéguen, 2010). A classical case study that reflects permanent and transitional marked variations during various earthquakes is the Millikan library (Figure 4.4).

Such transitory frequency shifts have also been observed in the studied building (Figure 4.5). The variation of the two first modes during the two above presented moderate seismic events is shown in Table 4.1. The reduction of the natural frequencies is transitory and the events did not cause damage in the structure.

Todorovska (2009b) evaluates the wandering of the fundamental frequency (denominated apparent frequency measured from the peaks of the transfer function, $f_{1;app}$) of Millikan library during earthquakes, which dropped up to 21% during the San Fernando 1970 earthquake (Udwadia and Trifunac, 1973b). She considers an infinite foundation horizontal stiffness ($f_H \to \infty$) and separate the effect of two components: a transitient drop (recoverable after

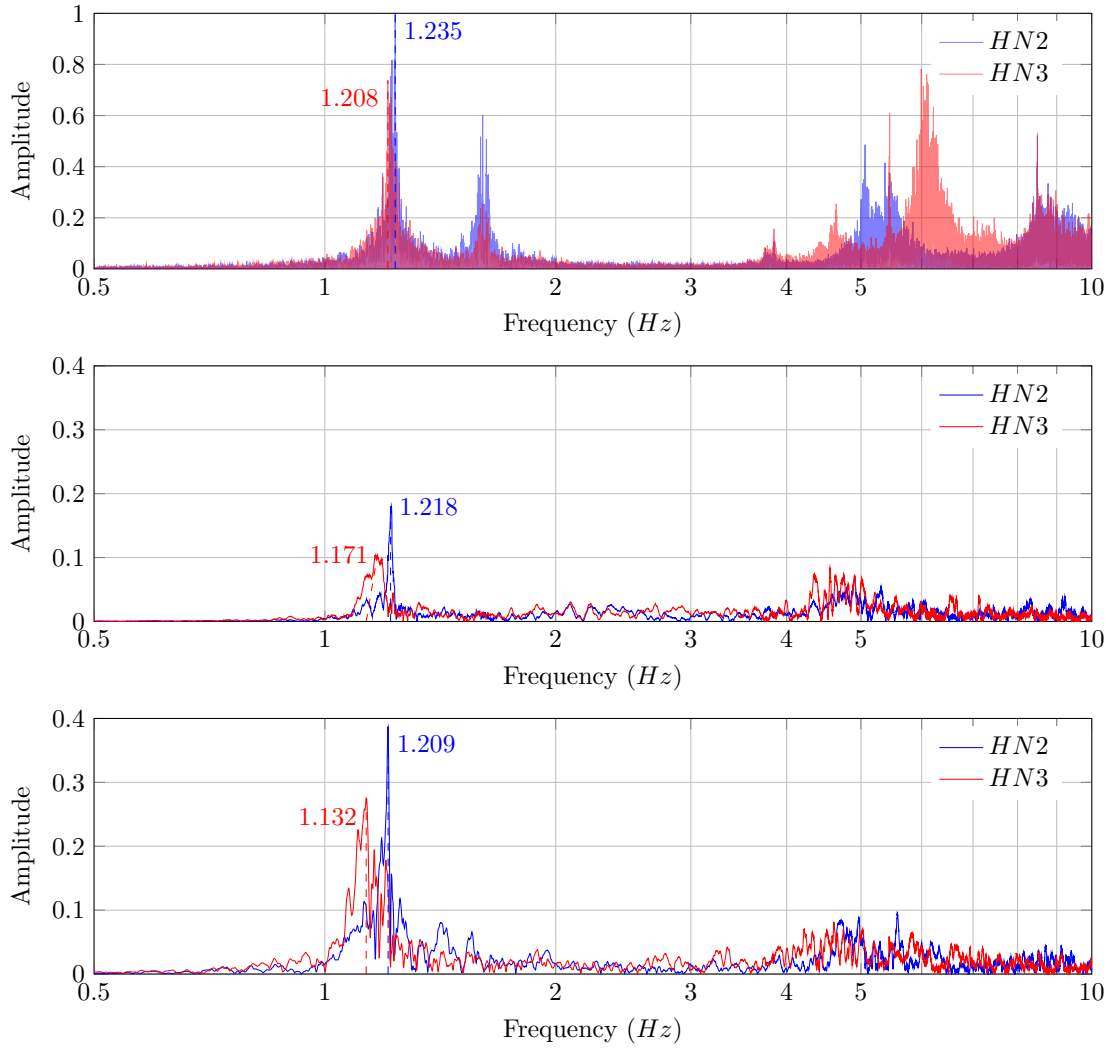

Figure 4.5 – Fourier transform of the recorded acceleration at the top of the building under ambient vibrations (top), during the 2012 Barcelonnette earthquake (middle) and during the 2014 Barcelonnette earthquake (bottom). The value of the first bending mode on each direction (HN2, HN3) is highlighted.

Table 4.1 – Natural frequencies variation with nature of input motion, measured as peaks of the Fourier transform (Noise, Barcelonnette 2012, Barcelonnette 2014).

Mode	Frequency		
	Noise [Hz]	M_w4.2 [Hz]	M_w4.9 [Hz]
1	1.208	1.171	1.132
2	1.235	1.218	1.209

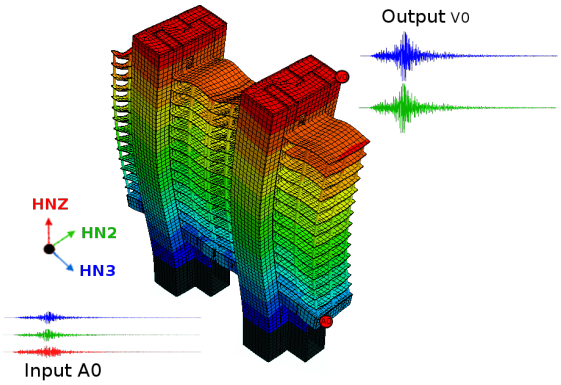

Figure 4.6 – Numerical simulation of the building by imposing a tri-axial signal recorded at A0 at the base of the model. Time-histories of horizontal acceleration (HN2, HN3) are obtained at the top of the building (V0).

the mainshock) and a permanent change (associated to degradation of structural stiffness). To evaluate the contribution of each part during the motion, the decrease of a fixed-base frequency, f_1, (asociated with structural damage) and rigid-body rocking frequency, f_R, (associated with soil interation) are separated. During the San Fernando earthquake, f_1 dropped by 24%, and f_R dropped by 18%, having a combined effect on the apparent frequency, $f_{1;app}$, of a 20.7% drop. These results shows that changes in f_R (soil) and f_1 (structure) contributed comparably to the observed drop.

A theoretical introduction of the effects of SSI on natural frequencies of a SDOF oscillator is presented in Section 2.1.5. The simulations carried out in this Chapter intend to numerically reproduce the influence of the structure-soil interaction to such transitory variation on the modal frequency content of the building.

4.3 Imposition of a single tri-axial input load (SI)

The three acceleration components (HN2, HN3 and HNZ in Figure 3.1c) of the 2012 and 2014 Barcelonnette earthquakes (Figure 4.2) recorded by one sensor (A0) are simultaneously imposed as excitation at the whole base of both towers in the FE model. The modal analysis procedure described in Section 2.1.6 is adopted. Records and numerical signals are filtered by a forth order Butterworth filter between 0.5 and 10 Hz, that is a band including the most relevant frequency content of the building. The numerical horizontal accelerations at the top of the instrumented tower (Figure 4.6) provided by the FE model (FEM2) are compared with records.

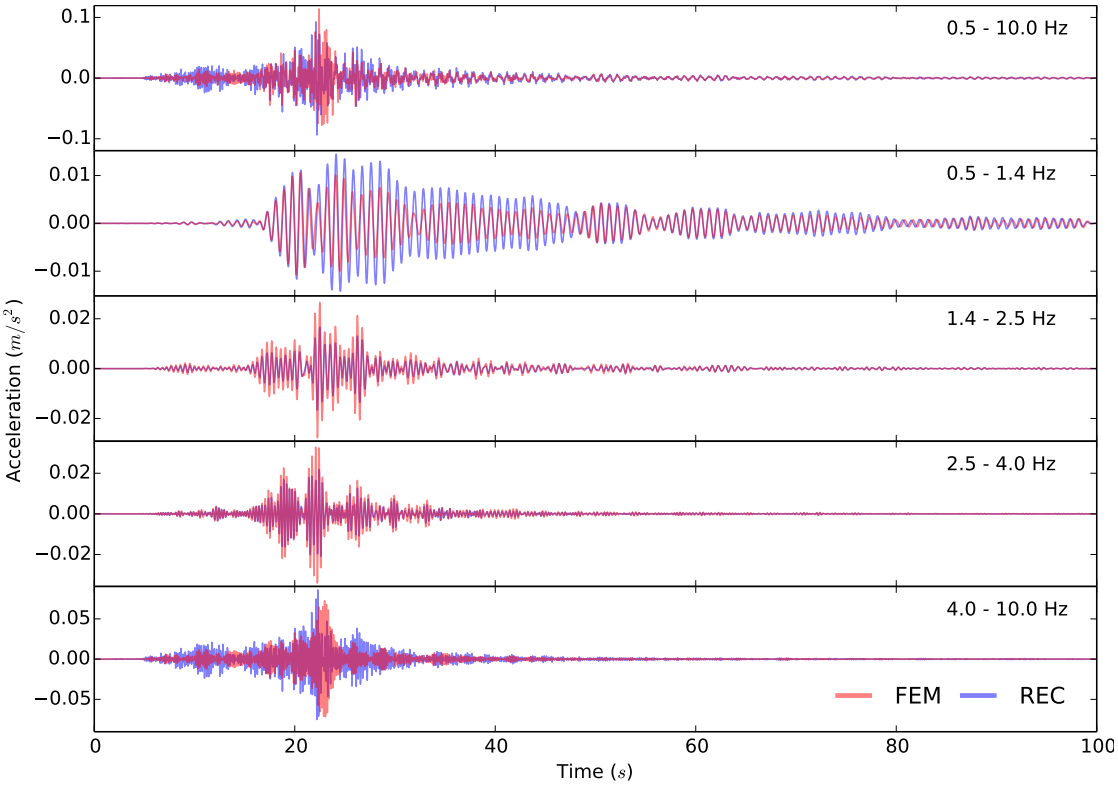

Figure 4.7 – Recorded (REC) and numerical (FEM) horizontal acceleration (HN3) at the top of the building (V0) during the 2012 Barcelonnette earthquake for different frequency bands. One triaxial signal is used as input in the numerical model.

The comparison of the horizontal component HN3, in different frequency bands (see Table 3.3), is presented in Figures 4.7 and 4.8, for 2012 and 2014 Barcelonnette earthquakes, respectively. The first, third and fourth modes are isolated in frequency bands B2, B3 and B4, respectively. Although the first two modes are in the same frequency band, only the first mode can be detected in B2 by the horizontal acceleration in direction HN3, due to the fact that the second mode is a translational motion in direction HN2. Records appear well reproduced in terms of amplitude. A misfit can be observed in the 0.5-1.4 Hz frequency band (B2) for the 2014 earthquake (Figure 4.8). Time-history accelerations appear to be well correlated in phase in the different observed frequency ranges.

The maximum stresses attained during these events corroborates the assumption of linear material behavior. The maximum stress reached during both the simulations is of 0.9 MPa (3% of 30MPa, that is the concrete resistance during conception).

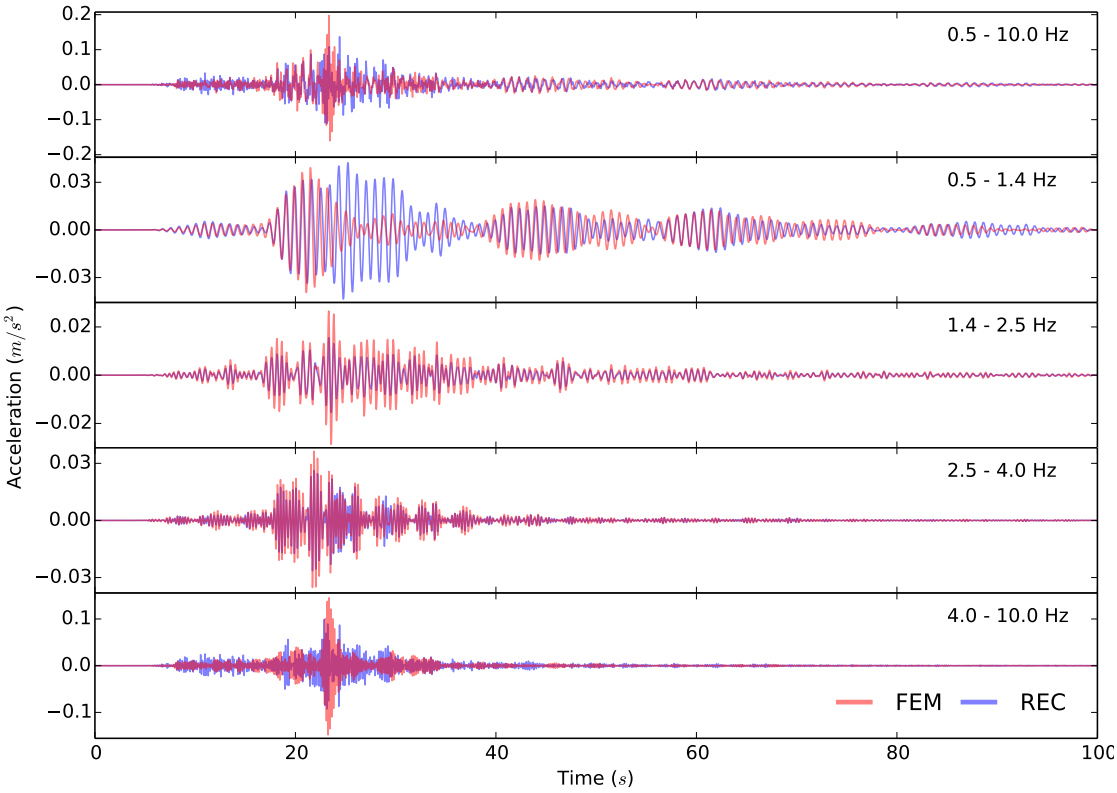

Figure 4.8 – Recorded (REC) and numerical (FEM) horizontal acceleration (HN3) at the top of the building (V0) during the 2014 Barcelonnette earthquake for different frequency bands. One triaxial signal is used as input in the numerical model.

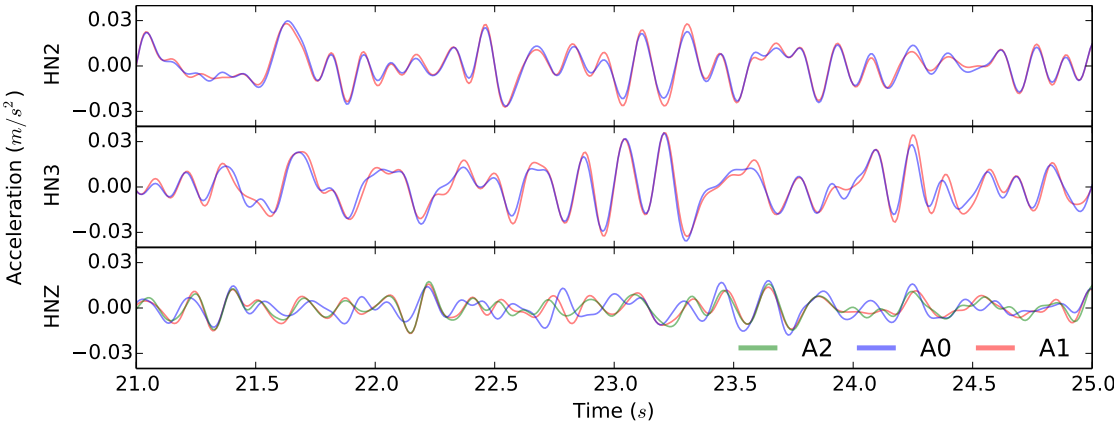

Figure 4.9 – Time window of the three components (HN2, HN3, HNZ) of 2014 Barcelonnette earthquake, recorded at different points at the base of the building (A0, A1, A2).

4.4 Imposition of multiple input loads (MI)

The imposition of the same signal at the base of the numerical model is generally accepted for the structural design of buildings. This simplification considers a completely rigid base neglecting the existing spatial variability among different base points and avoiding possible base rotations.

The instrumentation set-up at the base of the structure has two triaxial accelerometers and one monoaxial accelerometer in the vertical direction. A 4-second time window of 2014 Barcelonnette earthquake is shown in Figure 4.9, for the two horizontal components and the vertical component recorded by the two triaxial sensors (A0 and A1 in Figure 3.1c) and the vertical component recorded by a monoaxial sensor (A2).

The horizontal components are quite similar. However, the vertical components appear different, for this earthquake, in the observed points of the building base. According to this observation, the spatial variability is taken into account to improve the numerical results in the 0.5 - 1.4 Hz frequency range. The instrumented tower is excited with triaxial records (HN2, HN3 and HNZ) in points A0 and A1 and the monoaxial vertical record (HNZ) at the point A2 (Figure 4.10). Therefore, different input motions are imposed to the model. The implicit analysis described in Section 2.1.6 is adopted. Due to the lack of records in the non-instrumented tower of the building, the three-component signals recorded by the sensor at A0 are also imposed at the base of the second tower.

The comparison of numerical response at the top of the building, in the horizontal HN3 direction, with records of the 2014 Barcelonnette earthquake is shown in Figure 4.11, in

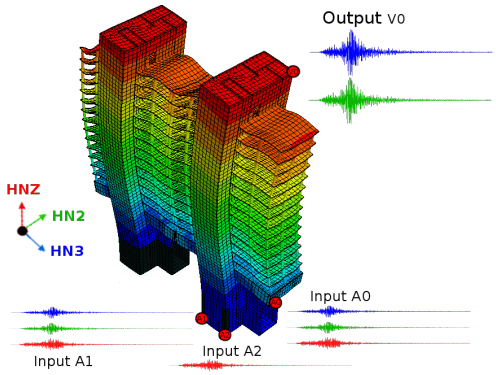

Figure 4.10 – Numerical simulation of the building by imposing multiple input (MI) signals at different points of the base of the model (A0, A1, A2). Time-histories of horizontal acceleration (HN2, HN3) are obtained at the top of the building (V0).

the case of multiple input signals. The response in the 0.5-1.4 Hz frequency range is better reproduced using the multiple signal input. Therefore, rocking effects are relevant in the analyzed high-rise building. Applying the recorded acceleration time-history at different locations, as seismic loading at the base of the building model, permits to take into account rocking effects caused by soil-structure interaction. These effects are not considered by the actual European building code for structural design, nevertheless they can not be neglected in seismic risk assessment for existing buildings.

Spectrograms obtained using short time Fourier transform of the horizontal component (HN3) and the vertical one (HNZ), at the base of the building (A0), are displayed in Figure 4.12, for the 2014 Barcelonnette earthquake. Spectrograms comparing the time-frequency content of the numerical and recorded acceleration at the top of the building are shown in Figure 4.13. Similar results are obtained for the 2012 Barcelonnette earthquake (not shown here). Numerical signals show good agreement with records. However, the FE model amplify the energy content associated to building deformation at low and medium frequencies (B2, B3 and B4) and reduce it for high frequencies (B5).

Comparing the spectrograms at the top (Figure 4.13) and at the base (Figure 4.12) of the building, an expected amplification of the amplitude is observed at the top around the natural frequencies of the structure. Such amplification is specially noticed around the fundamental frequency of the building (1.2 Hz).

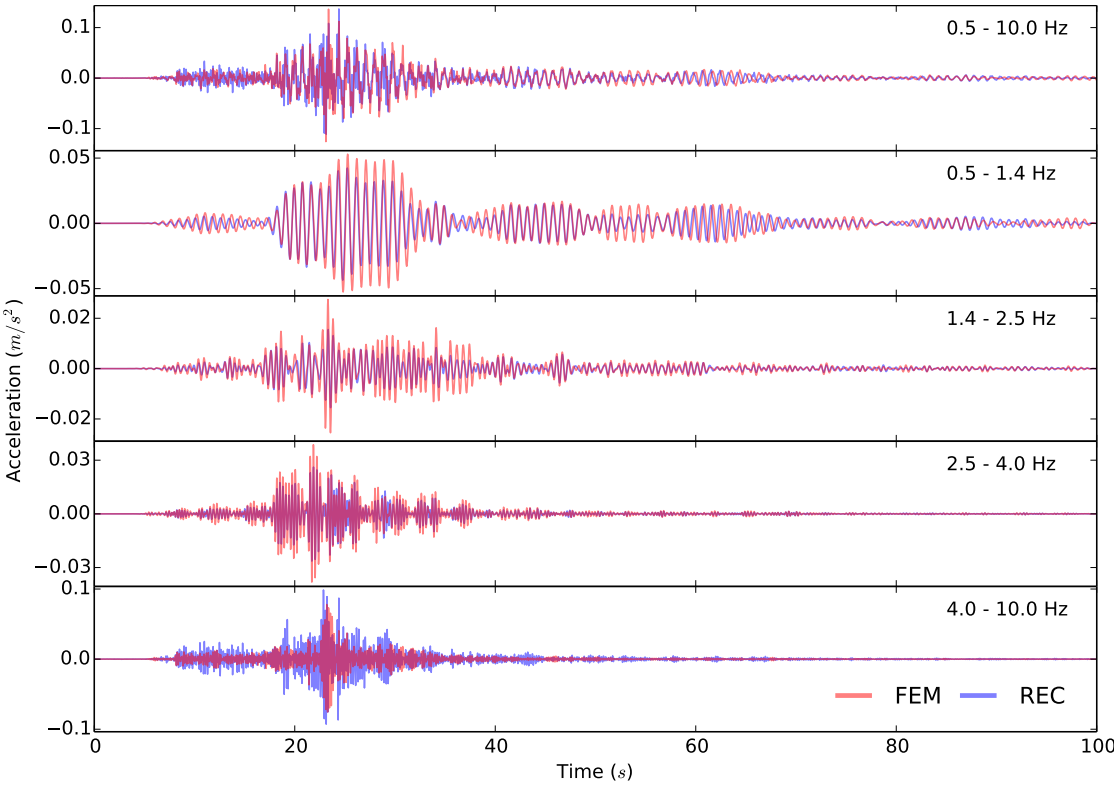

Figure 4.11 – Recorded (REC) and numerical (FEM) horizontal acceleration (HN3) at the top of the building (V0) during the 2014 Barcelonnette earthquake for different frequency bands. Multiple recorded signals are simultaneously applied at different points of the base of the building in the numerical model.

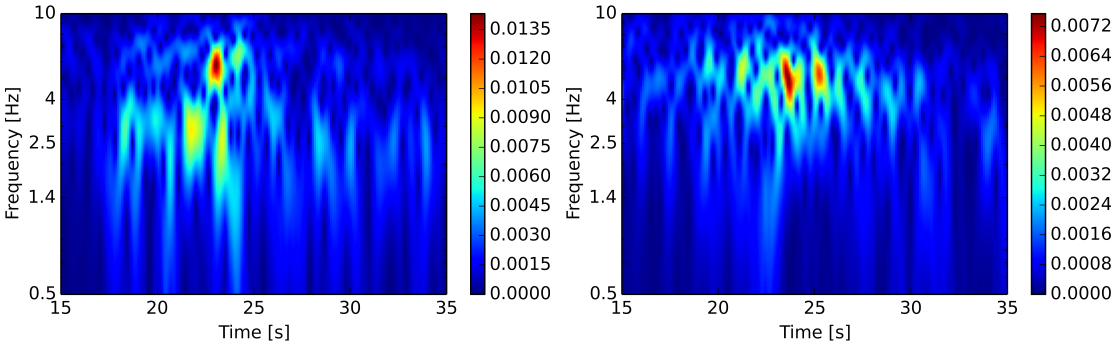

Figure 4.12 – Short time Fourier transform of the horizontal HN3 (left) and vertical HNZ (right) acceleration at the base of the building (A0) during the 2014 Barcelonnette earthquake.

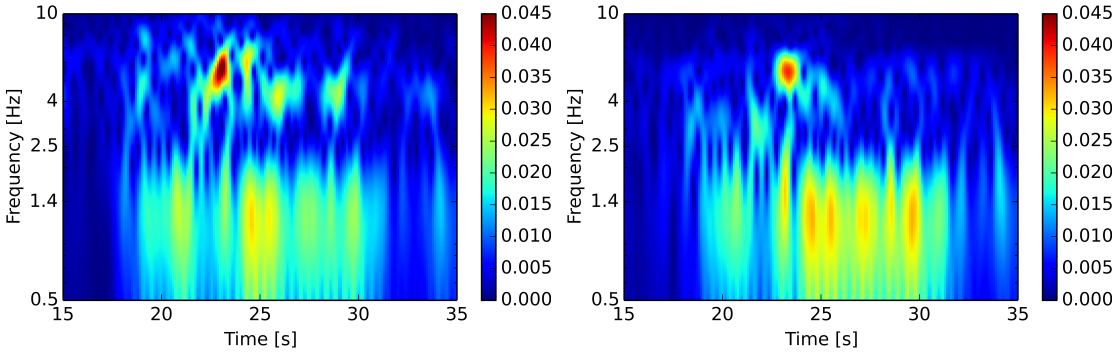

Figure 4.13 – Short time Fourier transform of the horizontal HN3 acceleration at the top of the building (V0) during the 2014 Barcelonnette earthquake for records (left) and FE simulation (right).

4.5 Quantitative comparison of goodness of fit: SI vs MI

Numerical time histories provided by the finite element analysis appear consistent with records in terms of acceleration amplitude and frequency content as seen in Section 4.4. Nevertheless, a validation based on statistical characteristics, to measure the GoF of the numerical seismogram, is undertaken using Anderson's criteria (Anderson, 2004). The use of a quantitative comparison enables further evaluation of the differences between the SI and MI approaches. Such criteria has already been used to adjust numerical models of buildings to records (Perrault, 2013). The similarity of ten parameters is quantified using the following equations:

$$S\left(p_n, p_r\right) = 10\left[1 - \max\left(\left|p_n - p_r\right|\right)\right] \tag{4.1}$$

$$S\left(p_n, p_r\right) = 10\exp\left(-\left[\frac{p_n - p_r}{\min(p_n, p_r)}\right]^2\right) \tag{4.2}$$

$$S\left(p_n, p_r\right) = 10\max\left(\frac{\int p_n(t)\, p_r(t)}{\left[\int p_n^2(t)\, dt\right]^{1/2}\left[\int p_r^2(t)\, dt\right]^{1/2}}, 0\right) \tag{4.3}$$

where p_n and p_r are the evaluated parameters for numerical and recorded seismograms, respectively. Equation 4.1 is applied for Arias duration (AD) and energy duration (ED). Equation 4.2 is used for Arias intensity (AI) (Arias, 1970), energy integral (EI), peak acceleration (PA), peak velocity (PV), peak displacement (PD), pseudo-acceleration floor response spectra (Sa) and Fourier spectra (FS). Equation 4.3 is adopted for the cross correlation (C*). The score for Fourier and response spectra is determined as the average of values obtained by equation 4.2 for all frequencies in the analyzed frequency range.

The integral of ground acceleration is related to the Arias intensity, I_A, using the equation

$$I_A = \frac{\pi}{2g} \int_0^T a^2(t)\, dt \tag{4.4}$$

where $a(t)$ is the acceleration time history, g is the acceleration of gravity, and T represents the complete duration of the recording. The energy integral, I_E, is integral of ground velocity

$$I_E = \int_0^\infty v^2(t)\, dt \tag{4.5}$$

where $v(t)$ is the velocity time history.

The agreement between signals is scored between 0 and 10, to interpret according to Anderson (2004) as: poor fit for a score bellow 4, fair fit between 4 and 6, good fit between 6 and 8, and excellent fit over 8. The evaluation is carried out at five different frequency bands as previously defined in Table 3.3.

The most relevant differences on the comparison of the single input and multi input approach are summarized in Figures 4.14 and 4.15. Figure 4.14 shows Anderson's scores of the SI and MI comparison with records in both global frequency band (left) and isolating the fundamental mode (right). The MI approach improves almost all the parameters used in the comparison. Figure 4.15 highlights the comparison of the Fourier spectra and the Arias intensity for the fundamental mode. It is observed that the energy distribution of the MI approach fits much better the records. The most interesting observation is that the MI signal reproduces a decrease on its frequency content (with respect to measures under noise excitation) of the same order as the seismic records (about 6%). On the other hand, the SI response does not show such decrease and has a frequency content that corresponds to the fixed-base mode.

A detailed representation of all the scores in both cases of single three-component motion and multiple signals are represented in Figure 4.16 for the 2012 and 2014 event. Numerical and recorded peak acceleration, velocity and displacement are reported in Table 4.2, for the 2014 Barcelonnette earthquake. Some other estimated parameters are shown in Figure 4.17. The first mode of the building (1.2 Hz) is excited as observed in Fourier spectra.

The broad-band response (frequency band B1 in Table 3.3) is well represented, giving good and excellent fit in most indicators. The multi-signal input improves the representation quality of the fundamental mode of the structure (band B2) in terms of acceleration time histories

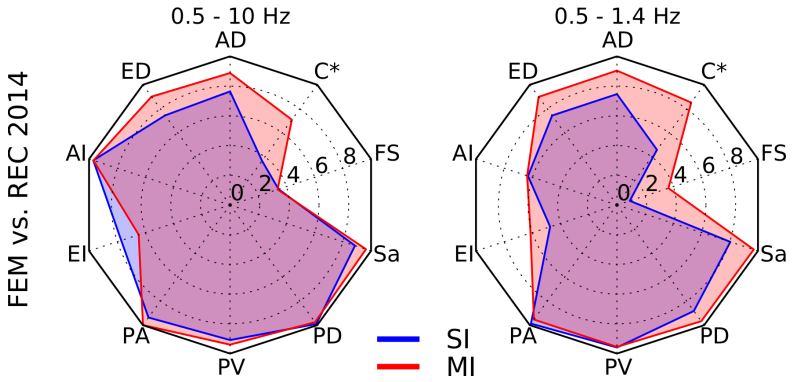

Figure 4.14 – Values of Anderson parameters for comparison with records of a horizontal component (HN3) at top of the building (V0), during the Barcelonnette 2014 earthquake, for the cases of modeling with an imposed mono-axial signal (SI) and multiple signals (MI).

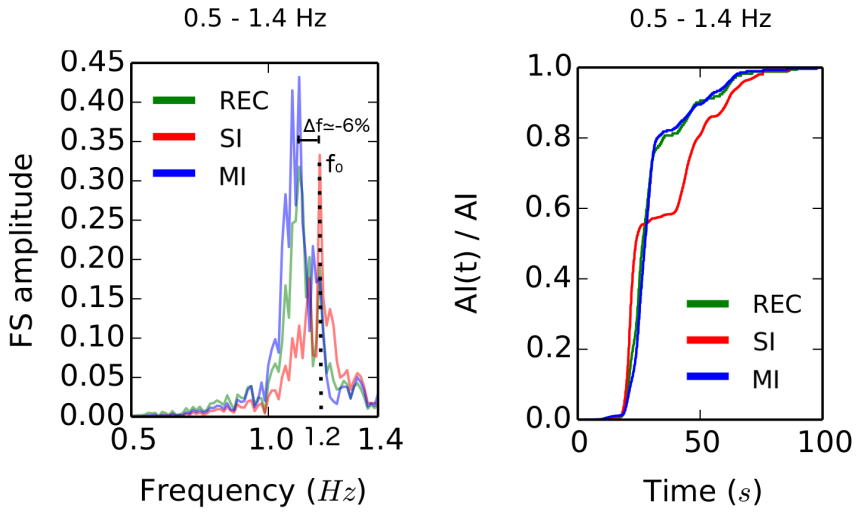

Figure 4.15 – Comparison of the Fourier spectrum (FS) and Arias intensity (AI) for a horizontal component (HN3) at top of the building (V0), during the Barcelonnette 2014 earthquake, for the cases of modeling with an imposed mono-axial signal (SI) and multiple signals (MI).

Table 4.2 – Values of Peak Acceleration, Velocity and Displacement for recorded and numerical horizontal component (HN3) at the top of the building (V0) during the 2014 Barcelonnette earthquake.

Band	PA [m/s^2] × 10^{-3}			PV [m/s] × 10^{-3}			PD [m] × 10^{-3}		
	REC	FEM1	FEM2	REC	FEM1	FEM2	REC	FEM1	FEM2
B1	133.18	167.42	136.23	7.44	9.73	9.28	1.00	0.91	1.16
B2	43.45	39.05	52.98	6.34	5.26	7.70	0.95	0.70	1.12
B3	15.52	28.51	27.48	1.30	2.33	2.23	0.11	0.20	0.19
B4	26.42	36.86	38.66	1.41	1.96	2.05	0.08	0.11	0.11
B5	91.45	121.15	77.15	2.47	3.39	2.19	0.07	0.10	0.06

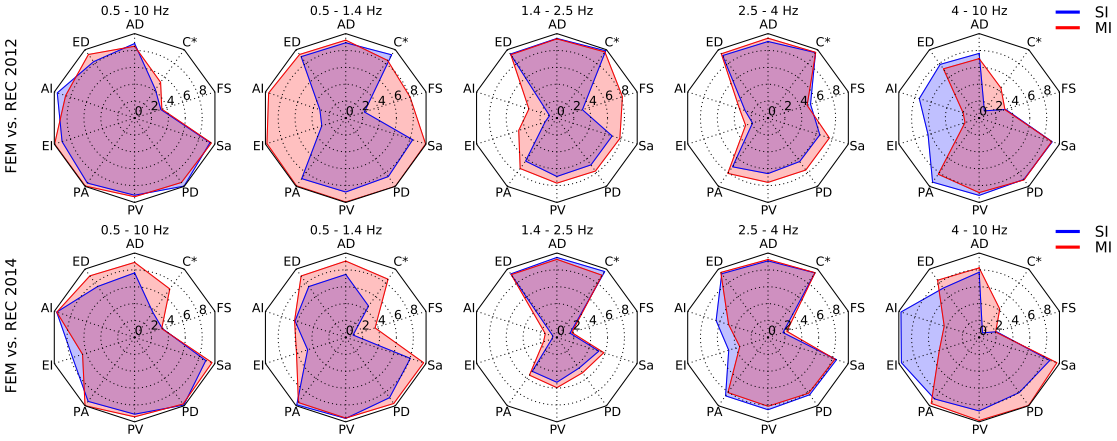

Figure 4.16 – Anderson's GoF scores for numerical horizontal component (HN3) at the top of the building (V0) during the 2012 (top) and 2014 (bottom) Barcelonnette earthquakes compared with records, in different frequency bands, in both cases of a single three-component signal applied as input to the whole base (SI) and multiple signal input (MI). Evaluated parameters include Arias duration (AD), energy duration (ED), Arias intensity (AI), energy integral (EI), peak acceleration (PA), peak velocity (PV), peak displacement (PD), pseudo-acceleration floor response spectra (Sa) and Fourier spectra (FS) and cross correlation (C*).

(as previously shown in Figures 4.8 and 4.11) and cross-correlation. The torsional mode (isolated in band B3) is fairly well represented. Acceleration, velocity and displacement are overestimated in frequency ranges B1, B2, B3, B4 (Table 4.2). The excellent cross-correlation value, in frequency ranges B2, B3 and B4, show the agreement in phase of both numerical and recorded signals (Figure 4.16). The Fourier spectra gives a poor fit in all cases, being the most difficult parameter to fit according to Anderson (2004). A good fit is obtained in the case of multiple signals as input at the base of the building (MI in Figure 4.16), for all parameters except Fourier spectrum, when the total frequency range is considered (B1).

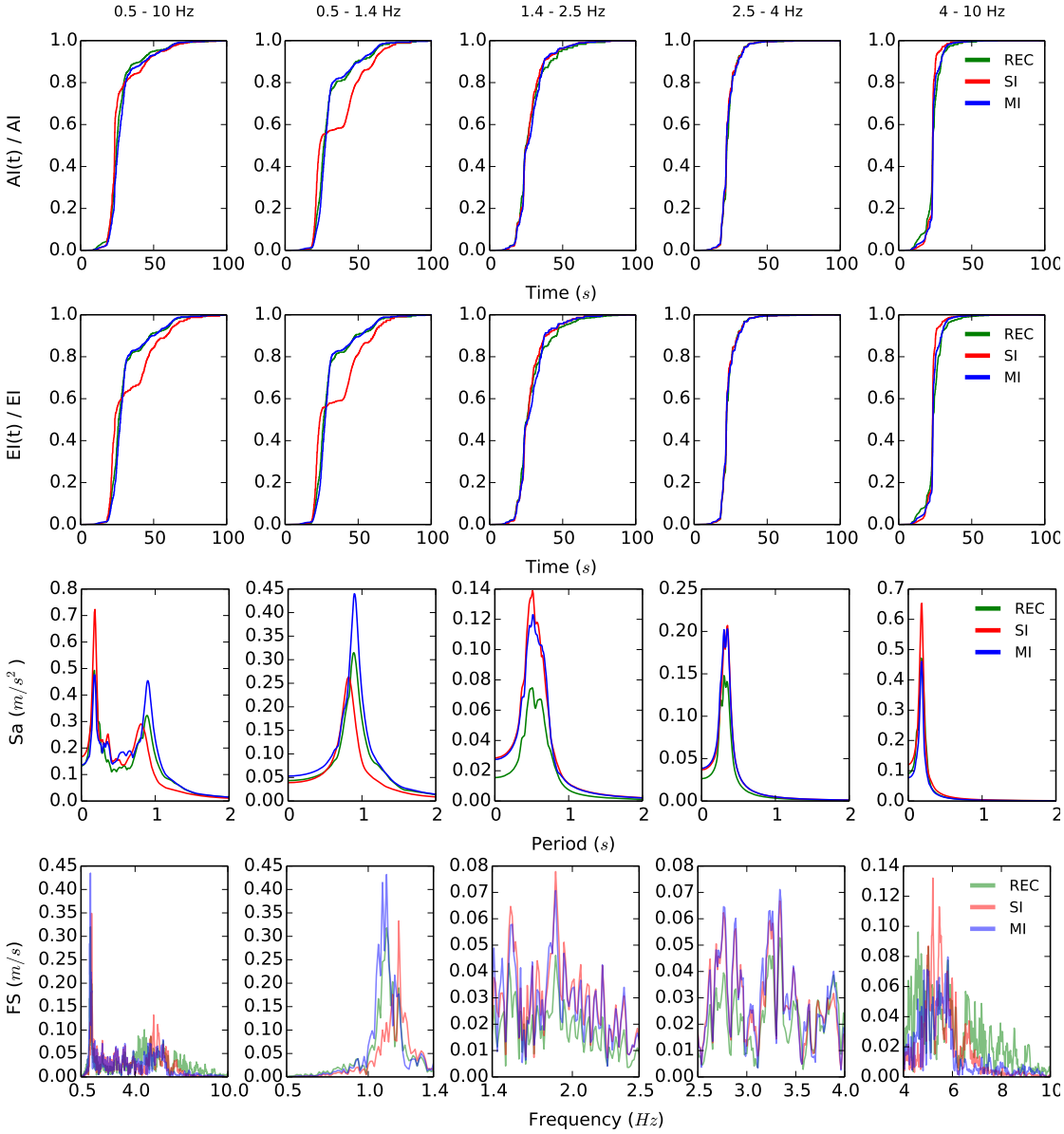

Figure 4.17 – Comparison of Arias integral, energy integral, elastic response spectrum in terms of pseudo-acceleration and Fourier spectrum for the horizontal acceleration component HN3 at the top of the building (V0), during the 2014 Barcelonnette earthquake: records (REC), FE model with single-input (SI) and FE model with multi-input (MI).

4.6 Conclusions

A detailed thee-dimensional finite element model of the Nice prefecture building, optimized using ambient vibration records to fit the service state of the structure, is used to reproduce the deformation time-history during past recorded earthquakes.

The numerical acceleration is compared with records at the top of the building. An initial case considers as input the same tri-axial exitation (SI) for the whole base of the model. An overall good simulation of the seismic response is observed using the SI model. However, considerable part of the behavior in the frequency range including the fundamental mode is not properly reproduced.

Comparison of the vertical component of seismic records at different locations at the underground level of the structure reveals the existence of spatial variability in the base motion. The differences are quite considerable during the strong motion (even if that sensors are separated by 10 to 20 m). In particular, out of phase signals may indicate that the building is suffering a rocking motion, which is ignored by the SI model.

An alternative model is adopted considering the observed spatial variability of the base motion (MI). A better agreement is achieved by imposing different signals at distinct points of the base of the building as input (MI), rather than the same three-components at the whole base (SI). Spatial variability on base motion has shown to have relevant effects on the response of the structure, in particular for the reproduction of the response in the frequency band including the fundamental mode shape.

A quantitative comparison, using Anderson's criteria, show that the goodness of fit of simulations compared with records is improved by considering the MI model. A transitory frequency shift of the fundamental frequency observed during moderate ground motions (of about 6% during Barcelonnette 2014 earthquake) is reproduced in the simulations by the MI model, when multiple input motions are imposed at different locations of the base, and hence its rotation is not blocked. The SI model does not allow a rocking behavior of the building and the maximum energy content of the signal corresponds to the value of the fixed-base fundamental frequency. Such effect appears to be caused by the soil-structure interaction, which even if it has not been explicitly modelled, it is included by the imposition of different records at the base to take into account the spatial variability of the ground motion. The energy distribution of the signal is also improved by the MI model.

Results show the considerable relevance of rocking effects for buildings, spatial variability of

the input motion and the importance of considering soil structure interaction to reproduce the building response to earthquakes. Actual seismic codes do not treat it directly, neither the transitory shift in terms of frequency during ground motions. These effects can put the structure under a very different solicitation that the one considered by the response spectrum analysis, and result in large changes in response amplitudes.

5 Response prediction from records: application of empirical Green's function approach to buildings

Contents

This Chapter proposes the application of empirical Green's functions (EGF), using a stochastic summation scheme, to generate synthetic signals at different heights of a building. Signals recorded during a small earthquake are used to predict the seismic motion for larger magnitude events from records.

The approach is adopted to investigate the dynamic behavior of the Nice prefecture building described in Section 3.2.

In this Chapter a selected observed scenario, with epicenter 100 km far away from the structure, is reproduced for a larger magnitude event in the same seismogenic zone. Ground motion of a

M_w 6.0 event at the base of the building is generated (using EGF in a traditional way) from records of Barcelonnette M_w 4.9 earthquake.

The application of the same summation scheme is adopted to generate empirical signals at different heights of the building (from records at the same level), extending the wave propagation path from the ground to the structure. An assumption of linear behavior of materials is adopted, justified by the low amplitudes and consequent reduced strain level of M_w 6.0 event at such a distance. Finite element simulations are used to produce reference signals to verify the validity of the EGF time history responses generated for the selected scenario. Empirical and numerical time histories of structural deformation are qualitatively and quantitatively compared.

A reviewed version of Kanai-Yoshizawa formulation is proposed (in combination with EGF approach) to approximate deformation time histories at different stories for greater earthquakes in the cases where only top recordings are available.

The proposed methodology allows structural deformation prediction for existing buildings, when records of small earthquakes are available at the building, without the need of construction drawings and mechanical parameters calibration (characteristic of deterministic numerical models).

The current limitations of the technique are discussed in Section 5.6.

5.1 Introduction

The deterministic approach for the evaluation of dynamic features and the simulation of structural response, to recorded and synthetic ground motions, is mainly based on numerical modeling. This approach demands the calibration of mechanical parameters (such as non-structural mass, damping properties and elastic moduli of materials) and the definition of consistent boundary conditions.

The comparison with records of the numerical structural response allows the assessment and improvement of numerical models. The application of combined numerical and empirical approaches is growing rapidly in the field of structural health monitoring (Brincker and Kirkegaard, 2010).

The ground seismic loading that is applied in a structural model can be defined among a set of selected records (empirical approach) or eventually be simulated (deterministic approach)

using a numerical model of the source rupture, the wave propagation and, in some cases, the interaction between soil and structures, if geological and geotechnical data are available. The prediction of ground motions stronger than the available records is essential in moderate seismicity areas for risk and structural vulnerability assessment. The use of small earthquake records to generate synthetic signals of large earthquakes is proposed by Hartzell (1978). According to this semi-empirical approach, each record represents the propagation effect between the source and the receiver and is considered as an empirical Green's function (EGF). Many methods are developed based on this concept for seismic hazard assessment. Some intend to represent large events in the near field, through a detailed description of the rupture process as an extended source (Hutchings, 1994; Ruiz et al., 2013). Others are more simply based on a point source assumption and a scheme of small record summation of earthquakes, that ensure a statistically good agreement with earthquake scaling laws (Joyner and Boore, 1986; Ordaz et al., 1995).

Analysis of wave propagation for structural response prediction to earthquakes dates from 1930s with the works of Sezawa and Kanai (1935, 1936). However, most of the interest of the earthquake engineering community focuses on a more vibrational approach with the introduction of the response spectrum method in 1932 (Biot, 1932; Trifunac, 2008b). In 1963, Kanai and Yoshizawa (1963) propose a simple formula to approximate the response at the base of the building from records at the roof level. The methodology is based on seeing the response of a structure as a superposition of propagating waves. Hence, the response at the base results on a superposition of two time shifts of the response at the roof. Such concept is considered as the predecessor of the impulse response method that conceptually inspired the impulse response method (Snieder and Safak, 2006; Todorovska, 2009a).

But, can we exploit empirical records to predict the building motion generated by a greater earthquake? Kanai-Yoshizawa formulation can only be applied to events for which we already have a record (hence past earthquakes), and has a limited utility for vulnerability evaluation. However, the main advantages of EGF method is that it naturally incorporates both regional propagation path features and local site effects, under the hypothesis of linear behavior of the medium through which seismic waves propagate. Assuming that the same physical principles are behind wave propagation in the soil and along a building, the propagating path can be extended to the building to predict the response to greater earthquakes, using EGF approach.

5.2 Seismic response at any story from records at the roof: KY formulation

The Kanai-Yoshizawa (KY) formulation is originally proposed to approximate the response at the base of a building from top records, under the assumption of linear elastic material with negligible damping. A one-dimensional nondispersive wave propagation is considered, assuming only shear deformations and neglecting base rocking. Structural deformation at the base and roof levels are, respectively

$$u_{tr}(0^+, t) = k_{tr} F(t) \tag{5.1}$$

$$u_{tr}(H, t) = k_{tr} F(t - H/V) \tag{5.2}$$

where $u_0 = F(t)$ is the incident base motion, k_{tr} is the transmission coefficient for the incident waves from the soil to the structure, H is the height of the building and V the apparent velocity of the vertically propagating waves.

Formulation of equation 5.1 has been recently revisited (Ebrahimian et al., 2016) and generalized to any level. The motion a the base of the building can be expressed as a sum of multiple waves

$$u(0,t) = k_{tr} F(t) + k_{tr} F\left(t - 2\frac{H}{V}\right) + k_{tr} k_{ref} F\left(t - 2\frac{H}{V}\right) + k_{tr} k_{ref} F\left(t - 4\frac{H}{V}\right) + \ldots \tag{5.3}$$

it can be decomposed in acausal and causal waves

$$u(0,t) = k_{tr} \sum_{n=0}^{\infty} k_{ref}^n F\left(t - 2n\frac{H}{V}\right) + k_{tr} \sum_{n=1}^{\infty} k_{ref}^{n-1} F\left(t - 2n\frac{H}{V}\right) \tag{5.4}$$

and simplified in the form

$$u(0,t) = k_{tr} F(t) + \sum_{n=1}^{\infty} \left(k_{ref}^n + k_{ref}^{n-1}\right) F\left(t - 2n\frac{H}{V}\right) \tag{5.5}$$

Similarly, the motion at the roof can be written as

$$u(0,t) = 2k_{tr}F\left(t-\frac{H}{V}\right) + 2k_{tr}k_{ref}F\left(t-3\frac{H}{V}\right) + 2k_{tr}k_{ref}^2F\left(t-5\frac{H}{V}\right) + \ldots \tag{5.6}$$

and simplified in the form

$$u(0,t) = 2k_{tr}\sum_{n=0}^{\infty} k_{ref}^n F\left(t-(2n+1)\frac{H}{V}\right) \tag{5.7}$$

By shifting the roof motion in time, of plus an minus H/V the following expressions are obtained

$$u\left(H,t-\frac{H}{V}\right) = 2k_{tr}\sum_{n=0}^{\infty} k_{ref}^n F\left(t-(2n+2)\frac{H}{V}\right) = 2k_{tr}\sum_{n=1}^{\infty} k_{ref}^{n-1} F\left(t-2n\frac{H}{V}\right) \tag{5.8}$$

$$u\left(H,t+\frac{H}{V}\right) = 2k_{tr}\sum_{n=0}^{\infty} k_{ref}^n F\left(t-2n\frac{H}{V}\right) = 2k_{tr}F(t) + 2k_{tr}\sum_{n=1}^{\infty} k_{ref}^n F\left(t-2n\frac{H}{V}\right) \tag{5.9}$$

A comparison of equations 5.8 and 5.9 with equation 5.7, reveals that

$$u(0,t) = \frac{1}{2}\left(u\left(H,t-\frac{H}{V}\right) + u\left(H,t+\frac{H}{V}\right)\right) \tag{5.10}$$

Hence, the KY formula can be extended to any level of the building according to the following

$$u(H-d,t) = \frac{1}{2}\left(u\left(H,t-\frac{d}{V}\right) + u\left(H,t+\frac{d}{V}\right)\right) \tag{5.11}$$

were d is the distance of the given level to the roof. Hence, if the motion at the roof and the apparent wave velocity V are known, the motion at any level can be computed as the superposition of two time shifts. The building is approximated to an uniform cantilever shear beam with $V = 4H/T_1$, where T_1 is the fixed-base fundamental period of vibration of the soil-structure system estimated from roof recordings. The formulation has been tested in 54 buildings in Los Angeles area, and despite its simplifying assumptions (one-dimensional wave propagation in a uniform shear beam), it works remarkably well, on RC and steel, height and

very height buildings, for both weak and strong motions. Such formulation may result to be useful to approximate motions at different floors in buildings by only disposing of a single earthquake recording.

Figure 5.1 shows the application of KY formulation using the motion records at the top of the Nice prefecture during the 2014 earthquake. The comparison with records (REC) at different floors shows a considerable overestimation of the response. Ebrahimian et al. (2016) observe that predicted displacements are, in certain cases, larger than the recorded ones using this technique. They attribute this effect to foundation rocking effects which affect taller structures (Trifunac, 2009a). Such assumption would be in agreement with the existence of important rocking effects on the present structure discussed in Section 4.4. Additionally, the high non-regularity in elevation of the studied building (see Section 3.2) can considerably contribute to distort results at intermediate levels.

5.3 Principles of the EGF method

EGF technique lies on the hypothesis of similarity between earthquake of different sizes, considering that small and big earthquakes are similar phenomena at a different scale (Aki, 1967) and that a seismic source can be reproduced using a large number of small sources.

The goal of EGF semi-empirical simulation methods is to generate synthetic signals of an event (target) of chosen magnitude and fixed localization, using the records of a smaller event with the same hypocenter, focal mechanism, but lower magnitude (small signal). The process of signal generation is illustrated in Figure 5.2.

5.3.1 Selection criteria for a small event

The selected small event must satisfy some conditions to can be assimilated to an empirical Green function:

- Same location : the rupture zone related to the stronger event to be generated is close to that of the small event (ideally containing it). This ensures the similarity of the wave transmission path between the source and the receiver. In the case of generating a future scenario, the fault is considered to be close to the hypocenter of the small earthquake.
- Same focal mechanism : in theory, both events have an identical focal mechanism. In the case of simulating a future scenario, the fault mechanism is considered to be the

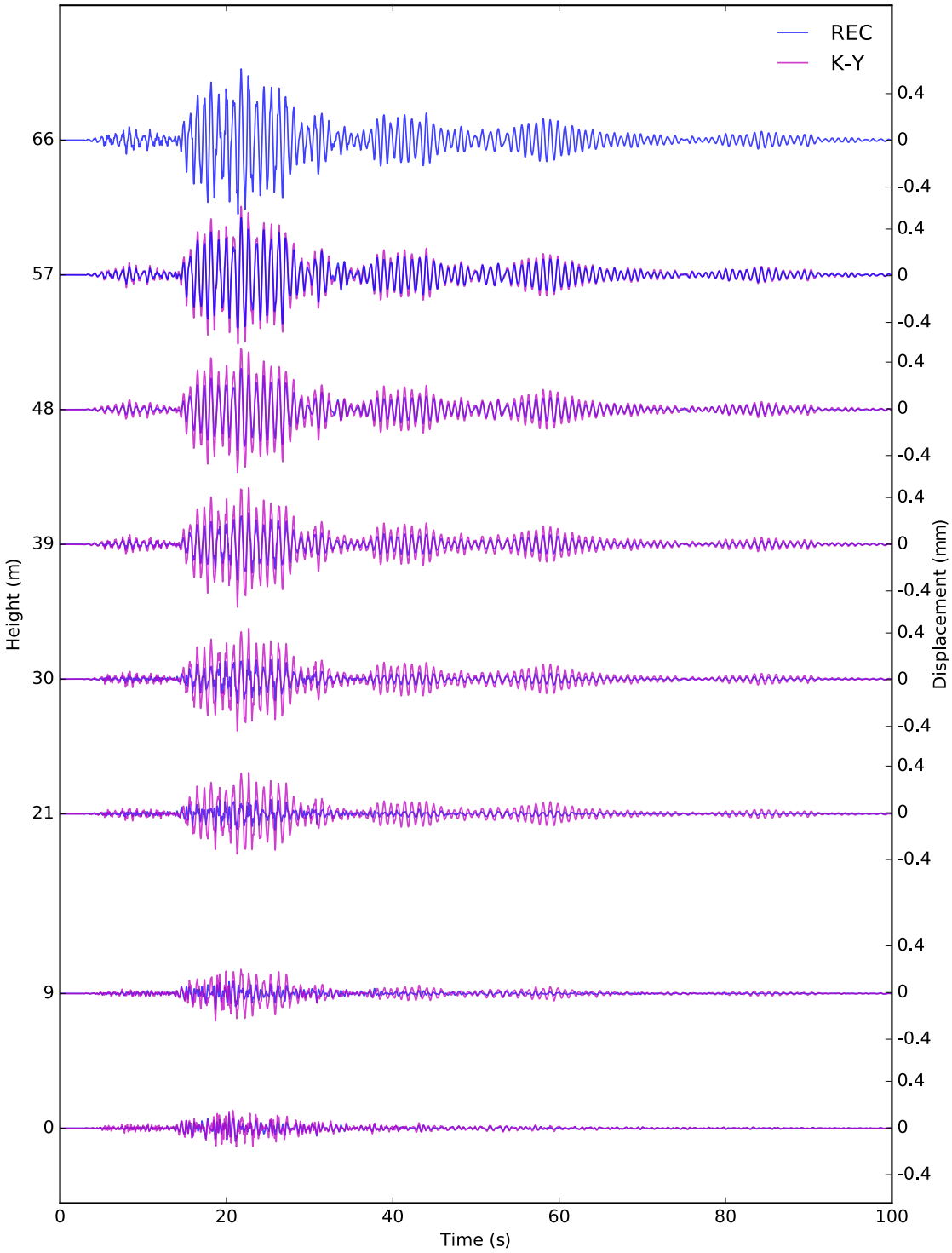

Figure 5.1 – HN3 horizontal component of structural deformation at different heights of the building, both recorded (REC) during the 2014 Barcelonnette earthquake and deduced using the record at the top of the building according to the revisited Kanai-Yoshizawa formulation (KY).

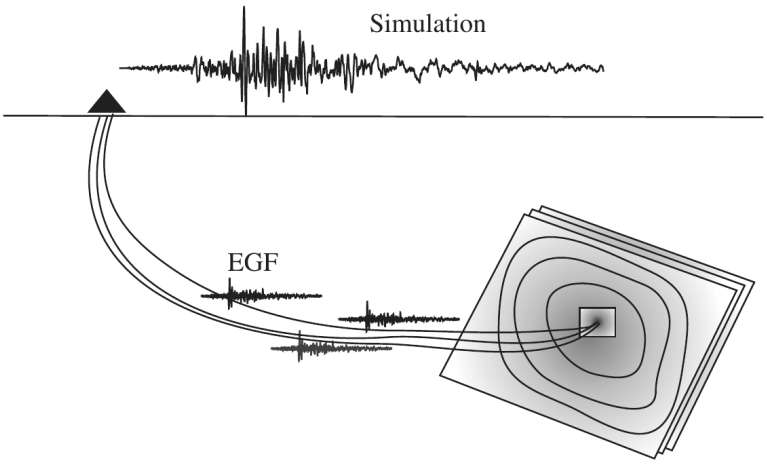

Figure 5.2 – Principle of the strong motion generation trough empirical Green's functions: the records of a single small earthquake are combined several times to produce synthetic recordings for a larger event at a given station (from Courboulex (2010)).

same of the small earthquake.

- Suitable signal to noise ratio : the selection of a small event is conditioned by its magnitude. The earthquake should be big enough to avoid being hidden by the seismic noise at low frequencies, but not too big in order to be consistent with the hypothesis of punctual source.

5.3.2 Applicability conditions

The assumed hypotheses in EGF technique represent some consequent limitations:

- Far field : a small event is representative of the propagation effect between each point of the source and the station, if records are taken far enough from the fault. The distance between the recording station and the fault must be greater than the fault lenght. (Bernard, 1987).

- Linearity : the technique does not take into account the effects of soil nonlinear behavior. The generation of a stronger ground motion by summation of small events requires the assumption of linear behavior.

5.3.3 Stochastic summation scheme

The stochastic method SIMULSTOC, based on the the two-step technique described by Kohrs-Sansorny et al. (2005), is used in this research to generate stronger earthquakes using records of small events. Records are called Green's functions as they describe the impulse response of the medium. The main advantage of this technique is the requirement of only two parameters: the seismic moment of the target earthquake and the stress-drop ratio (C), between small and target events. This method has been validated and tested on French Indies earthquakes (Courboulex et al., 2010) and in the south west of France to generate stronger earthquakes (Honoré et al., 2011). It has also been used to generate an offshore M_w 6.3 earthquake scenario in the city of Nice by Salichon et al. (2010).

The procedure consists in the generation of a large number k of Equivalent Source Time Functions (ESTFs) $R_k(t)$, that represent possible rupture processes. The large event signals $S_k(t)$ are obtained by a convolution operation $(*)$ applied to the small event record $s(t)$:

$$S_k(t) = R_k(t) * s(t) \tag{5.12}$$

The following stochastic summation is applied to reproduce the amplification effect between the source and the receiver:

$$R_k = \kappa \sum_{d=0}^{\eta_d - 1} \left[\sum_{c=0}^{\eta_c - 1} \delta(t - t_c - t_d) \right] \tag{5.13}$$

where κ is the scaling factor, η_c is a number of time shifts of duration t_c, randomly generated with a probability density $\rho_c(t)$, where t varies in a time interval having duration T_c and δ is the Dirac delta function. The other number of time shifts η_d, of duration t_d, is randomly generated with a probability density $\rho_d(t)$, where t varies in a time interval having duration $T_d \leq T_c$.

Probability densities $\rho_c(t)$ and $\rho_d(t)$ are chosen as proposed by Ordaz et al. (1995). The scaling factor κ and the total number of summed events $\rho = \rho_c \cdot \rho_d$ are selected to produce, on average, time histories that agree with the ω^{-2} model of seismic sources (Aki, 1967; Brune, 1970) and respect a non-constant stress-drop condition (Beeler et al., 2003; Kanamori and

Rivera, 2004) as:

$$\rho = N^4 \qquad k = \frac{C}{N} \qquad N = \frac{f_c}{F_c} \qquad C = \frac{\Delta\sum}{\Delta\sigma} \qquad T_c = \frac{1}{Fc} \tag{5.14}$$

where the energy is assumed distributed in the same way in both summation steps with $\rho_c = \rho_d = N^2$. The cutting frequency of the original signal f_c is obtained by comparison of the Fourier spectrum with the ω^{-2} model and its moment magnitude is estimated from records.

5.4 Generation of reference ground motion

A M_w 6.0 event at Barcelonnette (about 100 km from Nice) is generated, using acceleration time-histories recorded in Nice during the 2012 M_w 4.2 and 2014 M_w 4.9 Barcelonnette earthquake (see Section 4.2) as empirical Green's functions.

According to the EGF technique the seismogenic fault is assumed as a point source. The generated signal reproduces the transmission path between the source and the receiver, including the site effects in the basin. The simulated signal includes possible directivity effects as the EGF.

A total of 500 ESTFs are generated to represent the random rupture process of the source for each signal simulation. The ESTF with maximum value closer to the average maximum for all the ESTFs is selected for each component of motion. The calibration of the stress-drop ratio C is done by considering a rupture duration of 5.3 s, which is the average rupture duration for M_w 6.0 earthquakes according to automatic analysis of a large worldwide seismic event dataset by Vallée et al. (2011).

The ground motion of the original 2012 M_w 4.2 and 2014 M_w 4.9 events, as well as two corresponding M_w 6.0 synthetics, are displayed in Figure 5.3. The difference in terms of amplitude between the two generated signals, that should reproduce events of the same magnitude, is due to the directivity effect that characterize the 2012 event as presented by Courboulex et al. (2014). The fundamental period of the building (T_0 = 0.83 s) is higher than periods associated to the main energy content of these earthquakes, as indicated in Figure 5.4.

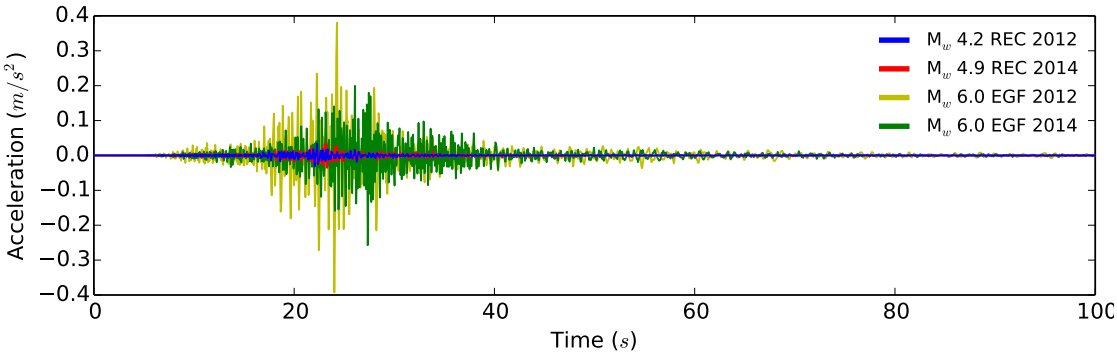

Figure 5.3 – HN3 acceleration component, recorded (REC) at the base of the building (A0) during the 2012 M_w 4.2 and 2014 M_w 4.9 Barcelonnette earthquakes and generated for the two M_w 6 earthquakes (EGF) using 2012 and 2014 events as EGF.

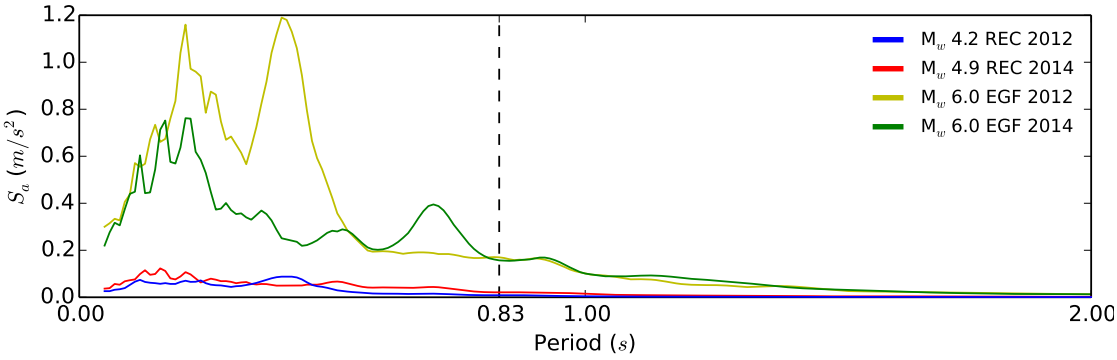

Figure 5.4 – Acceleration response spectra for HN3 component of motion, recorded (REC) at the base of the building (A0) during the 2012 M_w 4.2 and 2014 M_w 4.9 Barcelonnette earthquakes and generated for the two M_w 6 earthquakes using 2012 and 2014 events as EGF. The fundamental period of the structure is highlighted by a dashed line.

5.5 Generation of building deformation time histories

The stochastic summation procedure described in Section 5.4 is applied to predict the seismic response at the top of the building. As already explained, in the case of ground motion generation the procedure allows taking into account peculiarities of the propagation path between the source and the receiver at the base of the structure. Instead, for structural response prediction, the transmission path is extended to the building storys, considering the structure as a media through which the seismic waves propagate. The small earthquake, used as input of the signal generation procedure, is the acceleration component recorded at a selected building floor. This proposed procedure reproduces features of the propagation path between source and receiver on the building floor. It is a semi-empirical approach for structural response prediction.

The main advantage of the method is that no assumptions have to be made concerning the structure. It is only needed to have records in the position that the prediction is evaluated. The proposed method is applicable under the hypothesis of linear behavior of the medium through which waves propagate.

Acceleration time histories at each floor are generated for a M_w 6 event, adopting as small earthquake the records of 2014 Barcelonnette earthquake. A total of 500 ESTFs multiplied by 24 recording channels makes 12000 evaluated ESTFs for the whole building. Only accelerations at the top of the building are shown and discussed in this thesis.

5.5.1 Qualitative comparison

The verification of synthetics, obtained by EGF for a M_w 6 event at a given epicentral distance, is done by comparison with numerical signals provided by the FE model. The latter are considered as reliable, after the validation by comparison with records, presented in Section 3.4.4. The multi-input signal imposed in the FE model of the building in Nice is the reference signal for a M_w 6 event at Barcelonnette, obtained by applying the EGF procedure to signals recorded at the base of the building during the 2014 M_w 4.9 Barcelonnette earthquake. Acceleration time histories of the horizontal HN3 component at the top the building (V0 in Figure 3.1c), calculated by the proposed EGF procedure and the FE model (EGF+FEM), are compared in Figure 5.5.

The semi-empirical results are in good agreement with the finite element approach. The acceleration in some frequency bands is slightly overestimated by the FE model compared

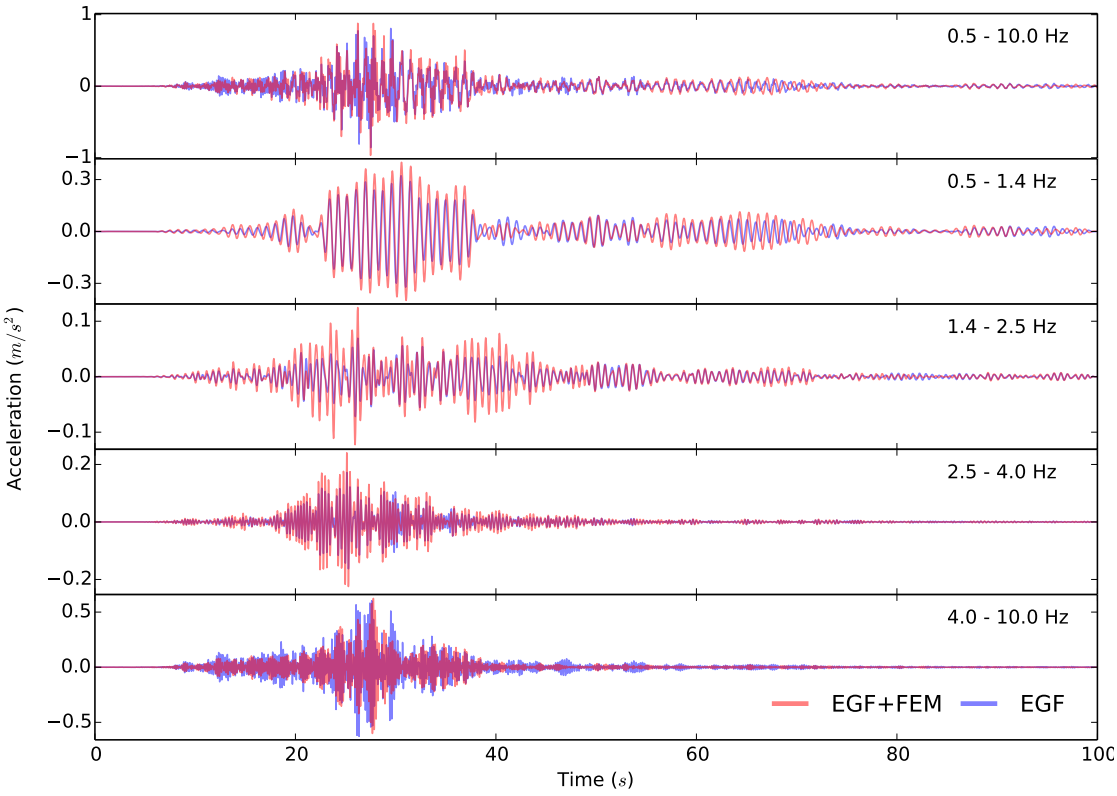

Figure 5.5 – HN3 horizontal acceleration component at the top of the building (V0), for different frequency bands: synthetic signal provided by EGF for a M_w 6 earthquake in Barcelonnette using 2014 event as small earthquake (EGF) and numerical signal obtained by the FE model with a synthetic ground motion as multiple input at the base (EGF+FEM) corresponding to a M_w 6 earthquake in Barcelonnette.

with both synthetics (Figure 5.5) and records (Figure 4.11). This remark allows concluding that generated synthetics reproduce records in a consistent way.

A comparison of time-frequency content using a short time Fourier transform of acceleration signals at the top of the building produced by EGF approach and FEM is shown in Figure 5.6. The results obtained using EGF show less amplification than the FE model at low and medium frequencies (B2, B3 and B4) and more for higher frequencies (B5). Consequently, spectrograms given by the proposed technique appear consistent with records (see Section 4.4).

The attained stress during the numerical simulation where the synthetic M_w 6 event related to the corroborates the assumption of linear material behavior. The maximum stress reached during the FEM simulation is of 6.78 MPa (22.6% of 30 MPa, that is the concrete resistance defined in the design phase).

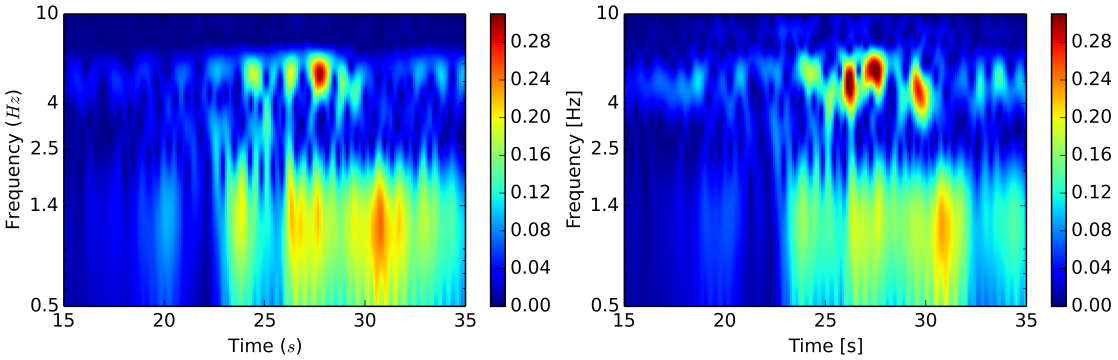

Figure 5.6 – Short time Fourier transform of the horizontal acceleration component HN3 at the top of the building (V0) given by EGF+FEM (left) and EGF (left) for a M_w 6 earthquake in Barcelonnette.

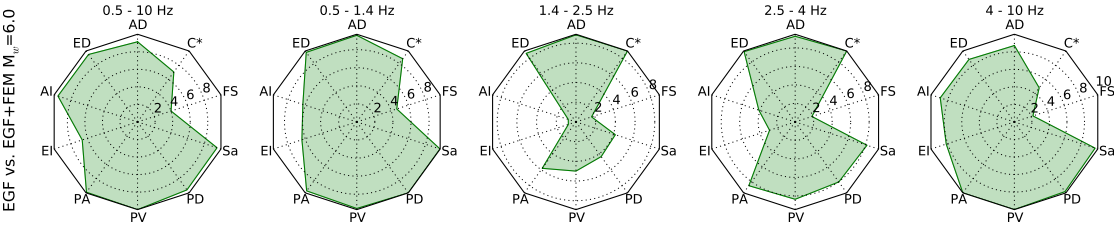

Figure 5.7 – Anderson's GoF scores for the comparison of the horizontal acceleration component HN3 at the top of the building (V0), obtained by EGF and EGF+FEM in the case of a M_w 6 earthquake in Barcelonnette, for different frequency bands. Evaluated parameters include Arias duration (AD), energy duration (ED), Arias intensity (AI), energy integral (EI), peak acceleration (PA), peak velocity (PV), peak displacement (PD), pseudo-acceleration response spectra (Sa) and Fourier spectra (FS) and cross correlation (C*).

5.5.2 Quantitative comparison

Figure 5.7 shows the GoF scores using Anderson's criteria (Anderson, 2004), presented in Section 4.5, obtained for synthetic and numerical signals at the top of the building, provided by the proposed EGF procedure and by the FEM with the stronger reference ground motion obtained by EGF as multi-input excitation at the base (indicated as EGF+FEM in the following figures).

The proposed procedure can not be directly validated by comparison with records because its goal is basically the generation of synthetic events with a magnitude higher than that of available records. Nevertheless, the trend of GoF scores is similar when comparing numerical signals, given by the FEM, with both records and synthetics provided by the proposed EGF technique. Consequently, generated synthetics appear consistent with records. A good fit is obtained for all parameters except Fourier spectrum, when the total frequency range is

considered (B1 in Figure 5.7). Peak acceleration, velocity and displacement are reported in Table 5.1. Some other parameters are compared in Figure 5.8.

Table 5.1 – Values of Peak Acceleration, Velocity and Displacement for synthetic (EGF) and numerical (FEM) horizontal component (HN3) at the top of the building (V0) during the reference M_w 6 earthquake at Barcelonnette.

Band	PA [m/s^2] $\times 10^{-3}$		PV [m/s] $\times 10^{-3}$		PD [m] $\times 10^{-3}$	
	EGF	EGF+FEM	EGF	EGF+FEM	EGF	EGF+FEM
B1	879.49	965.53	65.93	68.42	7.53	9.10
B2	321.94	399.59	49.00	59.24	7.41	8.71
B3	71.85	124.69	6.46	11.84	0.59	1.14
B4	171.82	240.57	8.72	12.41	0.45	0.67
B5	608.88	616.47	18.77	18.16	0.61	0.54

5.5.3 Prediction at any story from records at the top of the building

The proposed application of EGF can be used to predict the response of the building at any level where recordings are available. However, a combination of such approach with Kanai-Yoshizawa formulation (Section 5.2) enables to estimate the response at any level (from EGF simulations) in the case where only one recording is available at the top of the building. Figure 5.9 shows the comparison of the empirical signals generated directly from records at the floor level (EGF) with the application of KY formulation to the empirical simulation at the top of the building (EGF+KY), for the M_w 6.0 event (presented in Section 5.4). Similarly to the comparison with records (see Figure 5.9), the KY formulation overestimates the story responses on the Nice prefecture building. This effect is probably explained because the studied building has an important bending behavior (ignored by the KY formulation which only consider shear deformations) and rocking effects. It seems to work better for many structures (as shown in Ebrahimian et al. 2016).

The combination of EGF + KY enables to approximate the response at any level of the building, to an earthquake, by only having a sensor at the top of the building. This is extremely interesting since it is the configuration of many existing instrumented buildings (and it is cheaper than disposing a dense array).

5.6 Actual limitations of the semi-empirical approach

The application of EGF to recordings at different floors of a building has some limitations that should be carefully considered. First, it acquires all limitations of the conventional EGF

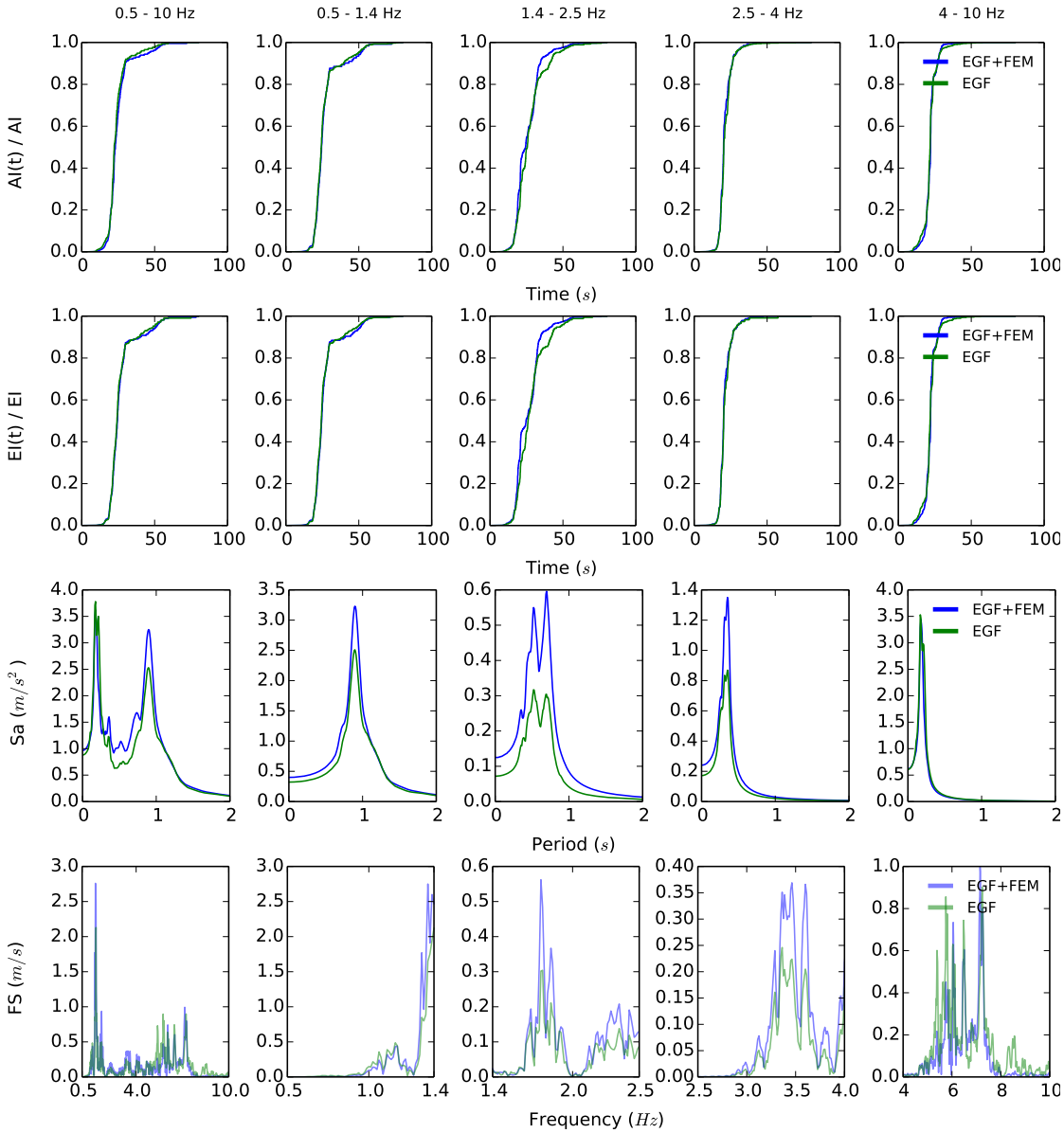

Figure 5.8 – Comparison of Arias integral, energy integral, elastic response spectrum in terms of pseudo-acceleration and Fourier spectrum for the HN3 horizontal acceleration component in the cases of synthetic signals generated at the top (V0) of the building (EGF) and numerical signals obtaining usisng EGF as seismic loading (EGF+FEM), during the reference M_w 6 earthquake in Barcelonnette.

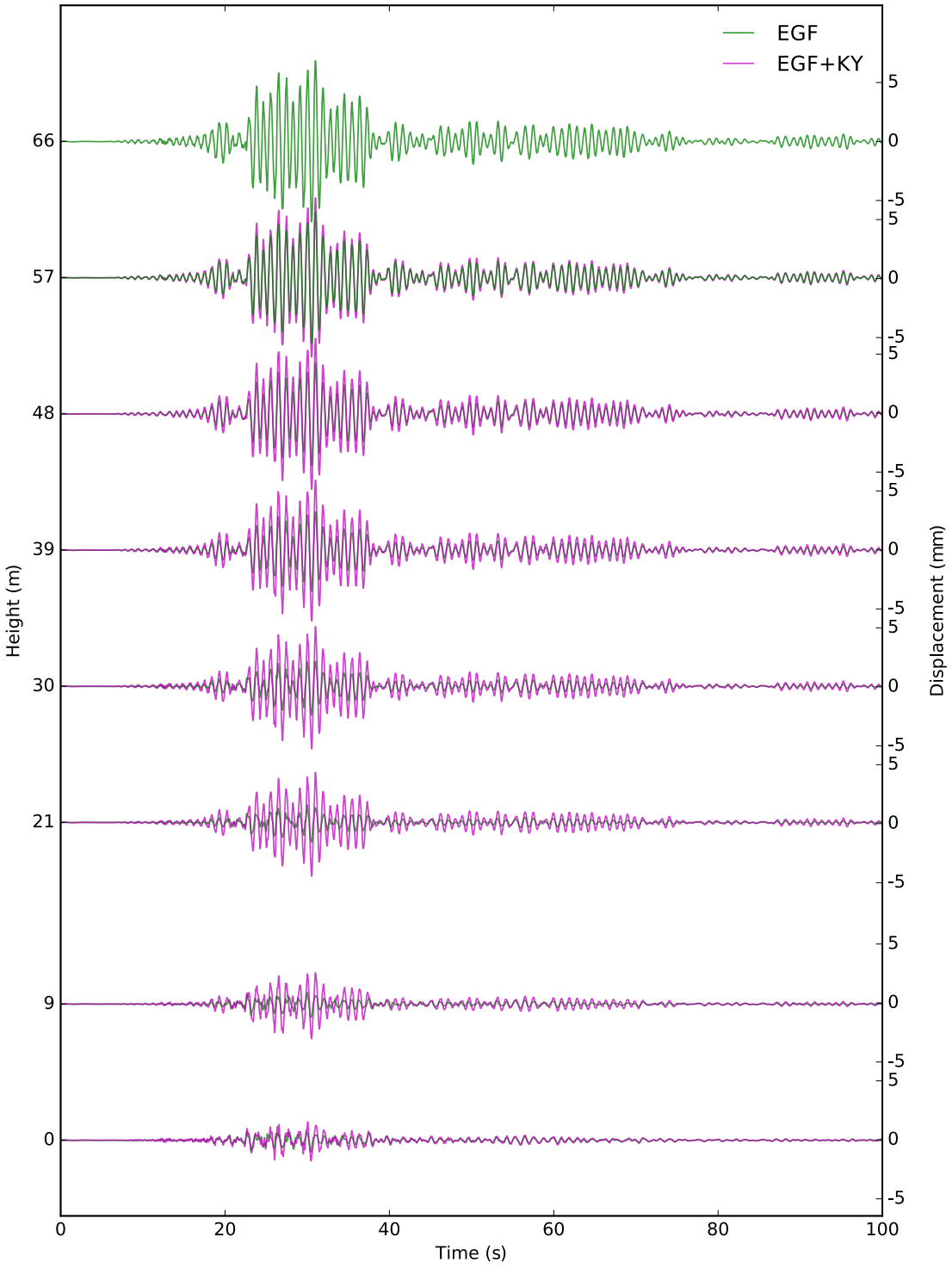

Figure 5.9 – Comparison of HN3 horizontal component of structural deformation at different heights of the building generated applying EGF procedure to records at the floor level (EGF) and approximated using Kanai-Yoshizawa formulation to EGF simulation at the top of the building (EGF + KY) related to the reference M_w 6 earthquake in Barcelonnette.

procedure as listed in Sections 5.3.1 and 5.3.2:

- The technique requires a record seismic event, with a suitable signal to noise ratio.
- The synthetic event has the same location and focal mechanism than the signal used as EGF.
- Only far field events (distance greater than the fault length) must be considered.
- The EGF simulation is currently based on linear superposition and do not account for nonlinear effects.

The last assumption represent a limitation also for the reproduction of building strong motion response, as it does not account for the nonlinearity of structural materials. Furthermore, soil-structure interaction causes considerable transitory reductions on resonant frequencies (observed also in the range of behavior of materials) during ground motions. Such effects are not present on the recorded event and the frequency content of the synthetic signals do not reveal such variation. This could lead to underestimations of the seismic response. These limitations are acceptable for a simplified approach to avoid modeling and computing time demanded by numerical simulation, when construction plans and material properties are not available for existing buildings.

Further work is done to take into account nonlinear effects on EGF ground simulations. The transfer function (TF) of a soil providing where local site effects are observed suffer, under strong motions, modifications with respect to the case of small seismic events and consequent linear behavior of soil (Beresnev et al., 1995a,b). Régnier et al. (2013) quantify the impact of such nonlinear behavior of the site response in terms of amplitude modification and frequency shift. A benchmark of numerical methods that try to reproduce such effects is carried out in the context of the PRENOLIN project (Régnier et al., 2015b,a). A similar tendency is observed in the TF of buildings under strong motion (decrease of amplitude and frequency values). According to the TF modification, a correction can be done for the generation of stronger ground motion using EGF and the same approach could be applied for buildings.

In the case of the EGF + KY formulation, where acceleration signals at the floor level are obtained from EGF synthetics at the roof level, it need to be considered that the approach is based on a shear beam theory and base rotations are neglected. Hence, buildings presenting rocking effects may not be well reproduced (as the studied building).

5.7 Conclusions

An extension of the empirical Green's function method is proposed to generate the structural response of existing buildings to earthquakes, stronger that those registered in the analyzed seismic area, from records of previous events. Such approach do not require to consider a model of the structure or to calibrate any mechanical parameter. Hence, it could be used as simplified approach when structural plans or information about materials are not available to allow precise numerical modeling.

Acceleration time histories at different floors of the building are generated (for a refence M_w 6.0 earthquake) using empirical Green's functions (from records of Barcelonnette M_w 4.9 earthquake at an epicentral distance of 100km). Numerical responses using a detailed three-dimensional model (MI) are obtained (by imposing the simulated ground motion of the M_w 6.0 earthquake) to verify the validity of the proposed approach. A quantitative comparison is done measuring acceleration, velocity and displacement peaks, as well as Arias intensity, energy integral, Fourier spectra and response spectra. The signals generated trough EGF show an excellent goodness of fit with numerical signals, without the need of any modeling hypothesis.

Applying EGF approach to reproduce building response appears interesting to reduce modeling and computing time for existing buildings in spite of limitations. The hypothesis of linear constitutive behavior of the medium through which waves propagate is adopted. Additionally, the source of the simulated event has the same location and focal mechanism than the original event.

Consequently, this method can be used to generate moderate amplitude synthetic signals in buildings at large enough epicentral distances. In the case where only records at the roof of the structure are available, Kanai-Yoshizawa formulation can be used to estimate the structural deformation at different floors, or even the ground motion.

Finally, note that the implementation of certain nonlinearities in EGF is possible and is currently object of research.

6 Identification of mechanical parameters from ambient vibration interferometry: modeling buildings as fixed-base Timoshenko beams

Contents

An identification procedure of mechanical parameters from ambient vibration records, for a dynamically equivalent beam model of buildings, is presented in this Chapter. The equivalent model can be used to simulate the response of the building to earthquakes, without the need of structural details or strong motion records.

Section 6.2 introduces how deconvolution interferometry can be used to identify dynamical properties of an existing building from records. The selected equivalent model that fit the dynamic behavior of the studied building is a Timoshenko beam, the theory and formulation is presented in Section 6.3. In Section 6.4, transfer functions and a wave dispersion imaging technique are used to fit the model in terms of wave dispersion, natural frequencies, and shear to compressional wave velocities in the medium. The selection of equivalent cross-sectional dimensions, Poisson ratio and modulus of elasticity to mass density ratio, estimated under the assumption of homogeneous isotropic material, is done in Section 6.5. Section 6.6 compares the time-history responses of the equivalent model, during earthquakes, with records.

The proposed method can be applied to buildings having bending-type structural behavior under seismic loading. Moreover, it is shown in Section 6.4.2 that wave propagation velocities in the building exhibit transitory variations with environmental conditions. Using short time windows of sixty seconds of noise is enough to obtain stable impulse response functions, which remain dependent of environmental variability, while stacking long time windows of noise filters out such variations. Consequently, the proposed technique is suitable for rapid in-situ surveys.

6.1 Introduction

Numerical modeling of buildings requires construction drawings, information about structural components and the knowledge of mechanical parameters of materials. Expensive computations as site-city interaction simulations demand simplified models of buildings, that can be considered equivalent from a dynamic point of view.

Guéguen et al. (2002) use elementary oscillators to model the structure-soil-structure interaction (SSSI) at the scale of a city, considering a group of buildings in their urban environment. Kham et al. (2006) model site-city interaction using the boundary element method and consider buildings as elementary oscillators with only one degree of freedom. Mazzieri et al. (2013) simulate site-city interaction effects using the spectral element method and parallelepipeds to represent the buildings, which are modeled by homogeneous blocks rigidly connected to the soil. Taborda and Bielak (2011) and Isbiliroglu et al. (2015) propose to model three-dimensional SSSI on regional scale using a set of blocks and fitting mechanical properties that allow reproducing the fundamental frequency of buildings. In addition to three-dimensional numerical simulations, another approach to investigate effects of SSSI consist of experimental tests to conceive passive seismic control devices as that proposed by Cacciola and Tombari

(2015). Design of this kind of device requires the knowledge of dynamic properties of structures that must be protected.

Computation time and modeling difficulties, especially when structural plans are not available, can be avoided by taking advantage of identification techniques. In this context, the global dynamic behavior of a building can be reproduced using a fixed-base beam model, whose mechanical parameters can be obtained by the analysis of motion recordings. However, extensive measurement campaigns need an easy procedure for dynamic identification of buildings, in the perspective of post-earthquake damage detection.

The proposed procedure has the aim to obtain dimensions and mechanical parameters of a fixed-base beam model, composed of an homogeneous and isotropic material, dynamically equivalent to a building whose geometry and material properties are unknown. In this context, Hans et al. (2005) and Boutin et al. (2005) relate mode shapes and natural frequencies of buildings, obtained from in-situ measurements, to their mechanical properties. They define a seismic integrity threshold to assess structures during seismic diagnosis, concluding that the Timoshenko beam model describes the dynamic behavior of the analyzed buildings with good accuracy. Michel (2007) use the natural frequency ratios to determine if the building response is principally controlled by bending or shear behavior, fitting an equivalent Timoshenko beam. He tests the model on five buildings, showing good reproduction of frequency values and modal shapes for the three first modes of the structures. Rahmani and Todorovska (2013) propose an equivalent one-dimensional system for applications such as structural health monitoring, using earthquake recordings and seismic interferometry for identification of buildings. The model consists of a layered shear beam and the fitting is done in terms of impulse response functions (IRF). Ebrahimian et al. (2014b) analyze the wave propagation and dispersion in buildings, showing the reliability of using a Timoshenko beam model for bending type structural behavior under seismic loading, compared with a layered beam model. The previous research of Ebrahimian et al. (2014a) concludes that Timoshenko beam model may be appropriate for reinforced concrete buildings with shear walls. Wave dispersion in a Timoshenko beam is mainly caused by bending and, consequently, it is suitable for representing a bending type structural behavior. Cheng and Heaton (2015) simulate the response of a building using modal summation on a Timoshenko beam model that considers soil-structure interaction. They use the first two translational modes in a particular direction to derive building dynamic properties. Su et al. (2016) describes the response spectrum analyses on a non-uniform Timoshenko beam model to provide a rapid assessment of the seismic performance of an existing building from in-situ vibration tests.

Seismic interferometry is a classical technique to estimate the Green's function between pairs of receivers. In a vertical array configuration, the objective is to determine the local wave velocity profiles between the deepest and the topmost sensors, under the hypothesis of vertical incident plane waves (Mehta et al., 2007a,b; Snieder, 2007; Miyazawa et al., 2008; Parolai et al., 2009). Applied to buildings, it enables to observe the wave propagation across the structure and it is a tool employed in several studies where earthquake recordings are used (Snieder et al., 2006; Snieder and Safak, 2006; Kohler et al., 2007; Todorovska and Trifunac, 2008a,b). Ambient vibrations are recently used as source of excitation (Prieto et al., 2010; Nakata and Snieder, 2013; Bindi et al., 2014). Nakata and Snieder (2013) observe that wave velocities in the medium obtained from ambient noise vibrations are more stable than those issued from earthquake data. The exploitation of noise vibration is of special interest in regions with low seismicity, avoiding the need to wait for an earthquake to happen, and providing data with temporary measurement campaigns using non-permanent instrumentation installed inside the structures.

In seismic interferometry, long time windows of noise are traditionally analyzed. Prieto et al. (2010) use a window between one and fifty days in thirty second intervals, while Nakata and Snieder (2013) stack two weeks of data to obtain a stable velocity estimation. Bindi et al. (2014) analyze different duration intervals, from few hours to days. The present study intends to evaluate if short range time windows of ambient noise can give stable IRFs with enough signal-to-noise ratios. In such context, the variability of building dynamic properties with environmental conditions has to be considered. Mikael et al. (2013) show the strong influence of temperature in natural frequencies and damping. It is discussed in this Chapter that wave velocity, as other dynamic parameters of the building, may exhibit transitory variations depending on external factors.

The resistance to lateral loads, in the high-rise reinforced concrete building of the case study (Section 3.2), is assured by structural walls. Following Ebrahimian et al. (2014b), a Timoshenko beam model, equivalent to the analyzed building, is assumed in this research with the perspective of structural identification. A frequency-wavenumber slant-stack technique, which is generally employed in dispersion imaging of the subsurface using ambient noise data and enables to obtain the phase velocity of a propagating pulse at different frequencies, is applied to IRFs. The resulting velocity image can be fitted using the analytical dispersion curve for forced vibration response of a Timoshenko beam (Timoshenko, 1921) excited by base motion. The fitting of the equivalent beam model to the real structure is done in terms of natural frequencies and wave propagation velocities, which allows the identification of mechanical

parameters.

6.2 Application of interferometry to buildings

A great starting point to get into the application of seismic interferometry on buildings are the works of Snieder and Safak (2006). They show how the building motion depends not only on the building structure mechanical properties, but also on the interaction with soil and the frequency content of excitation. They observe the propagation of waves across the structure and how a virtual source can be placed at any level of the building by setting a reference sensor and deconvolve recordings of sensors in other positions against with respect to the reference one. Curtis et al. (2006) give a further explication of the underlying physics of seismic interferometry.

The choice of the virtual source location allows isolating the structure from the soil if the reference sensor is at the ground level and consider the whole structure-soil system if the reference sensor is at the roof level. As seen in Figure 6.1, interferograms change considerably by changing the position of the reference sensor.

The resonant frequencies can be identified by observing the amplitude of the spectrum of waves deconvolved with respect to records of a sensor at the ground level. The velocity of the shear waves propagating across the building are found by picking interferograms obtained by deconvolution with respect to recordings of a sensor at the roof level.(Figure 6.1b).

Deconvolution with respect to records at the ground level enables to identify modal properties as done using other OMA techniques, but with the advantage of be able to isolate the building from the soil-structure coupling. Deconvolution with respect to recordings at the roof level provides interesting data that allow an equivalent beam model of the building to be constrained.

6.3 Equivalent beam model of a building

A one-dimensional model for buildings is adopted in the case where a detailed structural model is not necessary or available. This research aims to determine mechanical parameters and cross-sectional dimensions of the equivalent homogeneous fixed-base beam, whose length corresponds to the building height. The values obtained by the proposed identification procedure do not correspond to the mechanical parameters of the building material, or dimensions in the floor plan of the building. They represent numerical values that match the

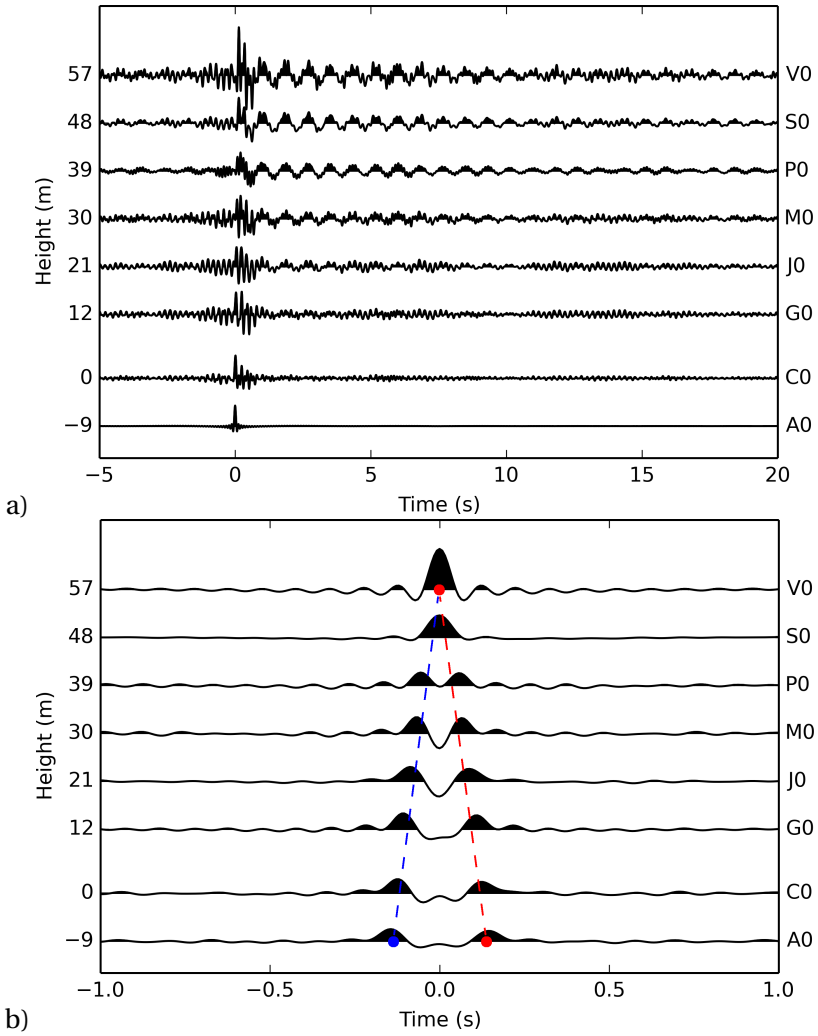

Figure 6.1 – Interferograms using records of the 2014 Barcelonnette earthquake deconvolved with respect to the sensor at the bottom (a) and by the sensor at the top of the building (b). The identification of the propagation path from the acausal and causal waves to estimate the wave velocity is shown in blue and red, respectively.

Figure 6.2 – (a) Perspective view of the Nice prefecture building. (b) Horizontal section of building structure.

dynamic behavior of the structural system as a whole, including soil-structure interaction effects.

6.3.1 Case study

The proposed methodology is applied to the Nice prefecture building (Figure 6.2a), located in southern France. The high-rise reinforced concrete building is composed of two identical 66 m high towers with cantilever reinforced concrete shells rigidly fixed at each floor and it is permanently monitored by 24 accelerometers at different levels. A detailed explanation of the instrumental set-up can be found in Section 3.2.

The seismic response of a building as a whole, excited by base motion, can be distinguished in

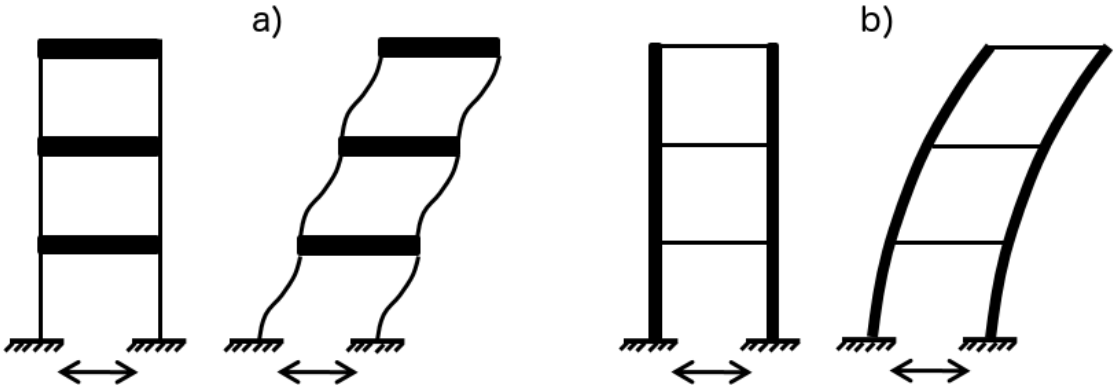

Figure 6.3 – Shear (a) and bending (b) type structural behavior of a building under seismic loading.

shear type structural behavior (Figure 6.3a), in the case of a frame system with stiffer floors compared with columns, and bending type structural behavior (Figure 6.3b), for a wall bearing structure or a dual frame-wall system. The adopted Timoshenko beam model considers a high-rise building where resistance to lateral loads is contributed mainly by structural walls. In this model, wave dispersion is principally caused by bending and it is derived from the uncoupled equations of motion of the beam (Timoshenko, 1921; Reis, 1978).

6.3.2 Timoshenko beam model

Timoshenko beam theory assumes small deformations and cross-sections that remain plane but not normal to the beam axis during deformation. The model accounts for shear and flexural deformation and rotary inertia. The equivalent building model is a uniform cantilever Timoshenko beam, excited by horizontal motion $u_g(t)$ at the base (Figure 6.4a). The beam length is assumed equal to the building height H. Material properties are the mass density ρ and moduli of elasticity in compression and shear, E and $G = E/(2(1+\nu))$, respectively, where ν is the Poisson ratio. Cross-section shape parameters are the shear correction coefficient, assumed as $\chi = 5(1+\nu)/(6+5\nu)$ (Timoshenko, 1922; Kaneko, 1975) and the radius of gyration $r = \sqrt{I/A}$, where $A = bh$ is the area of the rectangular cross-section of width h and depth b (Figure 6.4) and I is the moment of inertia according to the horizontal motion direction. The Timoshenko beam approach considers a not negligible shear strain γ, with loss of orthogonality between cross-section and the beam axial direction z. Consequently, the transverse deformation becomes $\partial u/\partial z = \phi + \gamma$, where $u(z,t)$ and $\phi(z,t)$ are the relative transverse displacement and the rotation of the cross-section at the location z (Figure 6.4), at a time instant t. According to Timoshenko (1921), the dynamic equilibrium equations of a

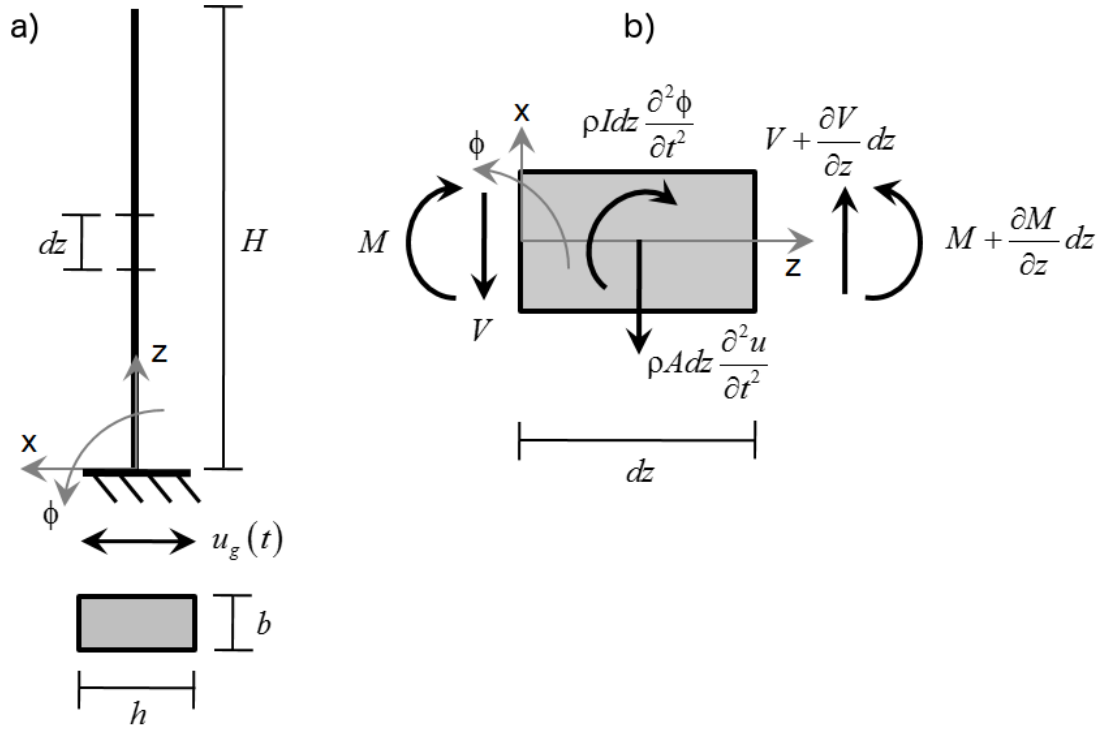

Figure 6.4 – (a) Cantilever Timoshenko beam equivalent to the analyzed building. (b) Free body diagram of a beam segment.

beam segment (Figure 6.4b) can be expressed as

$$\begin{cases} \frac{\partial V}{\partial z} dz - \rho A dz \frac{\partial^2 u}{\partial t^2} = 0 \\ \frac{\partial M}{\partial z} dz + V dz - \rho I dz \frac{\partial^2 \phi}{\partial t^2} = 0 \end{cases} \tag{6.1}$$

where generalized stresses V and M are the shear force and flexural moment, respectively, defined as $V = \chi GA\gamma = \chi GA(\partial u/\partial x - \phi)$ and $M = EI\partial\phi/\partial x$. Replacing these expressions, equation (6.1) becomes

$$\begin{cases} c_s^2 \left(\frac{\partial^2 u}{\partial z^2} - \frac{\partial \phi}{\partial z} \right) - \frac{\partial^2 u}{\partial t^2} = 0 \\ c_p^2 \frac{\partial^2 \phi}{\partial z^2} + \frac{c_s^2}{r^2} \left(\frac{\partial u}{\partial z} - \phi \right) - \frac{\partial^2 \phi}{\partial t^2} = 0 \end{cases} \tag{6.2}$$

where $c_p = \sqrt{E/\rho}$ and $c_s = \sqrt{\chi G/\rho}$ have dimensions of propagation velocities in the medium. According to the formulation presented by Reis (1978), replacing in equation (6.2) transverse

displacement and rotation, expressed as

$$\begin{cases} u(z,t) = U \exp\left[i\left(kz - \omega t\right)\right] \\ \phi(z,t) = \Phi \exp\left[i\left(kz - \omega t\right)\right] \end{cases} \tag{6.3}$$

yields

$$\begin{cases} \left(\omega^2 - c_s^2 k\right) U - \left(i\, k c_s^2\right) \Phi^2 = 0 \\ \left(i\, \frac{k c_s^2}{r^2}\right) U + \left(\omega^2 - c_p^2 k^2 - \frac{c_s^2}{r^2}\right) \Phi = 0 \end{cases} \tag{6.4}$$

that are two coupled linear equations in U and Φ. In equation (6.3), U and Φ are the displacement and rotation amplitudes, respectively, ω is the angular frequency and k is the wavenumber. The dispersion relation

$$c_s^2 c_p^2 k^4 - \left(c_s^2 + c_p^2\right) \omega^2 k^2 + \omega^4 \left(1 - \frac{c_s^2}{\omega^2 r^2}\right) = 0 \tag{6.5}$$

is obtained by imposing the determinant of the coefficient matrix of the system of equations (6.4) equal to zero. Equation (6.5) is a biquadratic equation which has the following four roots:

$$k = \pm \frac{\omega}{\sqrt{2} c_p} \sqrt{\left(1 + \frac{c_p^2}{c_s^2}\right) \pm \sqrt{\left(1 - \frac{c_p^2}{c_s^2}\right)^2 + 4 \frac{c_p^2}{\omega^2 r^2}}} \tag{6.6}$$

The solution

$$k_1 = + \frac{\omega}{\sqrt{2} c_p} \sqrt{\left(1 + \frac{c_p^2}{c_s^2}\right) + \sqrt{\left(1 - \frac{c_p^2}{c_s^2}\right)^2 + 4 \frac{c_p^2}{\omega^2 r^2}}} \tag{6.7}$$

gives a propagating wave and it is the one used in this research. Two other solutions give an evanescent wave until a cut-off frequency and a propagating wave afterward. The reader is referred to Ebrahimian et al. (2014b) for a complete discussion about the solutions of equation (6.6) and their domain of validity. The variation of the analytical dispersion curve in equation (6.7), by modifying E/ρ, is shown in Figure 6.5 for a given beam with different cross-sections, but having length equal to the analyzed building height.

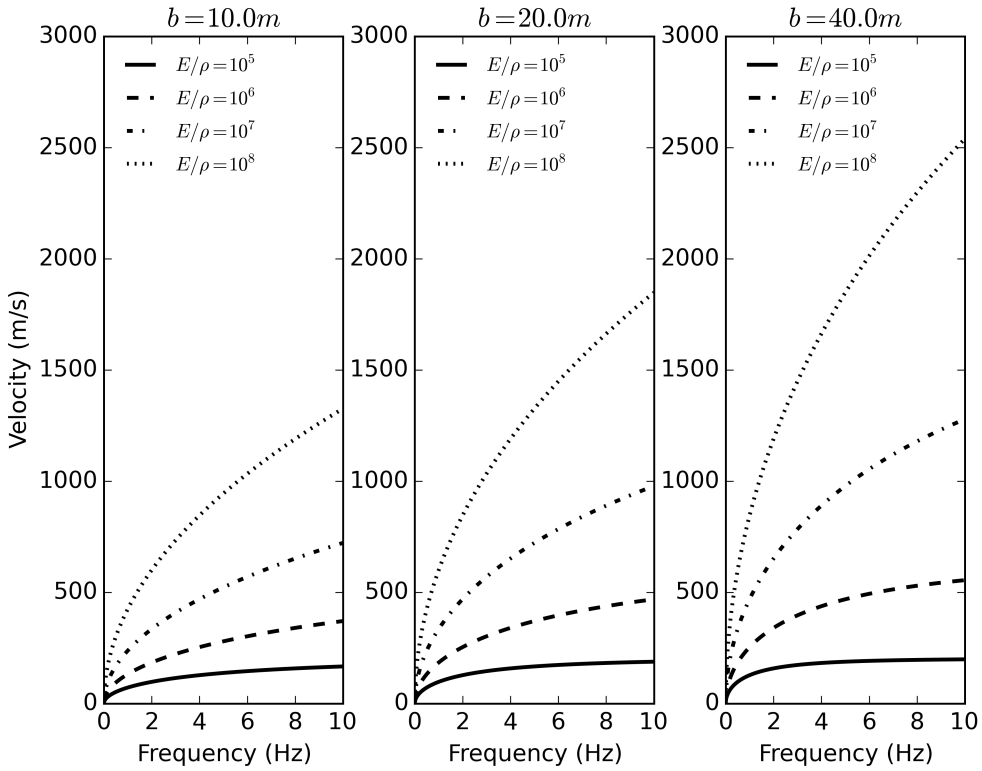

Figure 6.5 – Variation of the dispersion curve with the elasticity modulus to density ratio for a beam of 66 m long, H, with rectangular cross-section of different width, b, and a constant depth, h, of 40m.

6.3.3 Fundamental frequencies of a 3D Timoshenko beam

Fundamental fixed-base frequencies of a 3D Timoshenko beam (Figure 6.4a), are obtained solving the $6n_e$-dimensional eigenproblem $(\mathbf{K}-\omega^2\mathbf{M})\Phi = \mathbf{0}$, where n_e is the number of 2-node beam elements used in the spatial discretization (refer to Timoshenko 1921, for a more detailed derivation of the problem). Each 2-node beam element has 6 degrees of freedom per node. Roots of the eigenproblem ω are the natural angular frequencies and Φ is the modal matrix. The mass-normalization of matrix Φ implies $\Phi^T\mathbf{M}\Phi = \mathbf{I}$ and $\Phi^T\mathbf{K}\Phi = \Omega^2$, where Ω is the diagonal matrix of natural frequencies and $\mathbf{I}$ is a $6n_e$-dimensional identity matrix. The mass matrix $\mathbf{M}$ and stiffness matrix $\mathbf{K}$ result from the assemblage of (12x12)-dimensional matrices as $\mathbf{M}_e$ and $\mathbf{K}_e$, respectively, of each beam element e, which are expressed in global coordinates xyz as $\mathbf{K}_e = \Lambda^T\bar{\mathbf{K}}_e\Lambda$ and $\mathbf{M}_e = \Lambda^T\bar{\mathbf{M}}_e\Lambda$. The (12x12)-dimensional rotation matrix Λ^T permits to transform displacements and rotations from local to global coordinates.

The stiffness and mass matrix for a Timoshenko beam element, expressed in local coordinates, for a 2-node beam element e of length H_e, employed for the spatial discretization of the beam model of the building, are evaluated, respectively as

$$
\tilde{\mathbf{K}}_e = \begin{pmatrix}
\frac{AE}{H_e} & 0 & 0 & 0 & 0 & 0 & -\frac{AE}{H_e} & 0 & 0 & 0 & 0 & 0 \\
0 & \frac{12EI_y}{H_e^3(\psi_x+1)} & 0 & 0 & 0 & \frac{6EI_y}{H_e^2(\psi_x+1)} & 0 & -\frac{12EI_y}{H_e^3(\psi_x+1)} & 0 & 0 & 0 & \frac{6EI_y}{H_e^2(\psi_x+1)} \\
0 & 0 & \frac{12EI_x}{H_e^3(\psi_y+1)} & 0 & -\frac{6EI_x}{H_e^2(\psi_y+1)} & 0 & 0 & 0 & -\frac{12EI_x}{H_e^3(\psi_y+1)} & 0 & -\frac{6EI_x}{H_e^2(\psi_y+1)} & 0 \\
0 & 0 & 0 & \frac{GJ}{H_e} & 0 & 0 & 0 & 0 & 0 & -\frac{GJ}{H_e} & 0 & 0 \\
0 & 0 & -\frac{6EI_x}{H_e^2(\psi_y+1)} & 0 & \frac{EI_x(\psi_y+4)}{H_e(\psi_y+1)} & 0 & 0 & 0 & \frac{6EI_x}{H_e^2(\psi_y+1)} & 0 & \frac{EI_x(-\psi_y+2)}{H_e(\psi_y+1)} & 0 \\
0 & \frac{6EI_y}{H_e^2(\psi_x+1)} & 0 & 0 & 0 & \frac{EI_y(\psi_x+4)}{H_e(\psi_x+1)} & 0 & -\frac{6EI_y}{H_e^2(\psi_x+1)} & 0 & 0 & 0 & \frac{EI_y(-\psi_x+2)}{H_e(\psi_x+1)} \\
-\frac{AE}{H_e} & 0 & 0 & 0 & 0 & 0 & \frac{AE}{H_e} & 0 & 0 & 0 & 0 & 0 \\
0 & -\frac{12EI_y}{H_e^3(\psi_x+1)} & 0 & 0 & 0 & -\frac{6EI_y}{H_e^2(\psi_x+1)} & 0 & \frac{12EI_y}{H_e^3(\psi_x+1)} & 0 & 0 & 0 & -\frac{6EI_y}{H_e^2(\psi_x+1)} \\
0 & 0 & -\frac{12EI_x}{H_e^3(\psi_y+1)} & 0 & \frac{6EI_x}{H_e^2(\psi_y+1)} & 0 & 0 & 0 & \frac{12EI_x}{H_e^3(\psi_y+1)} & 0 & \frac{6EI_x}{H_e^2(\psi_y+1)} & 0 \\
0 & 0 & 0 & -\frac{GJ}{H_e} & 0 & 0 & 0 & 0 & 0 & \frac{GJ}{H_e} & 0 & 0 \\
0 & 0 & -\frac{6EI_x}{H_e^2(\psi_y+1)} & 0 & \frac{EI_x(-\psi_y+2)}{H_e(\psi_y+1)} & 0 & 0 & 0 & \frac{6EI_x}{H_e^2(\psi_y+1)} & 0 & \frac{EI_x(\psi_y+4)}{H_e(\psi_y+1)} & 0 \\
0 & \frac{6EI_y}{H_e^2(\psi_x+1)} & 0 & 0 & 0 & \frac{EI_y(-\psi_x+2)}{H_e(\psi_x+1)} & 0 & -\frac{6EI_y}{H_e^2(\psi_x+1)} & 0 & 0 & 0 & \frac{EI_y(\psi_x+4)}{H_e(\psi_x+1)}
\end{pmatrix}
$$

$$
\bar{\mathbf{M}}_e = \rho AH \begin{pmatrix}
\frac{1}{3} & 0 & 0 & 0 & 0 & 0 & \frac{1}{6} & 0 & 0 & 0 & 0 & 0 & 0 & 0 \\
0 & \frac{13}{35}+\frac{6I_y}{5AH_e^2} & 0 & 0 & 0 & \frac{11H_e}{210}+\frac{I_y}{10AH_e} & 0 & \frac{9}{70}-\frac{6I_y}{5AH_e^2} & 0 & 0 & 0 & 0 & -\frac{13H_e}{420}+\frac{I_y}{10AH_e} & \\
0 & 0 & \frac{13}{35}+\frac{6I_x}{5AH_e^2} & 0 & -\frac{11H_e}{210}-\frac{I_x}{10AH_e} & 0 & 0 & 0 & \frac{9}{70}-\frac{6I_x}{5AH_e^2} & 0 & \frac{13H_e}{420}-\frac{I_x}{10AH_e} & 0 & 0 & \\
0 & 0 & 0 & \frac{J}{3A} & 0 & 0 & 0 & 0 & 0 & \frac{J}{6A} & 0 & 0 & 0 & \\
0 & 0 & -\frac{11H_e}{210}-\frac{I_x}{10AH_e} & 0 & \frac{H_e^2}{105}+\frac{2I_x}{15A} & 0 & 0 & 0 & -\frac{13H_e}{420}+\frac{I_x}{10AH_e} & 0 & -\frac{H_e^2}{140}-\frac{I_x}{30A} & 0 & 0 & \\
0 & \frac{11H_e}{210}+\frac{I_y}{10AH_e} & 0 & 0 & 0 & \frac{H_e^2}{105}+\frac{2I_y}{15A} & 0 & \frac{13H_e}{420}-\frac{I_y}{10AH_e} & 0 & 0 & 0 & 0 & -\frac{H_e^2}{140}-\frac{I_y}{30A} & \\
\frac{1}{6} & 0 & 0 & 0 & 0 & 0 & \frac{1}{3} & 0 & 0 & 0 & 0 & 0 & 0 & \\
0 & \frac{9}{70}-\frac{6I_y}{5AH_e^2} & 0 & 0 & 0 & \frac{13H_e}{420}-\frac{I_y}{10AH_e} & 0 & \frac{13}{35}+\frac{6I_y}{5AH_e^2} & 0 & 0 & 0 & 0 & -\frac{11H_e}{210}-\frac{I_y}{10AH_e} & \\
0 & 0 & \frac{9}{70}-\frac{6I_x}{5AH_e^2} & 0 & -\frac{13H_e}{420}+\frac{I_x}{10AH_e} & 0 & 0 & 0 & \frac{13}{35}+\frac{6I_x}{5AH_e^2} & 0 & \frac{11H_e}{210}+\frac{I_x}{10AH_e} & 0 & 0 & \\
0 & 0 & 0 & \frac{J}{6A} & 0 & 0 & 0 & 0 & 0 & \frac{J}{3A} & 0 & 0 & 0 & \\
0 & 0 & \frac{13H_e}{420}-\frac{I_x}{10AH_e} & 0 & -\frac{H_e^2}{140}-\frac{I_x}{30A} & 0 & 0 & 0 & \frac{11H_e}{210}+\frac{I_x}{10AH_e} & 0 & \frac{H_e^2}{105}+\frac{2I_x}{15A} & 0 & 0 & \\
0 & -\frac{13H_e}{420}+\frac{I_y}{10AH_e} & 0 & 0 & 0 & -\frac{H_e^2}{140}-\frac{I_y}{30A} & 0 & -\frac{11H_e}{210}-\frac{I_y}{10AH_e} & 0 & 0 & 0 & 0 & \frac{H_e^2}{105}+\frac{2I_y}{15A} &
\end{pmatrix}
$$

where beam cross-sectional parameters are the constant area A, the moments of inertia I_x and I_y with respect to x and y axis, respectively, shape factors xz and yz for transverse shear and the second moment of area J. Mechanical parameters of the material are the mass density ρ and the modulus of elasticity in compression and shear E and G, respectively.

A fixed base and free surface are imposed as boundary conditions at the bottom and the top, respectively.

6.4 Information obtained from records

Even if the dimensions in the horizontal plan of the studied building are very different (see Figure 6.2b), natural frequencies corresponding to the first two bending modes are closely spaced, due to the orientation of reinforced concrete towers. The results of a frequency domain decomposition analysis (Brincker et al., 2001a) are shown in Figure 6.6 to discuss modal properties of the structure. Two singular values of the power spectral density matrix are shown to enable the identification of close modes (this is necessary when rigidity in both horizontal directions are similar, hence selected modal frequencies have similar values that cannot be separated by looking at a Fourier spectrum). The first order bending modes in both horizontal directions are found around 1.2 Hz, a torsional mode around 1.6 Hz, and the second order bending modes are located around 3.8 Hz.

All analyzed accelerometric recordings are linearly detrended and tapered using a 5% Hanning window. A fourth-order Butterworth filter is used each time the signals are filtered. HN2 horizontal component of acceleration, recorded at different heights of the building, during the 8^{th} April 2014 M_w 4.9 Barcelonnette earthquake (epicentral distance of 100 km northwards from the building) and an arbitrary ambient noise time window, are shown in Figure 6.7a and Figure 6.7b, respectively.

6.4.1 Transfer function and deconvolution procedure

The transfer function (TF) provides information about the relationship between the frequency content of signals at different locations. It is defined as the ratio of Fourier transform of acceleration at different heights and it is expressed as

$$TF^{z}_{z_0}(\omega) = \frac{\mathscr{F}_z(\omega)}{\mathscr{F}_{z_0}(\omega)} \tag{6.8}$$

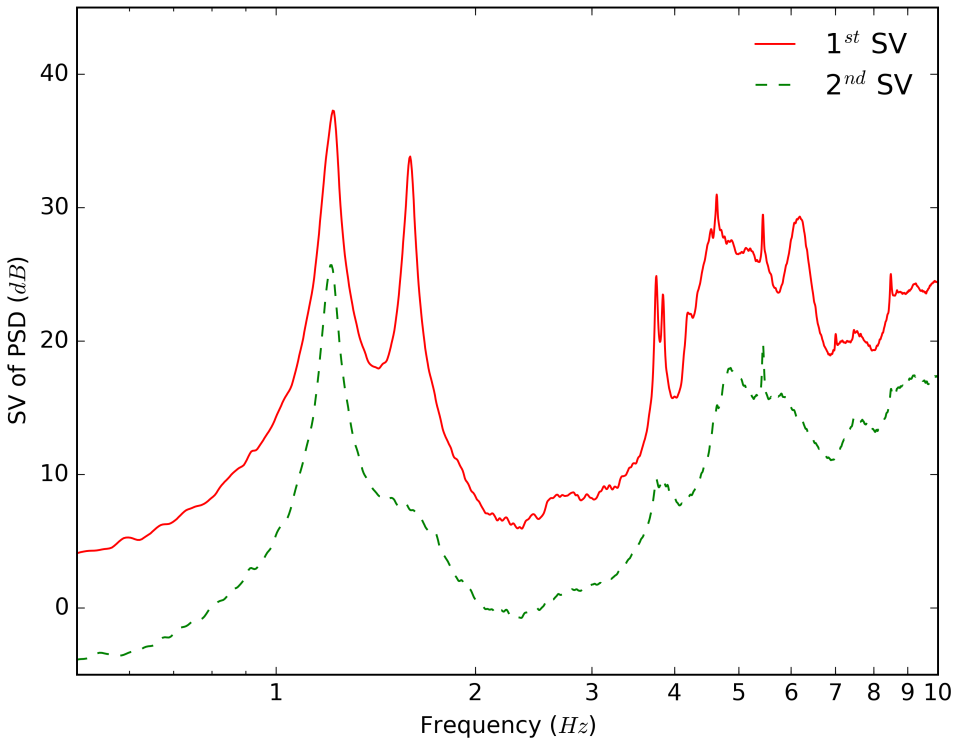

Figure 6.6 – Two first singular values of power spectral density obtained using the frequency domain decomposition analysis for the studied building.

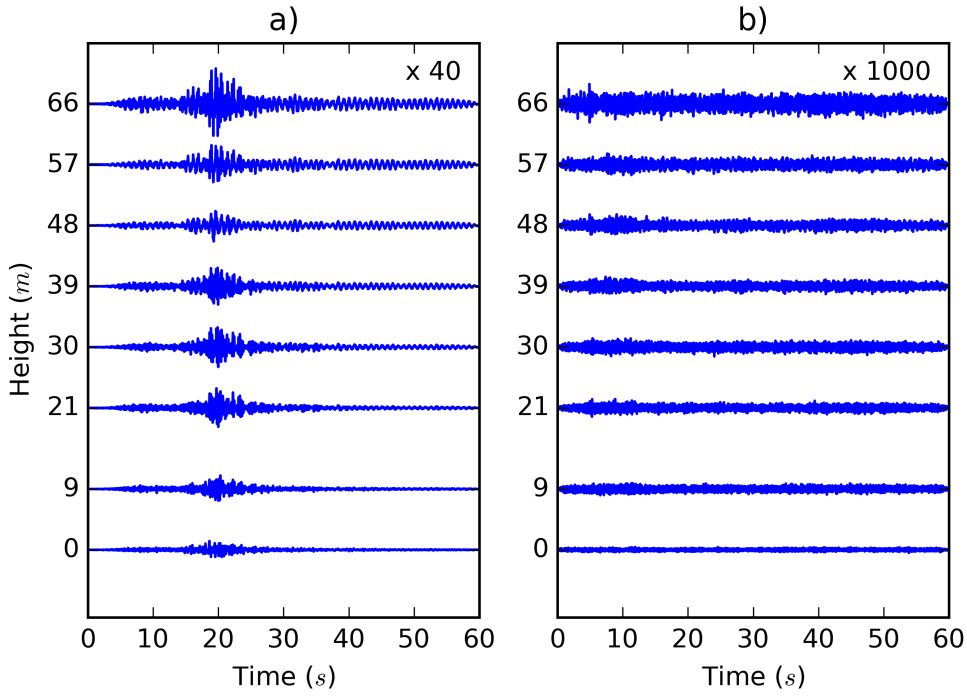

Figure 6.7 – Horizontal acceleration recordings (HN2 component) at different floors of the building during (a) the 2014 Mw 4.9 Barcelonnette earthquake and (b) 60s of ambient vibration.

where $\mathscr{F}_z(\omega)$ and $\mathscr{F}_{z_0}(\omega)$ are the Fourier transform of acceleration at an observed height z and at a reference height z_0, respectively.

According to the description of Nakata and Snieder (2013), the calculation of an impulse response function (IRF) using deconvolution is carried out as

$$IRF^{z}_{z_0}(t) = \sum_{n=1}^{N}\left[\mathscr{F}^{-1}\left\{\frac{\mathscr{F}^{n}_{z}(\omega)}{\mathscr{F}^{n}_{z_0}(\omega)}\right\}\right] \approx \sum_{n=1}^{N}\left[\mathscr{F}^{-1}\left\{\frac{\mathscr{F}^{n}_{z}(\omega)\mathscr{F}^{n*}_{z_0}(\omega)}{\left|\mathscr{F}^{n}_{z_0}(\omega)\right|^2 + \alpha\langle\left|\mathscr{F}^{n}_{z_0}(\omega)\right|^2\rangle}\right\}\right] \tag{6.9}$$

where N is the number of time windows of the stacking process (required for stability), $\mathscr{F}^{n}_{z}$ is the Fourier transform of the n^{th} time window of motion component recorded at height z, ω is the angular frequency, t is time, $\mathscr{F}^{-1}$ is the inverse Fourier transform operator, $*$ represents the complex conjugate, $\langle|\mathscr{F}_z|^2\rangle$ is the average power spectrum of $\mathscr{F}_z$ and $\alpha = 0.5\%$ is a regularization parameter stabilizing the deconvolution. Basically, the IRF represent the TF in the time-domain, which leads to a clearer visual interpretation of the phase content of the signal.

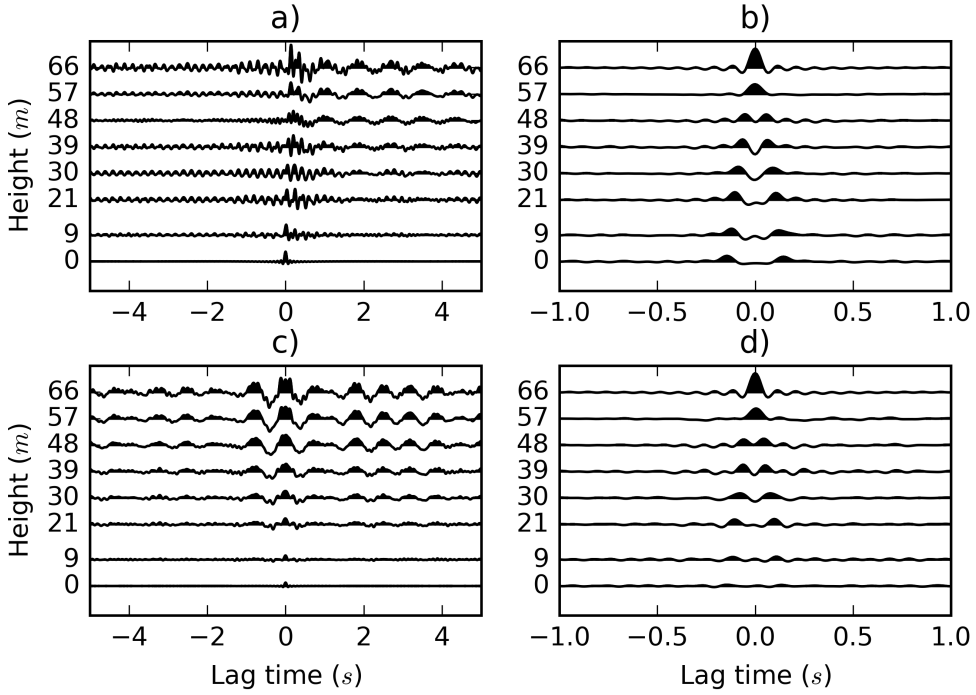

Figure 6.8 – Impulse response functions of the recorded HN2 component of motion, obtained by deconvolution with respect to the signal at the base (a) and top (b) of the building during the 2014 M_w 4.9 Barcelonnette earthquake and at the base (c) and top (d) of the building during 60 s of ambient vibration. High frequencies are removed for clarity purpose using a 10 Hz low pass filter.

6.4.2 IRFs for building identification

Interferometry has been more often applied, in buildings, to earthquake data than to ambient noise recordings. Figure 6.8a and Figure 6.8b show the IRFs of accelerometric data from the 2014 M_w 4.9 Barcelonnette earthquake deconvolved by the bottom and the top, respectively. Accelerometric records used to produce IRFs in Figure 6.8 are low pass filtered to 10 Hz.

Deconvolution with respect to the recording of sensor at the building base represents a spectral division by the input motion at the ground level, enhancing the modal content of the structure. The building response continues after the excitation has passed creating stationary IRFs (created by different waves that are related to the modal shapes of the building). Seismic IRFs are characterized by a more important contribution of higher frequency modes (Figure 6.8a), compared to those obtained from ambient noise (Figure 6.8a), directly related to the nature of the excitation. Deconvolution with respect to the recording of sensor at the top of the building represents a spectral division by the signal at the roof level, that is dominated by its modal

content, hence removing the participation of the stationary waves created by the modes of the structure. It leaves a single acausal (up-going) and causal (down-going) wave that propagates trough the building (Figure 6.8b and 6.8d), caused by the input motion that enters and leaves the building without making it enter in resonance (although it may seem like a single pulse, it contains different frequencies). Hence, the lag time of the maximum peak of the pulse can be measured picking from the IRFs, to estimate the phase wave propagation velocity in the building (in a given frequency range), expressed as

$$c_{a-b}^{ph} = \frac{H}{t_{a-b}} \tag{6.10}$$

where t_{a-b} is the time taken by causal (down going) waves, from seismograms filtered between frequencies a and b, to travel trough the structure.

As shown in Figure 6.9, the picked lag time from IRFs is strongly dependent on the analyzed frequency band. This happens because higher frequency waves propagate faster in the building, according to the dispersion curve for the Timoshenko beam model (see Figure 6.5).

Traditionally, long periods of noise are stacked when seismic interferometry is applied to soil characterization studies, to get a better signal-to-noise ratio and stabilize the IRFs. The same approach has been adopted for buildings, stacking several days of signals (Prieto et al., 2010; Nakata and Snieder, 2013; Bindi et al., 2014).

Figure 6.8c and Figure 6.8d show the impulse response functions of a sixty second noise window deconvolved by the bottom and the top, respectively. It is observed that the IRF has enough signal-to-noise ratio, however, if the analysis is repeated across a day, the IRF changes. Figure 6.10 shows the variation of wave velocity (measured according to equation (6.10) applying a 10 Hz low pass filter), fundamental frequency and temperature (measured at the exterior of the building) across three days, which suffers of daily variations, as also observed for the fundamental frequency This variability of wave velocity observed in Figure 6.10 is not due to measurement errors, but to transitory modifications of the structural behavior due to external factors (such as temperature oscillations).

The relation between environmental conditions (especially temperature) and building dynamic parameters has already been observed (Mikael et al., 2013). Stacking IRFs over a period of more than one day averages the results, filtering out the daily variation. However, even stacking several days, seasonal variations would not be taken into account. Sixty second noise windows are thus adopted in this analysis, to show that stable IRFs are obtained even without

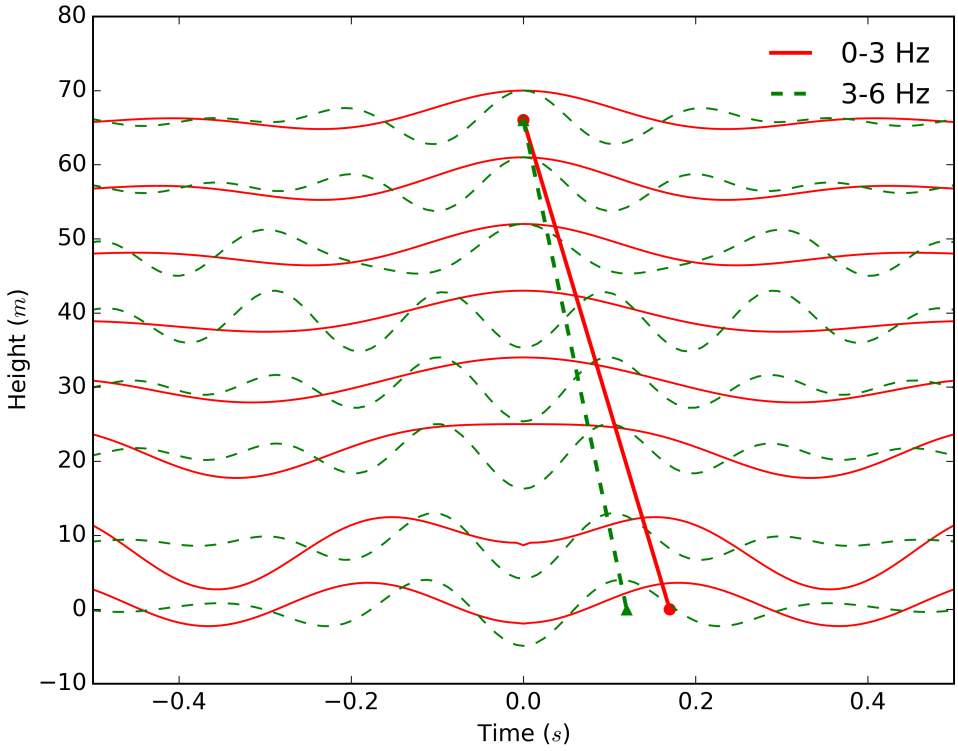

Figure 6.9 – Impulse response functions obtained by deconvolution with respect to the signal at the top of the building, filtering the signal in two different frequency bands. Thick lines represent the trajectory of causal waves by picking the phase lag time arrival at the bottom.

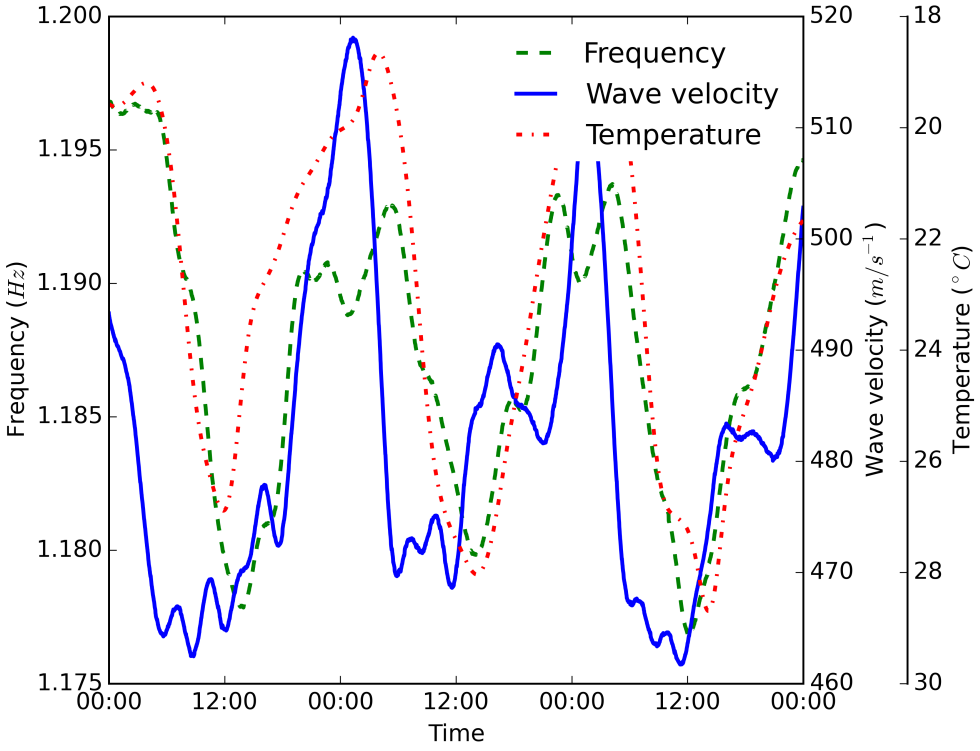

Figure 6.10 – Smoothed variation of wave velocity, fundamental frequency and temperature during three days. One sample per minute is calculated.

stacking, even though they are inevitably affected by the variation of structural parameters with environmental conditions.

6.4.3 Estimation of compression to shear wave velocity ratio

An array including vertical motion component allows the measurement of compressional wave velocity along the structure. The permanent instrumentation of the investigated building, installed in 2010, is composed, at the floor levels, of accelerometers recording only horizontal components of motion. Nevertheless, data from a temporary survey undertaken in 2007, using triaxial velocimeters recording at 250 Hz, has been exploited for this analysis. Vertical component of motion at the top and bottom of the building is used to measure compressional wave velocity through the structure.

Half an hour of recordings are stacked to produce smoothed IRFs using a Konno Ohmachi (Konno and Ohmachi, 1998) window, which enables to pick the lag times without need to filter high frequencies. Figure 6.11 shows the smoothed IRFs in the horizontal (HN2, HN3) and vertical (HNZ) directions. The shear wave velocity v_s, corresponding to each horizontal component of motion (v_{HN2} = 540 m/s, v_{HN3} = 490 m/s), and compressional wave velocity v_p (v_{HNZ} = 2750 m/s), are obtained by equation (6.10).

6.4.4 Dispersion images of recorded IRFs

A dispersion imaging technique is proposed for the analysis of IRF traces. It is a representation of variation in wave propagation velocity with frequency. IRF traces at different heights of the building can be processed as a common multi-offset record by a dispersion imaging technique commonly used for active seismic surveys under the assumption of plane wave propagation (Park et al., 1998). The scheme is based on the summation, at each frequency, of wave fields present in all traces traveling with a selected phase velocity. This operation produces a so-called dispersion image or dispersion spectrum. Similar techniques, known as slant-stack techniques, have been applied by Gouédard et al. (2008) to retrieve Rayleigh wave dispersion images from noise cross-correlations at local scale.

The procedure consists in an initial calculation of the time-frequency Fourier transform $\mathscr{F}_{z_j}(\omega)$ of each j^{th} IRF trace at height z_j. A phase-shift $\phi = -i\omega\Delta t_j = -i\omega z_j/c$ is applied to the Fourier transform of the j^{th} trace before summation, for each scanning phase velocity c. Then, the

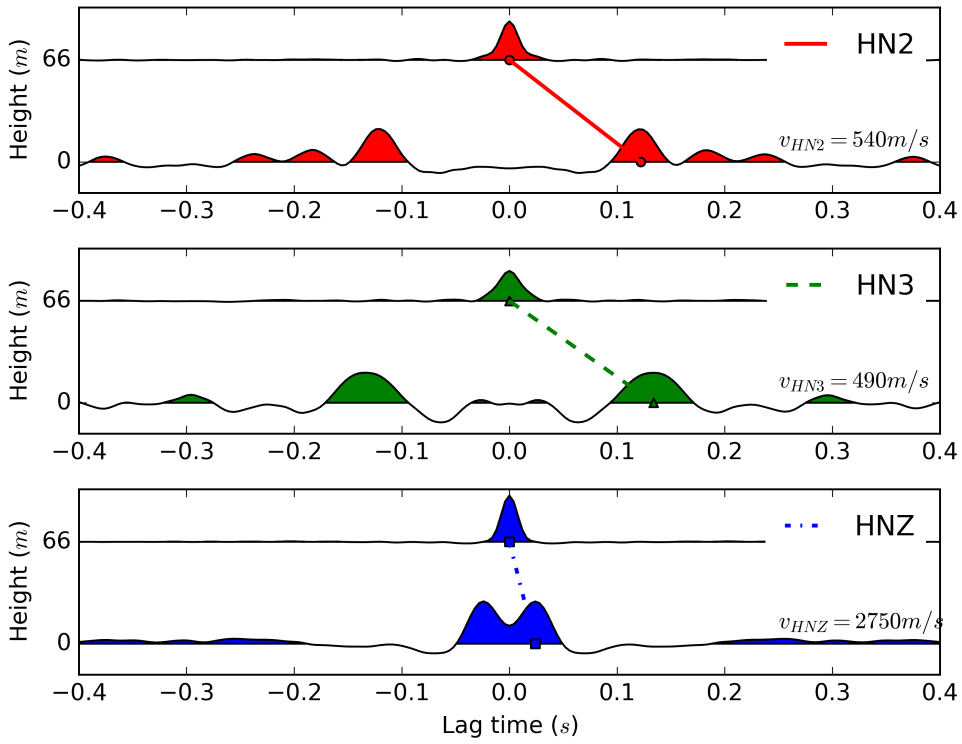

Figure 6.11 – Smoothed impulse response functions obtained using deconvolution with a virtual source at the top of the building, for different propagation directions (HN2, HN3, HNZ). Data have been acquired during a temporary instrumentation campaign where velocimeters have been used. Wave propagation arrival times are picked and the propagation paths are indicated.

relative spectral power $E(\omega, c)$ is calculated as

$$E(\omega, c) = \left| \sum_j \mathscr{F}_{z_j}(\omega) \cdot \exp\left(-i\omega z_j / c\right) \right| \tag{6.11}$$

for each angular frequency ω and scanning phase velocity c. Different amplitude normalization procedures to account for attenuation and/or noise spectral characteristics may enhance the dispersion imaging result (Park et al., 2004). No whitening or offset dependent normalization is applied in this study.

Figures 6.12 and 6.13 show the wave velocity image obtained using IRFs of 60s noise signal deconvolved by the bottom and the top, respectively. It is observed in Figure 6.12 that the deconvolutions by the bottom are dominated by the modal content of the building. The stationary content of the signals enables to identify the modal frequencies (Figure 6.12), but makes impossible to define a clear propagating pulse. When IRFs are calculated deconvolving by the top, the modal content is diminished and the voids in Figure 6.13 correspond to natural frequencies. The velocity of the propagating pulse can be determined corresponding to the frequencies that do not contribute to the building resonance (Figure 6.13).

According to the Timoshenko beam model, the wave propagation in the studied building follows the dispersion relation expressed in equation (6.7). As observed in Figure 6.13, the dispersion velocity image enables the identification of peaks that can be linked to provide a dispersion curve of waves propagating through the building. Such path can be matched using the analytical dispersion curve given by the Timoshenko beam theory (Figure 6.13).

The proposed methodology has limitations inherent to the array geometric characteristics. The range of wavelengths λ, considered as acceptable in this study, is limited by the aliasing limit $\lambda_{min} = 2d$ and the resolution limit $\lambda_{max} = 3D$, where d is the lower inter-station distance of neighboring stations and D is the maximum inter-station distance. The limits are chosen based on their reliability for phase velocity estimation in site characterization studies(Cornou et al., 2006). Aliasing and resolution limits are highlighted in Figures 6.12 and 6.13 by dashed lines. Wave velocities are also estimated using lag time picking c_{a-b}^{ph} (equation (6.10)) and from the building resonant frequencies of a uniform fixed-base layered beam c_n^{res} using the approximation $c_n^{res} = (4Hf_n)/(2n-1)$ (Ebrahimian et al., 2014a), where the n^{th} resonant velocity have the same natural frequency f_n as the building. The different values of wave velocities are displayed in Figure 6.13. As can be observed in this figure, the proposed dispersion velocity image enables a clearer interpretation of the propagation phenomena through the building

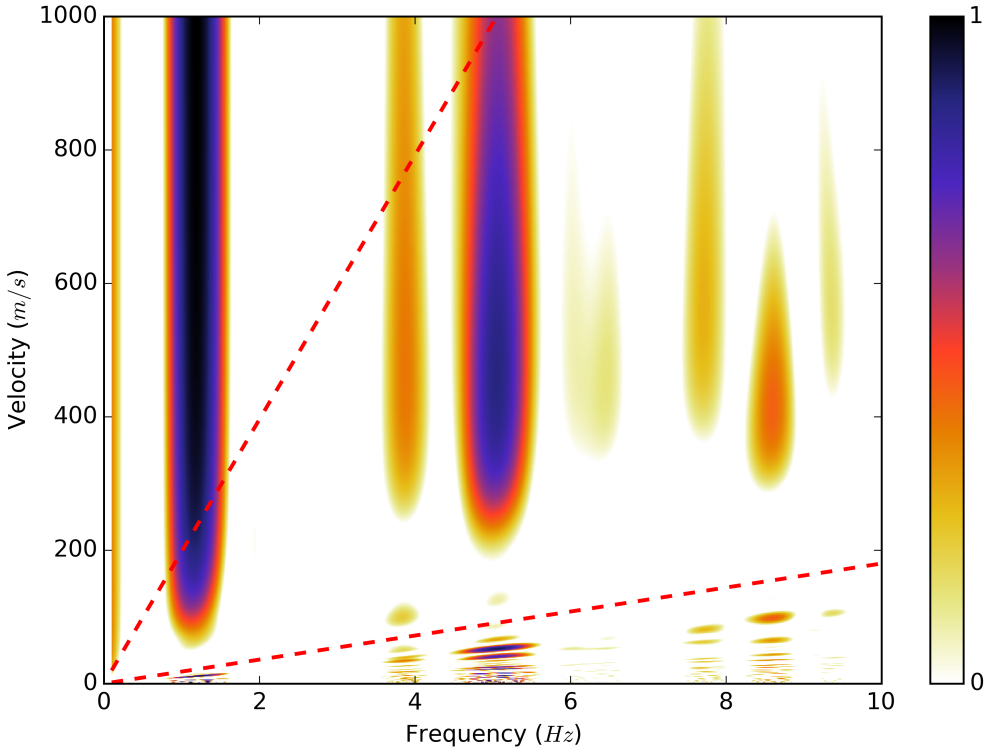

Figure 6.12 – Normalized wave velocity image with a virtual source at the bottom of the building. Considered frequency-wavenumber resolution limits are shown with a dashed line.

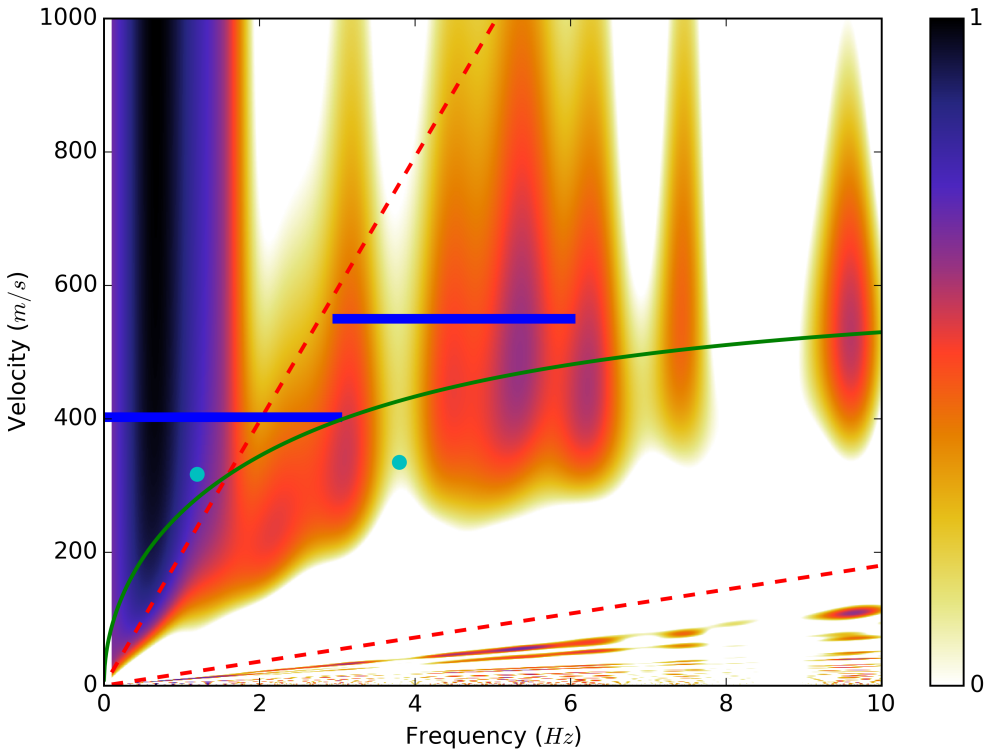

Figure 6.13 – Normalized wave velocity image with a virtual source at the top of the building. Frequency-wavenumber resolution limits are shown with dashed lines. Wave velocities estimated using resonant frequencies are highlighted by points and those points using picked phase arrival times by thick lines. Fitted analytical solution of the Timoshenko beam dispersion curve is shown using a thin straight line.

and enables to better constraint the dispersion curve given by the Timoshenko beam theory.

6.5 Identification of mechanical parameters for the equivalent model

The fitting of the Timoshenko beam model of a high-rise reinforced concrete building is undertaken through the comparison of the transfer functions, the dispersion images of phase velocity along the building and the ratio of compressional to shear wave velocities, obtained from in-situ recording analysis. The set of values (dimensions of the rectangular section and mechanical parameters) that represents the best agreement in terms of natural frequencies of the building and dispersion curve through the medium are selected as solution of the identification problem.

Boutin et al. (2005) observe that the $(n+1)^{th}$ to n^{th} natural frequency ratio for a fixed-base beam depend only on the dimensionless height H/r (building height to radius of gyration ratio) and the shear to compression modulus ratio G/E. Ebrahimian et al. (2014a) adopt cross-sectional dimensions for the beam model equal to the external width and depth of the building. Consequently, H/r is imposed and the unknown G/E is obtained using a first trial value deduced from the 2^{nd} to 1^{st} natural frequency ratio. The shear wave velocity is deduced by seismic interferometry.

In this work, no assumption is done about dimensions of the equivalent beam cross-section and its mechanical parameters. Only the beam length is assumed equal to the building height. In this manner, more accurate results can be obtained for buildings without equivalent stiffness in the two orthogonal directions.

The shear and compressional wave velocities in an elastic isotropic medium are related to the mechanical parameters according to the following expressions:

$$v_s = \sqrt{E/(2\rho(1+\nu))} \tag{6.12}$$

$$v_p = \sqrt{E(1-\nu)/(\rho(1+\nu)(1-2\nu))} \tag{6.13}$$

Then, the Poisson ratio can be obtained as function of the compressional to shear wave velocity

ratio, expressed as

$$\nu = (v_p^2/v_s^2 - 2)/(2(v_p^2/v_s^2 - 1)) \tag{6.14}$$

Numerical simulations considering simplified models of buildings require to assume a value of the Poisson ratio. For example, Mazzieri et al. (2013) considered that $v_p = 2.5v_s$ in buildings for a 3D site-city simulation. The measured compressional wave velocity is 5 to 6 times faster than shear wave velocities for the analyzed building (Figure 6.11). This yields to high values of ν (close to 0.5), being compressive stiffness much greater than the shear stiffness.

The values of width b, depth h, mass density ρ and modulus of elasticity in compression E for the equivalent beam, having assumed length equal to H, are obtained using the following procedure:

- Fix the Poisson ratio as function of the compressional to shear wave velocity ratio.
- The relative amount of shear to bending behavior that should be reproduced by the model is determined by the ratio between 1^{st} and 2^{nd} order flexural modes (in both horizontal directions).
- The section width, b, to depth, h, ratio is determined by the ratio between the 1^{st} flexural mode on each direction.
- The relation between the section dimensions to the homogeneous material properties (E and ρ) is determined by the value of the fundamental mode.

The specific values of E and ρ are irrelevant, the important is their ratio (as long as their ratio remains constant, the frequencies and dispersion curves remain identical, as can be observed in Figure 6.5). The final values of width b, depth h, mass density ρ and modulus of elasticity in compression E for the equivalent beam, having assumed length equal to H, are obtained by manual iteration until the best agreement between the numerical model and the recordings. It is important to remember that such values do not represent the properties of the reinforced concrete, but the whole building modeled as an homogeneous structure.

Natural frequencies and the analytical dispersion curve that fit the TF and the dispersion image, for the analyzed building, are plotted in Figure 6.14. The obtained geometrical and mechanical features are listed in Table 6.1. It is remarkably interesting to observe that the

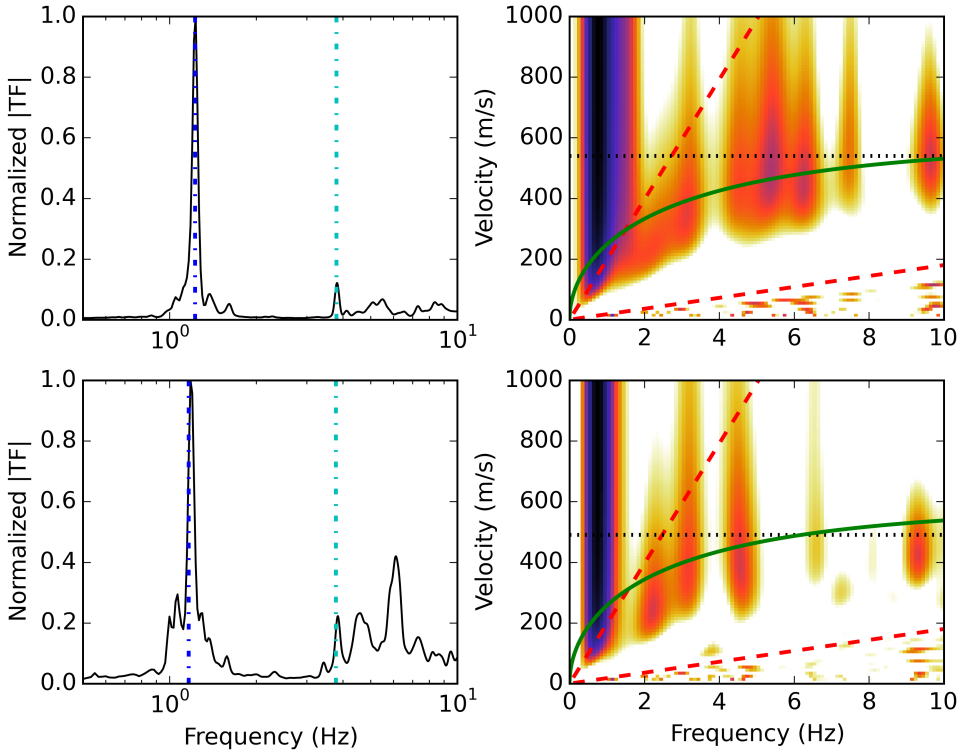

Figure 6.14 – Normalized transfer functions (left) and velocity spectrums (right), for the HN2 (up) and HN3 (down) horizontal components of the building motion. Natural frequencies (dash-point lines) of the building and analytical dispersion curve (straight line). Frequency-wavenumber resolution limits (dashed line). Picked shear wave velocities (dotted line).

section dimensions of the equivalent homogeneous model (35x38m) are quite different to those of the real building (17x60m), due to an non-uniform distribution of stiffness in both horizontal directions.

Table 6.1 – Values of parameters that fit the dynamic behavior of the building.

H (m)	b (m)	h (m)	ρ (kg/m^3)	E (GPa)	ν
66	35	38	830	1	0.48

6.6 Response simulation using a Timoshenko beam

The equivalent model using a Timoshenko beam is intended to be a simplification of a detailed three-dimensional finite element model. Some motivations for its use could be unavailability of structural details, time to create a detailed mesh, need of a less time consuming simulation.

The range of validity of the simplified model need to be determined.

The three-dimensional model of the Nice prefecture building has been presented in Section 3.4. The numerical seismic response to the 2014 Barcelonnette earthquake, in the case of fixed and non-rotating base and where the same seismic load is applied to all the base (FEM-SI), is shown in Section 4.3. An equivalent Timoshenko beam model is identified to verify the proposed procedure in terms of seismic response. The triaxial excitation, recorded at the bottom of the building during the 2014 Barcelonnette earthquake (Figure 4.2), is applied as seismic loading at the fixed base of the beam model (TB).

6.6.1 Qualitative comparison

The comparison of the horizontal component HN3 of both FEM-SI and TB models, in different frequency bands (see Table 3.3), is presented in Figure 6.15, for 2014 Barcelonnette earthquake. The first, third and fourth modes are isolated in frequency bands B2, B3 and B4, respectively. Acceleration time-history shows a good amplitude and phase correlation in these frequency ranges. If the perpendicular direction (HN2) is also analyzed, the first 5 modes are properly reproduced by the TB model.

However, higher modes (band B5) are not well reproduced, and their contribution to the broad response (band B1) of the TB model is almost neglected when compared to FEM-SI.

6.6.2 Quantitative comparison

A quantitative comparison of the goodness of fit of the deformation time history provided by the equivalent TB model is done using Anderson's criteria (Section 4.5). A representation of GoF scores of the seismic response of the Nice prefecture building to the 2014 Barcelonnette earthquake evaluated using the TB model, compared with the FEM-SI model, is shown in Figure 6.16. Numerical and recorded peak acceleration, velocity and displacement are reported in Table 6.2. Some other estimated parameters are shown in Figure 4.17.

The quantitative comparison confirms an excellent reproduction of lower modes (up to the fifth natural frequency), and the inability to reproduce higher modes (and consequently their contribution to the global response). As shown in Figure 6.18, modes higher than the 5^th correspond in this study case to local modes caracterized by the movement of fixed plates and hence cannot be reproduced using an homogeneous beam model.

The identification of building mode shapes higher than the first five trough the use of record-

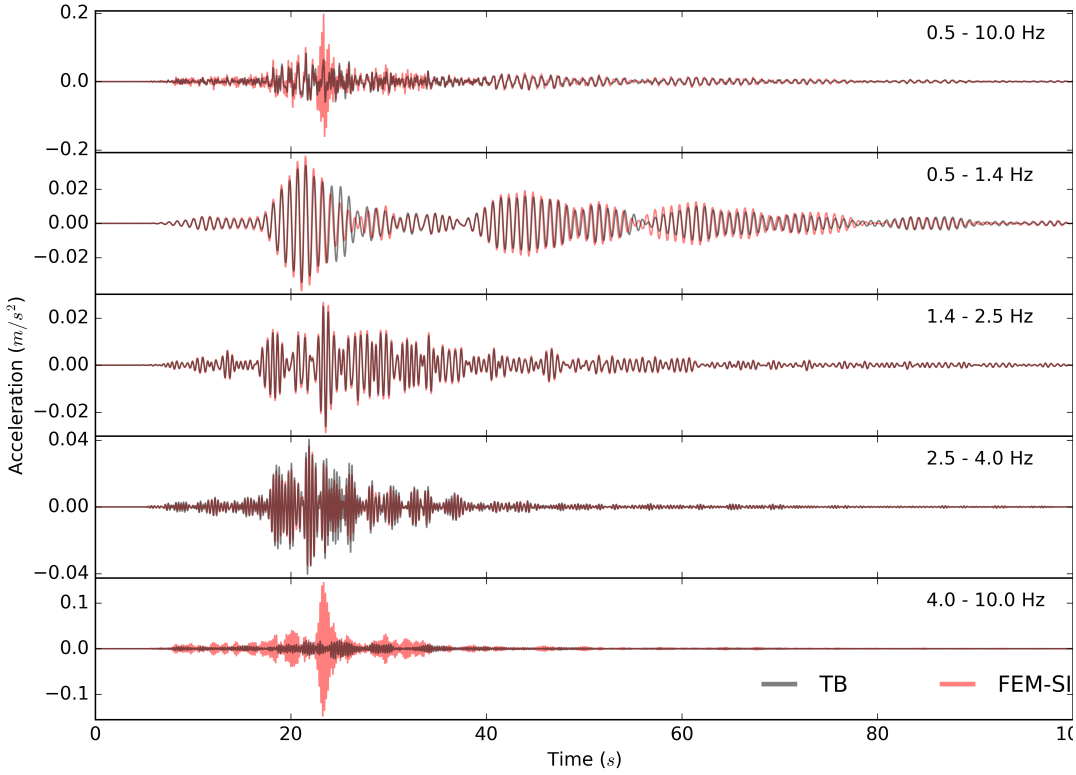

Figure 6.15 – Numerical response in terms of horizontal acceleration (HN3) at the top (V0) of the detailed 3D model of the building (FEM-SI) and the equivalent Timoshenko beam (TB) under the three components of the 2014 Barcelonnette earthquake for different frequency bands.

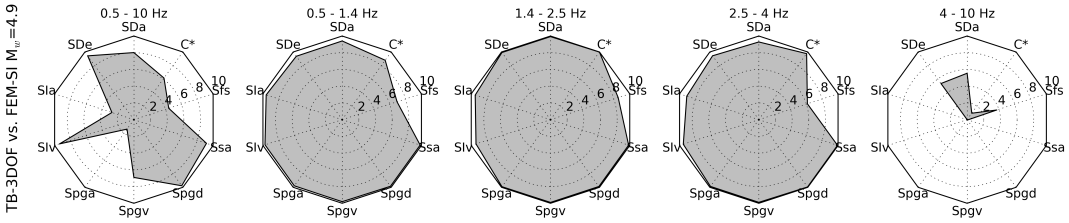

Figure 6.16 – Anderson's GoF scores for the comparison of the horizontal acceleration component HN3 at the top of the building (V0), obtained by an equivalent Timoshenko beam (TB) and a detailed three-dimensional model (FEM-SI) during the 2014 Barcelonnette earthquake, for different frequency bands. Evaluated parameters include Arias duration (AD), energy duration (ED), Arias intensity (AI), energy integral (EI), peak acceleration (PA), peak velocity (PV), peak displacement (PD), pseudo-acceleration response spectra (Sa) and Fourier spectra (FS) and cross correlation (C*).

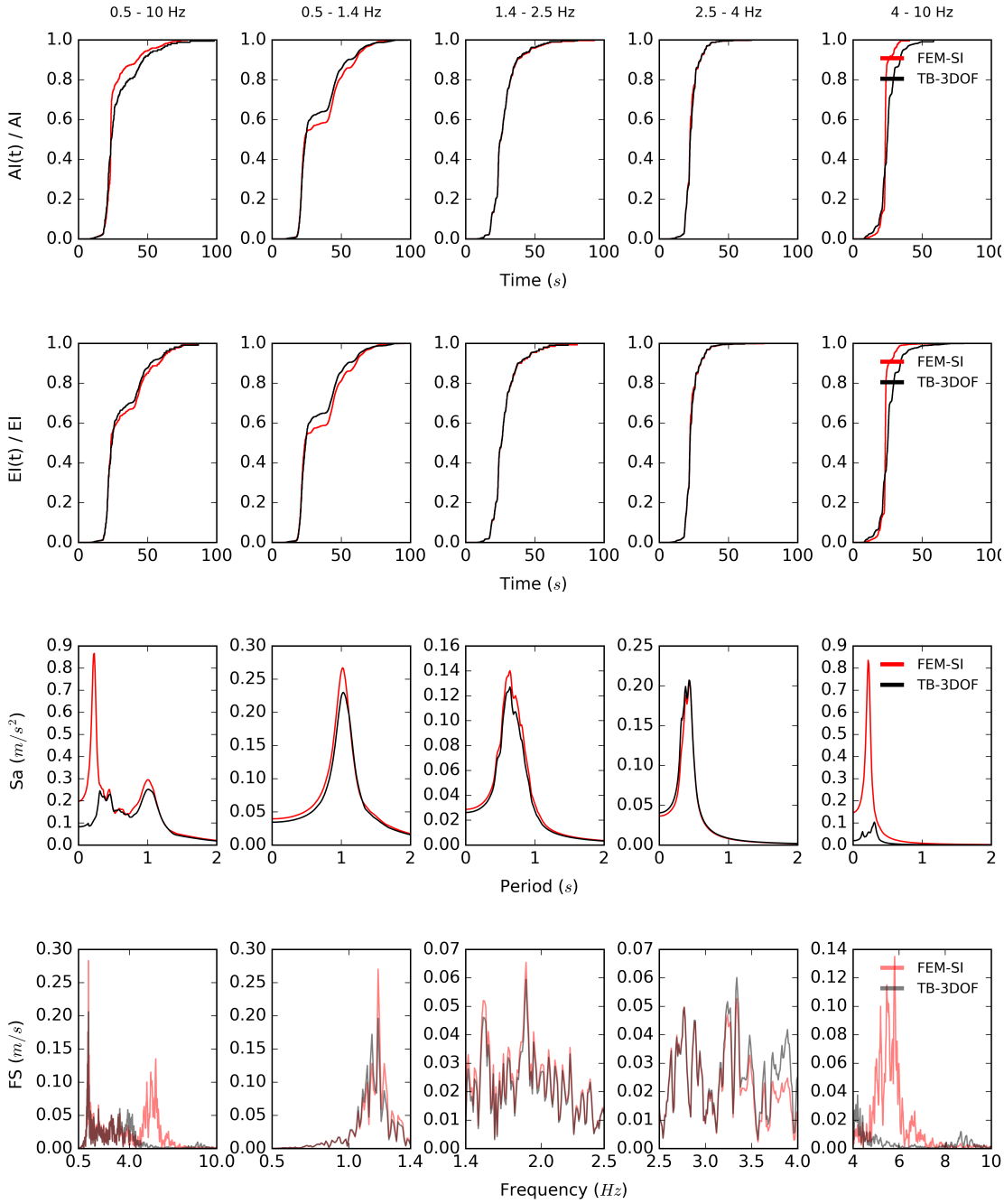

Figure 6.17 – Comparison of Arias integral, energy integral, elastic response spectrum in terms of pseudo-acceleration and Fourier spectrum for the horizontal acceleration component HN3 at the top of the building (V0), during the 2014 Barcelonnette earthquake: numerical simulations using an equivalent Timoshenko beam (TB) and a detailed three-dimensional model (FEM-SI).

Table 6.2 – Values of Peak Acceleration, Velocity and Displacement for numerical simulations using an equivalent Timoshenko beam (TB) and a detailed three-dimensional model (FEM-SI) for the HN3 horizontal component at the top of the building (V0) during the 2014 Barcelonnette earthquake.

Band	PA [m/s^2] × 10^{-3}		PV [m/s] × 10^{-3}		PD [m] × 10^{-3}	
	TB	FEM-SI	TB	FEM-SI	TB	FEM-SI
B1	82.187	197.442	6.645	10.685	0.795	0.917
B2	34.366	39.444	4.655	5.299	0.627	0.703
B3	26.132	28.673	2.141	2.356	0.183	0.204
B4	40.462	36.331	2.138	1.935	0.113	0.106
B5	19.585	147.121	0.581	4.197	0.023	0.120

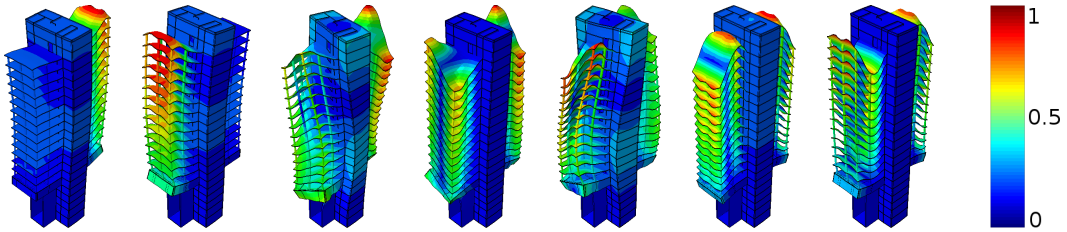

Figure 6.18 – 6^{th} to 12^{th} obtained using the finite element model under the hypothesis of independent dynamic behavior of the two towers (FEM1). Colormap shows the normalized displacement of nodes.

ings is not trivial task and is near current limitations of OMA techniques applied to buildings. Figure 6.19 shows the same results presented in Figure 6.15 in terms of displacement time histories. It can be observed that the global displacement is much better reproduced than the acceleration and that the contribution of higher modes is very low (the fundamental mode by itself produces a displacement amplitude about 10 times greater than all higher modes contained in the 4-10 Hz band).

6.7 Conclusions

Dimensions and mechanical parameters for a Timoshenko beam model of a high-rise reinforced concrete building, having bending type structural behavior under seismic loading, are obtained from the analysis of ambient noise recordings. The optimization of a Timoshenko beam model is achieved by fitting the natural frequencies, obtained using modal analysis, to those identified by transfer functions and, simultaneously, matching the analytical phase velocity dispersion curve to a dispersion image obtained from a slant-stack frequency-wavenumber analysis of the IRF sections.

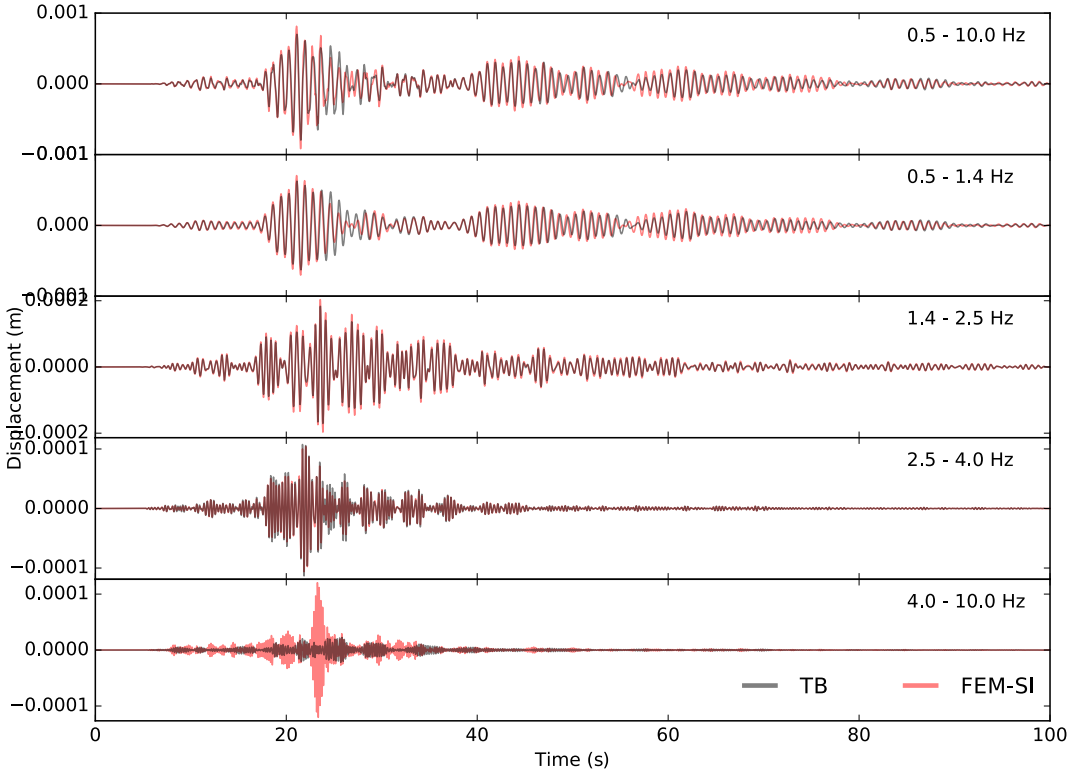

Figure 6.19 – Numerical response in terms of horizontal displacement (HN3) at the top (V0) of the detailed 3D model of the building (FEM-SI) and the equivalent Timoshenko beam (TB) under the three components of the 2014 Barcelonnette earthquake for different frequency bands.

The availability of vertical motion records enable to obtain the Poisson ratio, for the equivalent beam, deduced from the compressional to shear wave velocity ratio, where velocities are determined by direct lag time measurement of causal wave arrivals on IRFs. The measured compressional wave velocities are about 5 times faster than shear ones for the investigated building.

The use of dispersion imaging techniques enables a better understanding of wave propagation phenomena and corroborate that the dispersion, in bending type buildings, follows the analytical solution of a Timoshenko beam. A transitory variation of wave propagation velocity in the building is observed, influenced by environmental conditions. The procedure of stacking several days of noise filters out the daily variation due to temperature changes by providing an averaged value, however, seasonal variability would not be removed.

The proposed methodology does not need any information about disposition, dimensions or material of structural elements. The length of the equivalent beam is the only assumed parameter, imposed equal to the building height. It is confirmed that short windows of ambient vibrations are suitable as source of excitation for structural identification. The procedure can be carried out with only sixty seconds of recordings, allowing extensive temporary measurement campaigns for identification of dynamic properties of buildings by considering them as homogeneous structures.

The reproduction of the deformation time history of the equivalent fixed-base beam model is excellent for lower modes (the first five in the studied building). Higher modes, related to local displacements of the structure, cannot be reproduced using a homogeneous beam model. Their contribution is neglected by this approach. However, lower modes are the responsible of most displacement, hence the approach appears interesting as approximation.

7 Global conclusions and perspectives

The main purpose of this thesis is to estimate the seismic response of existing buildings, taking advantage of motion records and techniques that allow the characterization of their dynamic features using records. Detailed three-dimentional finite element models allow an accurate simulation of structural seismic response if the resistant structure, material properties and boundary conditions are adequately defined. The proposed simplified procedures appear to be useful alternatives when information about the structure and materials are not easily available. This thesis aims to propose the use of non-invasive measurements for identification of dynamic properties and simplified techniques to obtain the deformation time history of a building using these measures. The combination of numerical and empirical methods, as done in this study, allow correctly understanding the dynamic behavior of a building in its environment and avoid uncertainties due to the limitations of each approach. Some questions have been formulated in Chapter 1 to guide the reader through the manuscript and answers are formulated in these conclusions.

Can we reproduce the actual state of the structure starting from structural plans and adopted design conditions?

Structural identification of the case study building is presented in Chapter 3. Dynamic parameters are obtained from records using different OMA techniques and a detailed three-dimensional FE model is created according to structural plans. In-situ measures allows the calibration of the numerical model in order to fit the service condition of the structure that is different from the design condition in terms of loads, material properties, ageing of materials, boundary conditions, etc. The combined use of numerical modeling and records enables to observe that the seismic joint, present in the structural plans of the studied building, is not

working as expected. An error of almost 50% is identified on the first torsional frequency of the building by modeling the towers as dynamically isolated. Such error is reduced to less than 1% when considering that the seismic filling material provides a rigid connection between both parts. The observation of dynamic parameters in a long time interval period shows that the fundamental frequency suffers transitory variations (daily and annual) of about 4% between the winter and summer of the same year, mainly caused by external temperature variations.

Structural identification using records has a great potential in civil engineering industry and can be used, for example, to verify reinforcement operations, or to identify damaged buildings in a post-seismic context.

Can we obtain reliable numerical models to simulate the seismic response?

The numerical seismic response under past earthquakes is simulated using a three-dimensional FE model as presented in Chapter 4. The behavior of materials is assumed linear, due to the the lack of strong earthquakes recorded, in the analyzed seismic zone. An overall good simulation of the seismic response is obtained applying the three component of ground motion, recorded by one sensor, at the whole base of the model. However, considerable part of the behavior in the frequency range of the fundamental mode is not properly reproduced. The vertical component of earthquake, recorded by sensors relatively closely spaced at the base of the building, appears different in terms of amplitude and phase, indicating the presence of rocking effects and consequent rotation of the building base during the strong motion. The spatial variability of the base motion is considered by imposing different recorded excitation at different points of the numerical model. Imposing a multiple loading means reproduce the rigid rotation of the base, associated with the interaction between the building and the soil. According to a qualitative comparison of acceleration time histories, the rocking effect produces a transitory shift of the fundamental frequency (of about 6% during the 2014 M_w 4.9 Barcelonnette earthquake). This shift is numerically reproduced when a multiple input motion is imposed at different locations of the base, but it is neglected when the three components of motion recorded in a selected location are imposed to the whole base. Quantitative comparisons confirm better results when the spatial variability of the base motion is considered. It should be remarked that actual seismic codes do not take into account the spatial variability of ground motion for buildings and rocking effects.

Applying the same approach to other buildings would be interesting to determine if these effects are related to this study case or they can be observed for different types of buildings, in different environments.

Can we simulate the response to stronger earthquakes using past seismic records?

It is proposed in Chapter 5 to generate the dynamic response of existing buildings to earthquakes using records of previous smaller events. An extension of the empirical Green's function method is used for such purpose. It does not require to model the structure and to calibrate any mechanical parameter. Numerical responses evaluated using the detailed three-dimensional model, previously validated by comparison with records, are compared to the semi-empirically generated signals to verify the reliability of the procedure. The signals generated trough EGF show an excellent goodness of fit when compared with numerical signals and it is important to underline that not any modeling hypothesis is necessary about the building. This approach allows the reproduction of building response avoiding a time-consuming simulation. Hence, it could be used as simplified approach when structural plans or information about materials are not easily available. It is considered as simplified procedure due to several limitations that need to be taken into account. An hypothesis of linear constitutive behavior of the medium through which waves propagate is adopted. Nonlinearities along the transmission path (from the source to the structure) due to soil and building materials, site effects and soil-structure interaction are neglected. Additionally, the source of the simulated event has the same location and focal mechanism than the earthquake selected as EGF. Consequently, this method can be used to generate moderate amplitude synthetic signals in buildings at large enough epicentral distances. Additionally, in the case of having only records at the roof of the structure, Kanai-Yoshizawa formulation could be used to estimate the responses at different story locations (or even the ground motion).

The tendency is the increasing use of instrumentation in building, specially with the developments of affordable sensors. Applications of the proposed techniques helps to determine vulnerability of buildings before and after seismic events and to estimate the dynamic response for a stronger event selected as reference. The current limitations of the technique can be reduced by further research. The implementation of some nonlinearities in the EGF simulations is possible and it is the object of actual research.

Can we simulate the building seismic response using a simplified model and ambient vibration records?

In Chapter 6, a fixed-base beam model of a building, with equivalent dynamic behavior, is identified using ambient vibrations records. A Timoshenko beam model is fitted to observations, matching natural frequencies, wave propagation velocities and dispersion curves. All necessary mechanical parameters to model the structure can be obtained from a short noise

time window, without the need of any information about disposition, dimensions or material of structural elements. Only the building height is assumed. Poisson ratio, for the equivalent building, is deduced from the compressional to shear wave velocity ratio, showing that compressional wave velocities are about 5 times faster than shear ones (for the investigated building). The procedure can be applied using 60 second recordings of ambient vibration, allowing extensive temporary measurement campaigns for identification of dynamic properties of buildings. The reproduction of the deformation time history using the equivalent beam model is excellent for the lower modes (first five mode shapes for the studied building). However, modeling the building as an homogeneous beam does not allow taking into account local modes, and their contribution is neglected. Lower modes are often related to the most part of displacement. Hence, the proposed approach could be interesting as approximation. Such proposed methodology can be of especial interest for numerical simulations in a large scale, with a large number of buildings (as site-city interaction simulations), where modeling and computation time would be very important if all buildings were modeled in detail. The main advantage of an equivalent beam model of a building is that no structural details are needed to reproduce the seismic response of the building.

The Timoshenko beam reproduces well the seismic response of the structure, but the assumption of an uniform section do not consider mass eccentricities and do not accurately fit torsional modes. Results obtained for the Nice prefecture building are satisfying because it is symmetric respect to both orthogonal directions in the horizontal plane. Torsional modes may be poorly reproduced in buildings with strong eccentricities. A reformulation of the analytical equations considering an eccentric hole across the homogeneous section would allow a better simulation of torsional effects.

Bibliography

Aki, K. (1957). Space and time spectra of stationary stochastic waves, with special reference to microtremors. *Bulletin of the Earthquake Research Institute*, 35:415–457.

Aki, K. (1965). A note on the use of microseisms in determining the shallow structures of the earth's crust. *GEOPHYSICS*, 30(4):665–666.

Aki, K. (1967). Scaling law of seismic spectrum. *Journal of Geophysical Research*, 72(4):1217–1231.

Allemang, R. J. and Brown, D. L. (1982). A correlation coefficient for modal vector analysis. In *Proceedings of the 1st international modal analysis conference*, volume 1, pages 110–116. SEM, Orlando.

Anderson, J. G. (2004). Quantitative measure of the goodness-of-fit of synthetic seismograms. In *13th World Conference on Earthquake Engineering Conference Proceedings, Vancouver, Canada, Paper*, volume 243.

Arai, H. and Tokimatsu, K. (2004). S-Wave Velocity Profiling by Inversion of Microtremor H/V Spectrum. *Bulletin of the Seismological Society of America*, 94(1):53–63.

Arias, A. (1970). Measure of Earthquake Intensity. In Robert J. Hansen, editor, *Seismic Design for Nuclear Power Plants*, pages 438–483. The M.I.T. Press, Cambridge, MA.

Asten, M. and Henstridge, J. (1984). Array estimators and the use of microseisms for reconnaissance of sedimentary basins. *GEOPHYSICS*, 49(11):1828–1837.

Asten, M. W. (1978). Geological control on the three-component spectra of Rayleigh-wave microseisms. *Bulletin of the Seismological Society of America*, 68(6):1623–1636.

Atakan, K. (2002). Site Effects Assessment Using Ambient Excitations (SESAME). WP 2: Controlled instrumental specifiations. Technical report.

Banerji, S. K. (1925). Microseisms and the Indian Monsoon. *Nature*, 116:866.

Bard, P. Y., Duval, A. M., Bertrand, E., Vassiliadès, J. F., Vidal, S., Thibault, C., Guyet, B., Mèneroud, J. P., Guéguen, P., Foin, P., and others (2005). Le risque sismique à Nice: apport méthodologique, résultats et perspectives opérationnelles. Final GEM-GEP Report.

Beeler, N. M., Wong, T.-F., and Hickman, S. H. (2003). On the expected relationships among apparent stress, static stress drop, effective shear fracture energy, and efficiency. *Bulletin of the Seismological Society of America*, 93(3):1381–1389.

Bendat, J. S. and Piersol, A. G. (1986). *Random data: measurement and analysis procedures*. Wiley, Hoboken, N.J.

Bendat, J. S. and Piersol, A. G. (1993). *Engineering applications of correlation and spectral analysis*. Wiley, New York, 2nd ed edition.

Beresnev, I. A., Wen, K.-L., and Yeh, Y. T. (1995a). Nonlinear soil amplification: Its corroboration in Taiwan. *Bulletin of the Seismological Society of America*, 85(2):496–515.

Beresnev, I. A., Wen, K.-L., and Yeh, Y. T. (1995b). Seismological evidence for nonlinear elastic ground behavior during large earthquakes. *Soil Dynamics and Earthquake Engineering*, 14(2):103–114.

Bernard, P. (1941). *Etude sur l'agitation microséismique et ses variations*. PhD thesis, Université de Paris 19.

Bernard, P. (1987). *Du caractere complexe et agressif des sources sismiques*. PhD thesis, Université de Paris 6.

Bertelli, T. (1872). Osservazioni sui piccoli movimenti dei pendoli in relazione ad alcuni fenomeni meteorologiche. *Boll. Meteorol. Osserv. Coll. Roma*, 9:10.

Bertrand, E., Deschamps, A., Santisi d'Avila, M. P., Guéguen, P., Tahmi, N., and Fernández Lorenzo, G. W. (2014). Seismological monitoring of a tall RC building in Nice, France. *SSA annual meeting, Anchorage, USA*.

Bindi, D., Petrovic, B., Karapetrou, S., Manakou, M., Boxberger, T., Raptakis, D., Pitilakis, K. D., and Parolai, S. (2014). Seismic response of an 8-story RC-building from ambient vibration analysis. *Bulletin of Earthquake Engineering*, pages 1–26.

Biot, M. (1933). Theory of elastic systems vibrating under transient impulse with an application to earthquake-proof buildings. *Proceedings of the National Academy of Sciences*, 19(2):262–268.

Biot, M. (1934). Theory of vibration of buildings during earthquake. *Journal of Applied Mathematics and Mechanics*, 14(4):213–223.

Biot, M. A. (1932). *Vibrations of buildings during earthquake*. PhD thesis, Calif. Inst. of Tech., Pasadena, CA.

Blume, J. A. (1972). Highrise building characteristics and responses determined from nuclear seismology. *Bulletin of the Seismological Society of America*, 62(2):519–540.

Bonnefoy-Claudet, S. (2004). *Nature du bruit de fond sismique: implications pour les études des effets de site*. PhD thesis, Université Joseph-Fourier - Grenoble I.

Bonnefoy-Claudet, S., Cotton, F., and Bard, P.-Y. (2006). The nature of noise wavefield and its applications for site effects studies: A literature review. *Earth-Science Reviews*, 79(3–4):205–227.

Boutin, C., Hans, S., Erdin, I., and Loriot, M. (1999). Approche de la vulnérabilité sismique par l'étude du comportement de bâtiments réels. *Rapport de recherche ENTPE, Lyon*, page 11.

Boutin, C., Hans, S., Ibraim, E., and Roussillon, P. (2005). In situ experiments and seismic analysis of existing buildings. Part II: Seismic integrity threshold. *Earthquake Engineering & Structural Dynamics*, 34(12):1531–1546.

Brincker, R. and Kirkegaard, P. H. (2010). Special issue on Operational Modal Analysis. *Mechanical Systems and Signal Processing*, 24(5):1209–1212.

Brincker, R., Ventura, C., and Andersen, P. (2001a). Damping estimation by frequency domain decomposition. pages 698–703, Kissimmee, USA.

Brincker, R., Zhang, L., and Andersen, P. (2001b). Output-only modal analysis by frequency domain decomposition. In *The International Conference on Noise and Vibration Engineering*, pages 717–723.

Brune, J. N. (1970). Tectonic stress and the spectra of seismic shear waves from earthquakes. *Journal of geophysical research*, 75(26):4997–5009.

Brunel, D. and Bertrand, E. (2010). Instrumentation de la Préfecture de Nice. La lettre d'information du RAP - Numéro 12.

Byerly, P., Hester, J., and Marshall, K. (1931). The natural periods of vibration of some tall buildings in San Francisco. *Bulletin of the Seismological Society of America*, 21(4):268–276.

Cacciola, P. and Tombari, A. (2015). Vibrating barrier: a novel device for the passive control of structures under ground motion. *Proc. R. Soc. A*, 471(2179):20150075.

Cameelbeeck, T., Grünthal, G., Basili, R., Glavatovic, B., Valensise, G., Crowley, H., Campos-Costa, A., Meletti, C., Woessner, J., Pinho, R., Fonseca, J., Lindholm, C., Stucchi, M., Musson, R., Demircioglu, M. B., Arvidsson, R., Pitilakis, K., Akkar, S., Stromeyer, D., Danciu, L., Sesetyan, K., Giardini, D., Cotton, F., Douglas, J., Rovida, A., Erdik, M., and Makropoulos, K. (2013). Seismic Hazard Harmonization in Europe (SHARE): Online Data Resource.

Capon, J. (1969). High-resolution frequency-wavenumber spectrum analysis. *Proceedings of the IEEE*, 57(8):1408–1418.

Capon, J., Greenfield, R. J., and Kolker, R. J. (1967). Multidimensional maximum-likelihood processing of a large aperture seismic array. *Proceedings of the IEEE*, 55(2):192–211.

Cara, M., Cansi, Y., Schlupp, A., Arroucau, P., Béthoux, N., Beucler, E., Bruno, S., Calvet, M., Chevrot, S., Deboissy, A., Delouis, B., Denieul, M., Deschamps, A., Doubre, C., Fréchet, J., Godey, S., Golle, O., Grunberg, M., Guilbert, J., Haugmard, M., Jenatton, L., Lambotte, S., Leobal, D., Maron, C., Mendel, V., Merrer, S., Macquet, M., Mignan, A., Mocquet, A., Nicolas, M., Perrot, J., Potin, B., Sanchez, O., Santoire, J.-P., Sèbe, O., Sylvander, M., Thouvenot, F., Woerd, J. V. D., and Woerd, K. V. D. (2015). SI-Hex: a new catalogue of instrumental seismicity for metropolitan France. *Bulletin de la Societe Geologique de France*, 186(1):3–19.

Carder, D. S. (1936). Observed vibrations of buildings. *Bulletin of the Seismological Society of America*, 26(3):245–277.

CETE (2007). Mesures de bruit de fond dans une sélection d'immeubles à Nice. Technical report, Projet d'instrumentation du RAP.

CETE (2010). Instrumentation du bâtiment de la préfecture des Alpes Maritimes, Nice (06), France. Technical report.

Cheng, M. H. and Heaton, T. H. (2015). Simulating Building Motions Using Ratios of the Building's Natural Frequencies and a Timoshenko Beam Model. *Earthquake Spectra*, 31(1):403–420.

Chopra, A. K. (2012). *Dynamics of structures: theory and applications to earthquake engineering*. Prentice Hall, Upper Saddle River, N.J, 4th ed edition.

Clinton, J. F. (2004). *Modern digital seismology - instrumentation, and small amplitude studues in the engineering world*. PhD thesis, California Institute of Technology.

Clinton, J. F., Bradford, S. C., Heaton, T. H., and Favela, J. (2006). The observed wander of the natural frequencies in a structure. *Bulletin of the Seismological Society of America*, 96(1):237–257.

Clough, R. W. and Penzien, J. (2003). *Dynamics of structures*. McGraw-Hill, New York.

Cole, H. A. (1973). *On-line failure detection and damping measurement of aerospace structures by random decrement signatures*, volume 2205. National Aeronautics and Space Administration.

Cornou, C., Ohrnberger, M., Boore, D. M., Kudo, K., and Bard, P.-Y. (2006). Derivation of structural models from ambient vibration array recordings: results from an international blind test. In *Third International Symposium on the Effects of Surface Geology on Seismic Motion*, Grenoble, France.

Courboulex, F. (2010). *Des petits seismes pour comprendre et prevoir les plus gros*. HDR, Université Nice Sophia Antipolis.

Courboulex, F., Converset, J., Balestra, J., and Delouis, B. (2010). Ground-motion simulations of the 2004 Mw 6.4 les Saintes, Guadeloupe, earthquake using ten smaller events. *Bulletin of the Seismological Society of America*, 100(1):116–130.

Courboulex, F., Delouis, B., Dujardin, A., Deschamps, A., Bertrand, E., Causse, M., Maron, C., Sira, C., and Cultrera, G. (2014). The two events of Barcelonnette (French Alps), 2012 (Mw4.1) and 2014 (Mw 4.9): the role of directivity on ground motions, macroseismic intensities and site effects. In *Second European conference on Earthquake Engineering and Seismology*, Istambul.

Courboulex, F., Dujardin, A., Vallée, M., Delouis, B., Sira, C., Deschamps, A., Honoré, L., and Thouvenot, F. (2013). High-Frequency Directivity Effect for an Mw 4.1 Earthquake, Widely Felt by the Population in Southeastern France. *Bulletin of the Seismological Society of America*, 103(6):3347–3353.

Curtis, A., Gerstoft, P., Sato, H., Snieder, R., and Wapenaar, K. (2006). Seismic interferometry—turning noise into signal. *The Leading Edge*, 25(9):1082–1092.

Datta, T. K. (2010). *Seismic Analysis of Structures*. John Wiley & Sons, Ltd, Chichester, UK.

Davison, C. (1924). Fusakichi Omori and his work on earthquakes. *Bulletin of the Seismological Society of America*, 14(4):240–255.

Dominique, P., Autran, A., Blès, J. L., Fitzenz, D., Samarcq, F., Terrier, M., Cushing, M., Gariel, J. C., Mohammadioun, B., Durouchoux, P. C. C., and others (1998). Part Two: Probabilistic approach, Seismic hazard map on the national territory (France). *Proceedings of the 11th ECEE, 6-11 Septembre, Paris, France*.

Dubar, M. (2003). The Holocene deltas of Eastern Provence and the French Riviera: geomorphological inheritance, genesis and vulnerability. *Géomorphologie : relief, processus, environnement*, 9(4):263–270.

Dunand, F. (2005). *Pertinence du bruit de fond sismique pour la caractérisation dynamique et l'aide au diagnostic sismique des structures de génie civil*. PhD thesis, Université Joseph-Fourier - Grenoble I.

Dunand, F., Rodgers, J. E., Acosta, A. V., Salsman, M., Bard, P.-Y., and Celebi, M. (2004). Ambient vibration and earthquake strong-motion data sets for selected USGS extensively instrumented buildings. Technical Report OFR - 2004-1375, United States Geological Survey.

Ebrahimian, M., Rahmani, M., and Todorovska, M. I. (2014a). Nonparametric estimation of wave dispersion in high-rise buildings by seismic interferometry. *Earthquake Engineering & Structural Dynamics*, 43(15):2361–2375.

Ebrahimian, M., Rahmani, M., and Todorovska, M. I. (2014b). Wave method for system identification and health monitoring of buildings–extension to fitting Timoshenko beam model. In *Proceedings of the 10th National Conference in Earthquake Engineering, Earthquake Engineering Research Institute, Anchorage, AK*.

Ebrahimian, M., Trifunac, M. D., and Todorovska, M. I. (2016). Prediction of building response at any level from recorded roof response: The Kanai–Yoshizawa formula revisited. *Soil Dynamics and Earthquake Engineering*, 80:241–250.

Erdik, M., Celebi, M., Mihailov, V., and Apaydin, N., editors (2001). *Strong Motion Instrumentation for Civil Engineering Structures*. Springer Netherlands, Dordrecht.

European Committee for Standardisation (2004a). *EN 1992-1-1: Eurocode 2: Design of concrete structures - Part 1-1: General rules and rules for buildings*.

European Committee for Standardisation (2004b). *EN 1998-1: Eurocode 8: Design of structures for earthquake resistance – Part 1: General rules, seismic actions and rules for buildings*.

Farrar, C. R., Cornwell, P. J., Hunter, N. F., and Lieven, N. A. (2005). Sensing and Data Acquisition Issues for Damage Prognosis. In Inman, D. J., Farrar, C. R., Junior, V. L., and Junior, V. S., editors, *Damage Prognosis*, pages 305–321. John Wiley & Sons, Ltd.

Farsi, M. N. and Bard, P. Y. (1998). Estimation of buildings periods and vulnerability in urban area of grenoble (france). In *Proceeding of the 11th European Conference on Earthquake Engineering, Rotterdam*.

Felber, A. J. (1993). *Development of a hybrid bridge evaluation system*. PhD thesis, University of British Columbia.

Friswell, M. and Mottershead, J. E. (1995). *Finite Element Model Updating in Structural Dynamics*. Springer Science & Business Media.

Fäh, D., Kind, F., and Giardini, D. (2001). A theoretical investigation of average H/V ratios. *Geophysical Journal International*, 145(2):535–549.

Gavin, H. P. (2014). Vibrations of Single Degree of Freedom Systems. Technical report, Duke University.

GEMGEP (2005). Étude de scénarios de gestion de crise. Définition de l'aléa, de la vulnérabilité et des enjeux. Étude d'un bâtiment de classe D: Préfecture des Alpes-Maritimes. Technical report.

Gouédard, P., Cornou, C., and Roux, P. (2008). Phase–velocity dispersion curves and small-scale geophysics using noise correlation slantstack technique. *Geophysical Journal International*, 172(3):971–981.

Guillier, B., Chatelain, J.-L., Perfettini, H., Oubaiche, E. H., Voisin, C., Bensalem, R., Machane, D., and Hellel, M. (2016). Building frequency fluctuations from continuous monitoring of ambient vibrations and their relationship to temperature variations. *Bulletin of Earthquake Engineering*, 14(8):2213–2227.

Gutenberg, B. (1911). *Die seismische bodenunruhe*. PhD thesis, University of Gottigen, Germany.

Gutenberg, B. (1958). Microseisms. *Advances in Geophysics*, 5:53–92.

Guéguen, P., Bard, P.-Y., and Chávez-García, F. J. (2002). Site-City Seismic Interaction in Mexico City–Like Environments: An Analytical Study. *Bulletin of the Seismological Society of America*, 92(2):794–811.

Guéguen, P., Langlais, M., Roux, P., Schinkmann, J., and Douste-Bacqué, I. (2014). Frequency and Damping Wandering in Existing Buildings Using the Random Decrement Technique. In *7th European Workshop on Structural Health Monitoring*.

Hans, S. (2002). *Auscultation dynamique de bâtiments et modélisation par homogénéisation : contribution à l'analyse de la vulnérabilité sismique*. Villeurbanne, INSA.

Hans, S., Boutin, C., Ibraim, E., and Roussillon, P. (2005). In situ experiments and seismic analysis of existing buildings. Part I: experimental investigations. *Earthquake Engineering & Structural Dynamics*, 34(12):1513–1529.

Hartzell, S. H. (1978). Earthquake aftershocks as Green's functions. *Geophysical Research Letters*, 5(1):1–4.

Herak, M. and Herak, D. (2010). Continuous monitoring of dynamic parameters of the DGFSM building (Zagreb, Croatia). *Bulletin of Earthquake Engineering*, 8(3):657–669.

Hisada, T. and Nakagawa, K. (1956). Vibration tests on various types of buildings up to failure. In *Proceedings of the First World Conference on Earthquake Engineering, Berkeley, California, Earthquake Engineering Research Institute (EERI), Paper*, page 11.

Honoré, L., Courboulex, F., and Souriau, A. (2011). Ground motion simulations of a major historical earthquake (1660) in the French Pyrenees using recent moderate size earthquakes. *Geophysical Journal International*, 187(2):1001–1018.

Housner, G. W. (1957). Interaction of building and ground during an earthquake. *Bulletin of the Seismological Society of America*, 47(3):179–186.

Housner, G. W. and Brady, A. G. (1963). Natural periods of vibration of buildings. *Journal of the Engineering Mechanics Division*, 89(4):31–65.

Hsu, T. T. C. and Mo, Y.-L. (2010). *Unified Theory of Concrete Structures*. John Wiley & Sons.

Huang, M. J. and Shakal, A. F. (2012). Building instrumentation objectives and models. In *Seventh U.S. National Conference on Earthquake Engineering (7NCEE)*, Boston, Massachusetts.

Hughes, T. J. R. (1987). *The Finite Element Method: Linear Static and Dynamic Finite Element Analysis*. Prentice Hall, Englewood Cliffs, N.J.

Hutchings, L. (1994). Kinematic earthquake models and synthesized ground motion using empirical Green's functions. *Bulletin of the Seismological Society of America*, 84(4):1028–1050.

Isbiliroglu, Y., Taborda, R., and Bielak, J. (2015). Coupled Soil-Structure Interaction Effects of Building Clusters During Earthquakes. *Earthquake Spectra*, 31(1):463–500.

Ishimoto, M. and Takahasi, R. (1929). Mesures des mouvements d'un batiment dans des conditions tranquilles. *Tokyo Imperial University Earthquake Research Institute*, 7(1):175–184.

Jeary, A. P. (1986). Damping in tall buildings—a mechanism and a predictor. *Earthquake engineering & structural dynamics*, 14(5):733–750.

Joyner, W. B. and Boore, D. M. (1986). On Simulating Large Earthquakes by Green's–Function Addition of Smaller Earthquakes. *Earthquake source mechanics*, pages 269–274.

Kanai, K. and Tanaka, T. (1951). Vibration test of actual reinforced concrete building. *Bulletin of the Earthquake Research Institute, Tokyo*, 29(4):617–626.

Kanai, K., Tanaka, T., and Suzuki, T. (1949). Vibration experiments with the actual buildings. *Bulletin of the Earthquake Research Institute, Tokyo*, 27(1-4):91–95.

Kanai, K. and Yoshizawa, S. (1952). On the damping of vibration in actual buildings. *Bull Earthq Res Inst*, 30:121–126.

Kanai, K. and Yoshizawa, S. (1963). Some New Problems of Seismic Vibrations of a Structure. Part 1. *Earthquake Research Institute of the University of Tokyo*, 41(4):825–833.

Kanamori, H. and Rivera, L. (2004). Static and dynamic scaling relations for earthquakes and their implications for rupture speed and stress drop. *Bulletin of the Seismological Society of America*, 94(1):314–319.

Kaneko, T. (1975). On Timoshenko's correction for shear in vibrating beams. *Journal of Physics D: Applied Physics*, 8(16):1927–1936.

Kashima, T., Koyama, S., Okawa, I., and Iiba, M. (2012). Strong motion records in buildings from the 2011 Great East Japan earthquake. *IJMA*, 139:20.

Kham, M., Semblat, J.-F., Bard, P.-Y., and Dangla, P. (2006). Seismic Site–City Interaction: Main Governing Phenomena through Simplified Numerical Models. *Bulletin of the Seismological Society of America*, 96(5):1934–1951.

Knopoff, L. (1964). Q. *Reviews of Geophysics*, 2(4):625–660.

Kohler, M. D., Heaton, T. H., and Bradford, S. C. (2007). Propagating waves in the steel, moment-frame factor building recorded during earthquakes. *Bulletin of the Seismological Society of America*, 97(4):1334–1345.

Kohrs-Sansorny, C., Courboulex, F., Bour, M., and Deschamps, A. (2005). A two-stage method for ground-motion simulation using stochastic summation of small earthquakes. *Bulletin of the Seismological Society of America*, 95(4):1387–1400.

Konno, K. and Ohmachi, T. (1998). Ground-motion characteristics estimated from spectral ratio between horizontal and vertical components of microtremor. *Bulletin of the Seismological Society of America*, 88(1):228–241.

Kramer, S. L. (1996). *Geotechnical earthquake engineering*. Prentice-Hall international series in civil engineering and engineering mechanics. Prentice Hall, Upper Saddle River, N.J.

Larroque, C., Béthoux, N., Calais, E., Courboulex, F., Deschamps, A., Déverchère, J., Stéphan, J. F., Ritz, J. F., and Gilli, E. (2001). Active deformation at the junction between southern French Alps and Ligurian basin. *Netherlands Journal of Geosciences*, 80:255–272.

Larroque, C., Scotti, O., and Ioualalen, M. (2012). Reappraisal of the 1887 Ligurian earthquake (western Mediterranean) from macroseismicity, active tectonics and tsunami modelling. *Geophysical Journal International*, 190(1):87–104.

LEGIFRANCE (2010). Code de l'environnement - Article D563-8-1.

Lestuzzi, P. (2008). *Séismes et construction: eléments pour non-spécialistes*. PPUR presses polytechniques.

Liu, H., Yang, Z., and Gaulke, M. S. (2005). Structural identification and finite element modeling of a 14-story office building using recorded data. *Engineering Structures*, 27(3):463–473.

Maia, N. M. M. and Silva, J. M. M. (1997). *Theoretical and experimental modal analysis*. Research Studies Press Taunton.

Martin, C., Combes, P., Secanell, R., Lignon, G., Carbon, D., Fioravanti, A., and Grellet, B. (2002). Révision du zonage sismique de la France. Etude probabiliste. *Rapport GEOTER GTR/MATE/0701*, 150.

Mazzieri, I., Stupazzini, M., Guidotti, R., and Smerzini, C. (2013). SPEED: SPectral Elements in Elastodynamics with Discontinuous Galerkin: a non-conforming approach for 3d multi-scale problems. *International Journal for Numerical Methods in Engineering*, 95(12):991–1010.

Mehta, K., Snieder, R., and Graizer, V. (2007a). Downhole Receiver Function: a Case Study. *Bulletin of the Seismological Society of America*, 97(5):1396–1403.

Mehta, K., Snieder, R., and Graizer, V. (2007b). Extraction of near-surface properties for a lossy layered medium using the propagator matrix. *Geophysical Journal International*, 169(1):271–280.

Meneroud, J.-P., Duval, A.-M., and Bard, P.-Y. (2000). Methodological study on seismic risk assessment. In *12 th World Conference on Earthquake Engineering. Auckland, New Zealand*.

Meschke, G., Borst, R. d., Mang, H., and Bicanic, N. (2006). *Computational Modelling of Concrete Structures: Proceedings of the EURO-C 2006 Conference, Mayrhofen, Austria, 27-30 March 2006*. CRC Press.

Michel, C. (2007). *Vulnérabilité Sismique de l'échelle du bâtiment à celle de la ville - Apport des techniques expérimentales in situ - Application à Grenoble*. PhD thesis.

Michel, C. and Guéguen, P. (2010). Time-frequency analysis of Transitory/Permanent frequency decrease in civil engineering structures during earthquakes. *Structural Health Monitoring*, 9(2):159–171. arXiv: 0803.1779.

Mikael, A., Guéguen, P., Bard, P.-Y., Roux, P., and Langlais, M. (2013). The Analysis of Long-Term Frequency and Damping Wandering in Buildings Using the Random Decrement Technique. *Bulletin of the Seismological Society of America*, 103(1):236–246.

Miyazawa, M., Venkataraman, A., Snieder, R., and Payne, M. (2008). Analysis of microearthquake data at Cold Lake and its applications to reservoir monitoring. *GEOPHYSICS*, 73(3):O15–O21.

Mouroux, P. and Brun, B. L. (2006). Risk-Ue Project: An Advanced Approach to Earthquake Risk Scenarios With Application to Different European Towns. In Oliveira, C. S., Roca, A., and Goula, X., editors, *Assessing and Managing Earthquake Risk*, number 2 in Geotechnical, Geological And Earthquake Engineering, pages 479–508. Springer Netherlands.

Nakamura, Y. (1989). A method for dynamic characteristics estimation of subsurface using microtremor on the ground surface. *Railway Technical Research Institute, Quarterly Reports*, 30(1).

Nakamura, Y. (1996). Real-time information systems for seismic hazards mitigation UrEDAS, HERAS and PIC. *Railway Technical Research Institute, Quarterly Reports*, 37(3).

Nakata, N. and Snieder, R. (2013). Monitoring a Building Using Deconvolution Interferometry. II: Ambient-Vibration Analysis. *Bulletin of the Seismological Society of America*, 104(1):204–213.

Nasser-Barakat, F. (2015). *Suivi automatique de variations modales à l'aide du technique de décrément aléatoire sans filtrage application à des enregistrements de vibrations ambiantes des bâtiments*. PhD thesis, Université Grenoble Alpes.

Nogoshi, M. and Igarashi, T. (1971). On the amplitude characteristics of microtremor (part 2). *Jour. Seism. Soc. Japan*, 24:26–40.

Omori, F. (1922). The semi-destructive earthquake of April 26, 1922. *Seismological notes (imperial earthquake investigation committee)*, 3:1–30.

Ordaz, M., Arboleda, J., and Singh, S. K. (1995). A scheme of random summation of an empirical Green's function to estimate ground motions from future large earthquakes. *Bulletin of the Seismological Society of America*, 85(6):1635–1647.

Park, C., Miller, R., and Xia, J. (1998). Imaging dispersion curves of surface waves on multi-channel record. In *Society of Exploration Geophysicists*, pages 1377–1380.

Park, C. B., Miller, R. D., Xia, J., and Ivanov, J. (2004). Imaging dispersion curves of passive surface waves. In *Society of Exploration Geophysicists*, pages 1357–1360.

Parolai, S., Ansal, A., Kurtulus, A., Strollo, A., Wang, R., and Zschau, J. (2009). The Ataköy vertical array (Turkey): Insights into seismic wave propagation in the shallow-most crustal layers by waveform deconvolution. *Geophysical Journal International*, 178(3):1649–1662.

Peeters, B. and De Roeck, G. (2001). Stochastic system identification for operational modal analysis: a review. *Journal of Dynamic Systems, Measurement, and Control*, 123(4):659–667.

Pequegnat, C., Guéguen, P., Hatzfeld, D., and Langlais, M. (2008). The French Accelerometric Network (RAP) and National Data Centre (RAP-NDC). *Seismological Research Letters*, 79(1):79–89.

Perrault, M. (2013). *Évaluation de la vulnérabilité sismique de bâtiments à partir de mesures in situ*. PhD thesis, Université de Grenoble.

Prevosto, M. (1982). *Algorithmes d'identification des caractéristiques vibratoires de structures mécaniques complexes*. PhD thesis, Université de Rennes I, Rennes.

Prieto, G. A., Lawrence, J. F., Chung, A. I., and Kohler, M. D. (2010). Impulse Response of Civil Structures from Ambient Noise Analysis. *Bulletin of the Seismological Society of America*, 100(5A):2322–2328.

Rahmani, M. and Todorovska, M. I. (2013). 1d system identification of buildings during earthquakes by seismic interferometry with waveform inversion of impulse responses—method and application to Millikan library. *Soil Dynamics and Earthquake Engineering*, 47:157–174.

Rainieri, C., Fabbrocino, G., Cosenza, E., and Manfredi, G. (2007). Implementation of OMA procedures using labview: theory and application. In *Proc. of the 2nd IOMAC Conference, Copenhagen, Denmark*, volume 30, pages 1–13.

Reis, M. d. A. (1978). *Wave propagation in elastic beams and rods.* PhD thesis, Massachusetts Institute of Technology.

RESIF (1995). RESIF-RLBP French Broad-band network, RESIF-RAP strong motion network and other seismic stations in metropolitan France. Technical report. DOI 10.15778/RESIF.FR.

Rodrigues, J. and Brincker, R. (2005). Application of the Random Decrement Technique in Operational Modal Analysis. In *Proceedings of the 1st International Operational Modal Analysis Conference*, pages 191–200, Copenhagen, Denmark. Aalborg Universitet.

Roux, P., Guéguen, P., Baillet, L., and Hamze, A. (2014). Structural-change localization and monitoring through a perturbation-based inverse problem. *The Journal of the Acoustical Society of America*, 136(5):2586–2597.

Ruiz, J. A., Baumont, D., Bernard, P., and Berge-Thierry, C. (2013). Combining a Kinematic Fractal Source Model with Hybrid Green's Functions to Model Broadband Strong Ground Motion. *Bulletin of the Seismological Society of America*, 103(6):3115–3130.

Régnier, J., Bonilla, L. F., Bard, P. Y., Kawase, H., Bertrand, E., Hollender, F., Marot, M., and Sicilia, D. (2015a). PRENOLIN Project: a Benchmark on Numerical Simulation of 1d Non-Linear Site Effect. 1–Verification Phase Based on Canonical Cases. In *6th International Conference on Earthquake Geotechnical Engineering*.

Régnier, J., Bonilla, L. F., Bard, P. Y., Kawase, H., Bertrand, E., Hollender, F., Marot, M., Sicilia, D., and Nozu, A. (2015b). PRENOLIN Project: a Benchmark on Numerical Simulation of 1d Non-linear Site Effects. 2-Results of the Validation Phase. In *6th International Conference on Earthquake Geotechnical Engineering*.

Régnier, J., Cadet, H., Bonilla, L. F., Bertrand, E., and Semblat, J.-F. (2013). Assessing Nonlinear Behavior of Soils in Seismic Site Response: Statistical Analysis on KiK-net Strong-Motion Data. *Bulletin of the Seismological Society of America*, 103(3):1750–1770.

Safak, E. and Celebi, M. (1991). Analyses of recorded responses of two high-rise buildings during the Loma Prieta earthquake of 18 October 1989. *Bulletin of the Seismological Society of America*, 81(5):2087–2110.

Salameh, C. (2016). *Vibrations ambiantes, contenu spectral et dommages sismiques: nouvelle approche adaptée à l'échelle urbaine. Application à Beyrouth.* PhD thesis, Université Grenoble Alpes.

Salameh, C., Guillier, B., Harb, J., Cornou, C., Bard, P.-Y., Voisin, C., and Mariscal, A. (2016). Seismic response of Beirut (Lebanon) buildings: instrumental results from ambient vibrations. *Bulletin of Earthquake Engineering*, pages 1–26.

Salichon, J., Kohrs-Sansorny, C., Bertrand, E., and Courboulex, F. (2010). A Mw 6.3 earthquake scenario in the city of Nice (southeast France): ground motion simulations. *Journal of Seismology*, 14(3):523–541.

Semblat, J. F., Duval, A. M., and Dangla, P. (2000). Numerical analysis of seismic wave amplification in Nice (France) and comparisons with experiments. *Soil Dynamics and Earthquake Engineering*, 19(5):347–362.

Sezawa, K. and Kanai, K. (1935). Decay in the Seismic Vibrations of a Simple or Tall Structure by Dissipation of their Energy into the Ground. 13(3):681–697.

Sezawa, K. and Kanai, K. (1936). Improved Theory of Energy Dissipation in Seismic Vibrations of a Structure. 14(2):164–188.

Shih, C. Y., Tsuei, Y. G., Allemang, R. J., and Brown, D. L. (1988). Complex mode indication function and its applications to spatial domain parameter estimation. *Mechanical Systems and Signal Processing*, 2(4):367–377.

Sira, C., Schulupp, A., Schaming, M., Chesnais, C., Cornou, C., Deschamps, A., Delavaud, E., and Maufroy, E. (2014). Séisme de Barcelonnette du 7 avril 2014. Technical report, BCSF.

Sira, C., Schulupp, A., Schaming, M., and Granet, M. (2012). Séisme de Barcelonnette du 26 février 2012. Technical report, BCSF.

Snieder, R. (2007). Extracting the Green's function of attenuating heterogeneous acoustic media from uncorrelated waves. *The Journal of the Acoustical Society of America*, 121(5):2637–2643.

Snieder, R. and Safak, E. (2006). Extracting the building response using seismic interferometry: Theory and application to the Millikan Library in Pasadena, California. *Bulletin of the Seismological Society of America*, 96(2):586–598.

Snieder, R., Sheiman, J., and Calvert, R. (2006). Equivalence of the virtual-source method and wave-field deconvolution in seismic interferometry. *Physical Review E*, 73(6):066620.

Stubbs, I. R. and MacLamore, V. R. (1973). The ambient vibration survey. In *Proceedings of Fifth World Conference on Earthquake Engineering*, pages 286–289.

Su, R. K. L., Tang, T. O., and Liu, K. C. (2016). Simplified seismic assessment of buildings using non-uniform Timoshenko beam model in low-to-moderate seismicity regions. *Engineering Structures*, 120:116–132.

Taborda, R. and Bielak, J. (2011). Full 3d integration of site-city effects in regional scale earthquake simulations. In *Proc. 8th Int. Conf. Struct. Dyn. EURODYN*, pages 511–518.

Timoshenko, S. (1922). On the transverse vibrations of bars of uniform cross-section. *Philosophical Magazine Series 6*, 43(253):125–131.

Timoshenko, S. (1953). *History of strength of materials, with a brief account of the history of theory of elasticity and theory of structures*. Courier Corporation.

Timoshenko, S. P. (1921). On the correction for shear of the differential equation for transverse vibrations of prismatic bars. *The London, Edinburgh, and Dublin Philosophical Magazine and Journal of Science*, 41(245):744–746.

Todorovska, M. I. (2009a). Seismic Interferometry of a Soil-Structure Interaction Model with Coupled Horizontal and Rocking Response. *Bulletin of the Seismological Society of America*, 99(2A):611–625.

Todorovska, M. I. (2009b). Soil-Structure System Identification of Millikan Library North-South Response during Four Earthquakes (1970-2002): What Caused the Observed Wandering of the System Frequencies? *Bulletin of the Seismological Society of America*, 99(2A):626–635.

Todorovska, M. I. and Trifunac, M. D. (2008a). Earthquake damage detection in the Imperial County Services Building III: analysis of wave travel times via impulse response functions. *Soil Dynamics and Earthquake Engineering*, 28(5):387–404.

Todorovska, M. I. and Trifunac, M. D. (2008b). Impulse response analysis of the Van Nuys 7-storey hotel during 11 earthquakes and earthquake damage detection. *Structural control and health monitoring*, 15(1):90–116.

Tokimatsu, K., Wakai, S., and Arai, H. (1998). Three-Dimensional Soil Stratification Using Surface Waves in Microtremors. *Proc. The 1st International Conference on Site Characterization-ISC98*, pages 537–542.

Trifunac, M. D. (2008a). 75th Anniversary of the response spectrum method—A historical review. *Soil Dynamics and Earthquake Engineering*, 28(9):675.

Trifunac, M. D. (2008b). Early history of the response spectrum method. *Soil dynamics and earthquake engineering*, 28(9):676–685.

Trifunac, M. D. (2009a). Review: Rotations in Structural Response. *Bulletin of the Seismological Society of America*, 99(2B):968–979.

Trifunac, M. D. (2009b). The role of strong motion rotations in the response of structures near earthquake faults. *Soil Dynamics and Earthquake Engineering*, 29(2):382–393.

Udwadia, F. E. and Trifunac, M. D. (1973a). Ambient vibration tests of full scale structures. In *Proceeding of the 5th world conference on earthquake engineering, Rome, Italy*, pages 1430–1439.

Udwadia, F. E. and Trifunac, M. D. (1973b). Time and amplitude dependent response of structures. *Earthquake Engineering & Structural Dynamics*, 2(4):359–378.

USGS (2016). NSMP Structural and Geotechnical Arrays. http://earthquake.usgs.gov/monitoring/nsmp/structures/.

Vallée, M., Charléty, J., Ferreira, A. M., Delouis, B., and Vergoz, J. (2011). SCARDEC: a new technique for the rapid determination of seismic moment magnitude, focal mechanism and source time functions for large earthquakes using body-wave deconvolution. *Geophysical Journal International*, 184(1):338–358.

Vandiver, J. K., Dunwoody, A. B., Campbell, R. B., and Cook, M. F. (1982). A mathematical basis for the random decrement vibration signature analysis technique. *Journal of Mechanical Design*, 104(2):307–313.

Venture, C. E., Brincker, R., Dascotte, E., and Andersen, P. (2001). FEM updating of the heritage court building structure. In *IMAC-XIX: A Conference on Structural Dynamics*, volume 1, pages 324–330.

VULNERALP (2007). Evaluation de la VULNérabilité Sismique à l'échelle d'une ville de Rhône-ALPes – Application à Grenoble. Technical report.

Welch, P. D. (1967). The use of fast Fourier transform for the estimation of power spectra: a method based on time averaging over short, modified periodograms. *IEEE Transactions on audio and electroacoustics*, 15(2):70–73.

Wolf, J. P. (1985). *Dynamic soil-structure interaction*. Prentice-Hall international series in civil engineering and engineering mechanics. Prentice-Hall, Englewood Cliffs, N.J.

WU (2016). Weather Underground website. https://www.wunderground.com/.

Xia, Y., Chen, B., Weng, S., Ni, Y.-Q., and Xu, Y.-L. (2012). Temperature effect on vibration properties of civil structures: a literature review and case studies. *Journal of Civil Structural Health Monitoring*, 2(1):29–46.

Zhang, L. and Brincker, R. (2005). An Overview of Operational Modal Analysis: Major Development and Issues. In *Proceedings of the 1st International Operational Modal Analysis Conference, April 26-27, 2005, Copenhagen, Denmark*, pages 179–190. Aalborg Universitet.

Résumé étendu de la thèse

L'objectif de cette thèse est de simuler l'histoire temporelle de la réponse d'un bâtiment de grande hauteur sous sollicitation sismique et de proposer des méthodologies simplifiées qui reproduisent correctement une telle réponse. Initialement, un modèle tridimensionnel par éléments finis est produit afin de valider sa fiabilité pour simuler le comportement réel du bâtiment pendant les mouvements du sol, enregistrés à l'aide d'accéléromètres. Il est proposé d'améliorer la précision du modèle numérique en imposant de multiples excitations, compte-tenu des effets de basculement et de la variabilité spatiale sur la sollicitation d'entrée. Le modèle d'éléments finis fournit d'excellents résultats lorsque les paramètres dynamiques sont calibrés pour correspondre à l'état de service de la structure. L'utilisation de fonctions de Green empiriques est proposée pour simuler la réponse sismique directement à partir d'enregistrements d'événements passés, sans avoir besoin de dessins de construction ni d'étalonnage des paramètres mécaniques. Une méthode de sommation stochastique, déjà utilisée pour prédire les mouvements du sol, est adoptée pour générer des signaux synthétiques à des hauteurs différentes du bâtiment, par extension du chemin de propagation des ondes du sol à la structure. La procédure montre une bonne concordance avec les signaux numériques fournis par le modèle d'éléments finis. Une représentation simplifiée du bâtiment comme une poutre homogène Timoshenko est proposée pour simuler la réponse sismique directement à partir des enregistrements des vibrations ambiantes. Des paramètres mécaniques équivalents sont identifiés à l'aide de l'interférométrie par déconvolution en termes de dispersion des ondes, de fréquences naturelles et de rapport de vitesse des ondes de cisaillement et de compression dans le milieu. La simulation de la réponse des modes inférieurs, jusqu'à la cinquième fréquence naturelle, est bien reproduite par le modèle simplifié. Les deux techniques proposées sont des alternatives à la modélisation par éléments finis, lorsque les enregistrements in situ (soit sismiques, soit bruit ambiant) sont disponibles, afin d'éviter les difficultés liées à l'absence d'informations sur la structure et les matériaux et liées au temps de calcul.

Mots clés : *simulation de la réponse sismique, bâtiment de grande hauteur, analyse modale opérationnelle, modélisation par éléments finis, fonction de Green empirique, interférométrie par déconvolution*

Présentation des problématiques

La population vivant dans les zones sismiques augmente et, en dépit des avancées scientifiques et techniques, continue à subir des dommages. Nombre de scénarios dramatiques récents tels qu'à Sumatra (2004), au Sichuan (2008), en Haïti (2010), à Tohoku (2011), au Népal (2015), en Equateur (2016), nous rappellent trop souvent la nature imprévisible et la puissance destructrice de ces événements naturels.

La principale cause des pertes humaines et économiques lors des événements sismiques est liée à l'effet qu'ont les tremblements de terre sur les structures civiles. Cela peut sembler évident, mais explique les raisons qui conduisent souvent à la catastrophe: sous-estimation du danger, dimensionnement structurel inapproprié, manque de ressources à disposition, mauvaise exécution, etc.

De nos jours, les codes sismiques fournissent des lignes directrices à suivre afin de protéger les biens et les vies dans les bâtiments en cas de tremblements de terre. De telles dispositions n'existent pas depuis longtemps. Les premières règles normatives pour les bâtiments ont été émises après le tremblement de terre de Lisbonne en 1755. Les événements de Messine (1908) et de Kanto (1923) ont conduit à des lignes directrices pour les ingénieurs afin de concevoir des bâtiments dans ces régions. Les codes modernes sont fortement influencés par la réglementation sismique Californienne, qui a été initiée après le tremblement de terre de Santa Barbara (1925). En France, le premier document technique lié à la construction parasismique est mis au point pour l'Afrique du Nord (PS55) après l'événement d'Orleansville en 1954. Les règles sismiques pour la France métropolitaine n'ont été établies qu'à partir de 1969 (PS69), suite au tremblement de terre d'Arette en 1967. Ces lignes directrices étaient facultatives. En 1977, ces règles deviennent obligatoires pour les bâtiments publics, et en 1983, pour toute nouvelle construction. Ces dispositions ont notamment été améliorées en 1995 (PS92) et en 2005 avec le début de l'Eurocode 8 qui a pour but d'harmoniser les normes de construction dans toute l'Europe. La plupart des bâtiments des villes françaises ont été construits avant le code sismique et aucune mesure anti-sismique n'a été appliquée.

Dans un tel contexte, savoir comment une structure existante va réagir contre le mouvement du sol produit par un tremblement de terre devient important. Mais, sait-on vraiment com-

ment modéliser la réponse réelle d'une structure face à un tremblement de terre? Nous n'avons pas souvent la possibilité de valider la fiabilité de la prédiction de la réponse sismique obtenue à l'aide de modèles numériques. L'instrumentation des structures permet d'enregistrer la réponse réelle des bâtiments lors de mouvements sismiques et fournit des mesures utilisables pour valider les simulations numériques. Lors d'un événement fort, la réponse du bâtiment aux tremblements de terre est fortement non linéaire (en raison de la rhéologie des matériaux et des effets tels que l'interaction sol-structure), et la plupart des efforts de recherche tentent de reproduire un tel comportement.

La France métropolitaine est caractérisée par une sismicité modérée et une ville comme Nice (dans le sud-est de la France) connaît des séismes destructeurs (avec des intensités MSK à leurs épicentres de VIII en 1565 et X en 1887). Par conséquent, l'approche anti-sismique est différente de celle dans les zones de risque sismique plus élevés et les efforts de recherche doivent être adaptés pour répondre aux besoins spécifiques (risque plus faible et moins de ressources disponibles). Cette étude se focalise sur les apports pouvant être fournis par l'instrumentation du bâtiment de la préfecture de Nice. Le bâtiment a été instrumenté en 2010. Aucun dommage n'a été identifié depuis que les capteurs ont été installés.

Le but de cette recherche est d'évaluer dans quelle mesure nous pouvons reproduire le comportement du bâtiment lors de tremblements de terre en utilisant des techniques de modélisation numérique et de proposer des techniques alternatives simplifiées afin de simuler la réponse du bâtiment, utilisables lorsque les plans de construction et les propriétés des matériaux ne sont pas facilement disponibles. À cette fin les questions suivantes seront développées:

1. Peut-on reproduire l'état réel de la structure à partir de plans structurels et des choix de conception?
2. Peut-on obtenir des modèles numériques fiables pour simuler la réponse sismique?
3. Peut-on simuler la réponse à des tremblements de terre plus forts en utilisant des enregistrements sismiques antérieurs?
4. Peut-on simuler la réponse sismique d'un bâtiment en utilisant un modèle simplifié et des données de vibrations ambiantes?

La simulation numérique par éléments finis nécessite de la modélisation, du temps de calcul, des connaissances sur la structure et sur les propriétés des matériaux. Cette approche pourrait

être remplacée par des méthodes simplifiées, particulièrement dans le cas d'un modèle de ville. Dans ce contexte, l'instrumentation de structures offre de nouvelles possibilités pour évaluer les propriétés dynamiques du bâtiment et reproduire sa réponse opérationnelle face à un tremblement de terre.

Afin de répondre à ces questions, la recherche suivante a été élaborée et se présente selon différents chapitres:

- **Identification structurelle** (Chapitre 3): Nous utilisons des mesures à partir des enregistrements in situ pour extraire les propriétés dynamiques du bâtiment. L'influence des propriétés des matériaux sur le comportement dynamique de la structure est mis en évidence. Un modèle tridimensionnel par éléments finis de l'immeuble est créé à partir des plans de construction. Il est montré comment les mesures empiriques peuvent être utilisées pour étalonner un modèle numérique afin de le faire correspondre à l'état de service de la structure et valider des hypothèse de modélisation. La variabilité de l'état de la structure avec des facteurs externes (notamment la température) est discutée.
- **Réponse par éléments finis** de textbf (Chapitre 4): Le modèle créé est utilisé pour reproduire les réponses des données in situ, à différents niveaux de la structure, en imposant le mouvement du sol enregistré lors de séismes passés. L'objectif est d'évaluer si un modèle numérique est capable de reproduire la réponse sismique du bâtiment. Une base fixe est choisie initialement (comme habituellement pour les bâtiments) et une charge sismique triaxial est imposée. Cependant, des variations transitoires des fréquences naturelles des bâtiments sont observées pendant les mouvements du sol (Udwadia and Trifunac, 1973b). Todorovska (2009b) associe ces modifications à l'interaction avec le sol, en lien avec un effet de basculement pendant la sollicitation. Ces chutes transitoires dans les fréquences naturelles existent et peuvent être considérables (Todorovska 2009b quantifie cette contribution à 18% de chute dans la fréquence de basculement d'un corps rigide). Mais sont-ils pertinents pour la réponse d'un bâtiment? Trifunac (2009b) est préoccupé par cette simplification communément adoptée. Il montre que négliger la composante rotationnelle du mouvement à proximité des failles peut conduire à une sous-estimation des déformations des étages par un facteur deux dans les bâtiments en cisaillement. Un modèle à base fixe est incapable de reproduire la rotation de la base et ces effets sont généralement négligés. En ajoutant la variabilité spatiale sur le mouvement d'entrée, plusieurs sources d'excitation enregistrées sont imposées aux parties pertinentes de la base de la structure afin de reproduire un tel comportement de basculement (le cas échéant). La comparaison de la réponse donnée par les deux modèles avec les enregistrements permet de quantifier l'importance

des effets de basculement sur la réponse d'un bâtiment.

- **Fonction de Green empirique** (Chapitre 5): L'analyse de la propagation des ondes pour prédire la réponse des structures face aux tremblements de terre date des années 1930 avec les travaux de Sezawa and Kanai (1935, 1936). En 1963, Kanai and Yoshizawa (1963) a proposé une formule simple pour approximer la réponse à la base du bâtiment à partir des données au niveau du toit, en observant la réponse d'une structure comme une superposition d'ondes se propageant. Par conséquent, la réponse à la base résulte en une superposition de deux décalages temporels de la réponse du toit. Ce concept est considéré comme le prédécesseur de la méthode de la réponse impulsionnelle (Snieder and Safak, 2006; Todorovska, 2009a). La formule de Kanai-Yoshizawa a été récemment revue et généralisée à tous les étages (Ebrahimian et al., 2016). Elle approxime bien la réponse des immeubles de grande et de très grande hauteur pour des mouvements faibles et forts. Une telle formulation peut estimer les mouvements à différents étages en disposant d'un seul enregistrement d'un séisme au niveau du toit. Mais, pouvons-nous utiliser ces enregistrements pour prédire le mouvement généré par un séisme plus important? La prédiction des mouvements du sol plus forts que les enregistrements disponibles est très habituel pour l'évaluation du risque et de la vulnérabilité structurelle. La charge sismique peut être simulée en utilisant un modèle numérique de la rupture de la source et du chemin de propagation des ondes (approche déterministe), ou définie parmi un ensemble d'enregistrements sélectionnés (approche empirique). L'utilisation de données de petits tremblements de terre pour produire des signaux synthétiques de grands séismes est proposée par Hartzell (1978). Selon cette approche semi-empirique, chaque enregistrement représente l'effet de propagation entre la source et le récepteur et est considéré comme une fonction de Green empirique. Le principal avantage de ces méthodes est qu'elles incorporent naturellement les caractéristiques du chemin de propagation et des effets de site locaux (difficiles à modéliser si les propriétés mécaniques du milieu ne sont pas connues ou si des effets 3D sont présents). Nous proposons une procédure de sommation stochastique (Kohrs-Sansorny et al., 2005), déjà utilisée pour générer des mouvements du sol, pour simuler la réponse d'un bâtiment à un tremblement de terre donné à partir d'enregistrements. La technique originale est développée afin de proposer des mouvements réalistes forts au champs libre, où seulement les événements de magnitude intermédiaire sont enregistrés, pour des événements caractéristiques de plus grande ampleur. Elle est basée sur la connaissance de la modification subie par les ondes à travers le milieu de propagation, de la source du tremblement de terre jusqu'au sol où la réponse doit être reproduite. La réponse d'un immeuble à un tremblement de terre peut être vue d'une manière similaire. Le bâtiment transforme le contenu des ondes d'entrée lors

de la propagation à travers la structure, selon son contenu fréquentiel. Par conséquent, il est logique de prolonger le chemin de propagation du bas vers le haut de la structure. Cette mise en œuvre ne nécessite pas de connaître les propriétés des matériaux ni les dimensions de la structure. Il n'y a pas besoin non plus d'effectuer de longs calculs. Un enregistrement unique de la réponse structurelle au cours d'un séisme est suffisante.

- **Interférométrie par déconvolution** (Chapitre 6): L'interférométrie est un autre domaine extrêmement intéressant de la séismologie. Les premières observations de bruit ambiant sismique datent de la fin du XIXe siècle (Bertelli, 1872). Le développement du matériel d'acquisition a amélioré la compréhension du bruit sismique et les informations qu'il contient. Des nouvelles techniques avec des réseaux de capteurs, mesurant le retard de propagation entre les différentes stations, permettent l'obtention de profils de vitesse du sol sur la base des propriétés de dispersion des ondes de surface. Deux méthodes différentes se distinguent par l'analyse du domaine fréquence -nombre d'onde (FK) (Capon et al., 1967; Capon, 1969), et la corrélation des signaux (Aki, 1957, 1965). Elles permettent de suivre la propagations des différentes ondes au travers de la terre, ce qui rend possible de déterminer leurs vitesses, et donc la rigidité du sol à travers lequel elles se propagent. Cela permet des prospections non invasives de couches de terrain sous la surface. Si l'on considère que la réponse d'un bâtiment est le résultat d'une onde qui se propage, il est donc judicieux d'utiliser ces méthodes pour suivre la propagation des ondes à travers la structure. Snieder et al. (2006) montre comment la propagation des ondes peut être suivie à travers la structure et comment les propriétés dynamiques du bâtiment peuvent être obtenues à partir d'interférogrammes. Quelques principes de l'interférométrie sont utilisés pour trouver des paramètres mécaniques d'un modèle équivalent au bâtiment de la préfecture de Nice afin de le modéliser comme une poutre Timoshenko. Ces paramètres mécaniques peuvent être obtenus à partir de l'analyse des données de vibration ambiante de la structure, sans nécessairement connaître en détail les éléments structurels.

Présentation des résultats

L'objectif principal de cette thèse est d'estimer la réponse sismique des bâtiments existants en utilisant les enregistrements et les techniques permettant de caractériser les propriétés dynamiques de bâtiments à partir des données. Un modèle tridimensionnel par éléments finis permet de simuler la réponse sismique d'un bâtiment d'une façon précise si la structure porteuse, les propriétés des matériaux et les conditions limites sont correctement définies. Les procédures simplifiées proposées semblent être des alternatives utiles lorsque l'information

sur la structure et les matériaux ne sont pas facilement disponibles. Cette thèse vise à proposer l'utilisation de mesures non invasives pour l'identification des propriétés dynamiques et techniques simplifiées afin d'obtenir des déformations temporelles d'un bâtiment à l'aide de ces mesures. Cette étude utilise des méthodes numériques et empiriques. Cette combinaison permet de comprendre correctement le comportement dynamique d'un bâtiment dans son environnement et éviter les incertitudes liées aux limitations de chaque approche. Certaines questions ont été posées dans le Chapitre 1 et les réponses sont formulées dans cette conclusion.

Peut-on reproduire l'état réel de la structure à partir de plans structurels et des choix de conception?

L'identification structurale du bâtiment de ce cas d'étude est présentée dans le chapitre 3. Les paramètres dynamiques sont obtenus à partir des enregistrements en utilisant différentes techniques d'analyse modale opérationnelle et un modèle par éléments finis en trois dimensions est créé selon les plans de construction. Des mesures in-situ permettent d'étalonner le modèle numérique afin d'adapter l'état de service de la structure qui diffère de la condition de conception en termes de charges, de propriétés des matériaux, de vieillissement des matériaux, de conditions limites, etc. L'utilisation combinée de la modélisation numérique et des données empiriques permet d'observer que le joint sismique, présent dans les plans de la structure du bâtiment étudié, ne fonctionne pas comme prévu. Une erreur de près de 50% est identifiée sur la première fréquence de torsion du bâtiment en modélisant les tours comme dynamiquement isolées. Cette erreur est réduite à moins de 1% lorsque l'on considère que le matériau de remplissage sismique fournit une liaison rigide entre les deux parties. L'observation des paramètres dynamiques dans un long intervalle de temps montre que la fréquence fondamentale subit des oscillations transitoires (journalières et annuelles) d'environ 4% entre l'hiver et l'été de la même année, principalement causées par les variations de la température extérieure.

L'identification structurelle à partir des données enregistrées dans l'industrie du génie civil a un grand potentiel et peut être utilisée, par exemple, pour vérifier les opérations de renforcement ou pour identifier les bâtiments endommagés dans une situation post-sismique.

Peut-on obtenir des modèles numériques fiables pour simuler la réponse sismique?

La réponse sismique numérique à des tremblements de terre passés est simulée à l'aide d'un modèle par éléments finis en trois dimensions qui est présenté dans le Chapitre 4. Le comportement des matériaux est supposé linéaire, en raison de l'inexistence de données sismiques plus fortes dans la zone analysée. Une bonne simulation globale de la réponse sismique est obtenue en appliquant les trois composantes du mouvement du sol enregistré par un capteur à l'ensemble de la base du modèle. Cependant, une partie considérable du comportement dans la bande de fréquence du mode fondamental n'est pas correctement reproduite. La composante verticale du tremblement de terre enregistré à la base du bâtiment par des capteurs relativement rapprochés est différente en termes d'amplitude et de phase. Cela indique la présence d'effets de basculement qui lui-même implique une rotation de la base de la structure au cours d'un mouvement fort. La variabilité spatiale du mouvement de la base est prise en compte en imposant de multiples excitations enregistrées à différents points du modèle numérique. L'imposition de multiple charges permet de reproduire la rotation de la base rigide associée à l'interaction entre le bâtiment et le sol. Une comparaison qualitative des histoires temporelles d'accélération montre que l'effet de basculement produit une décroissance transitoire de la fréquence fondamentale (d'environ 6% au cours de séisme de Barcelonnette 2014 M_w 4.9). Cette décroissance est numériquement reproduite quand un mouvement d'entrée multiple est imposé à différents endroits de la base, mais elle est négligée lorsque les trois composantes du mouvement enregistré en un point sont imposées à l'ensemble de base. Les comparaisons quantitatives confirment de meilleurs résultats lorsque la variabilité spatiale du mouvement de la base est prise en compte. Il faut remarquer que les codes sismiques actuels ne tiennent pas compte de la variabilité spatiale des mouvements du sol pour les bâtiments, ni de ces effets de basculement.

L'application de cette même approche à d'autres bâtiments serait intéressante pour déterminer si ces effets sont liés à ce cas d'étude ou s'ils peuvent être observés sur différents types de bâtiments ou dans d'autres environnements.

Peut-on simuler la réponse à des tremblements de terre plus forts en utilisant des enregistrements sismiques antérieurs?

Il est proposé dans le Chapitre 5 de générer la réponse dynamique aux séismes des bâtiments existants à partir d'enregistrements d'événements précédents plus petits. Une extension de la méthode des fonctions de Green empiriques est utilisée à cette fin. Elle ne nécessite pas de modéliser la structure ni de calibrer des paramètres mécaniques. Les réponses numériques,

évaluées à l'aide du modèle tridimensionnel préalablement validé par comparaison avec les données, sont comparées aux signaux générés de façon semi-empirique afin de vérifier la validité de la procédure. Les signaux générés à partir des EGF présentent une excellente qualité d'ajustement quand ils sont comparés aux signaux numériques. Il est important de souligner qu'aucune hypothèse de modélisation n'est imposée. Cette approche permet de reproduire la réponse du bâtiment en évitant une situation coûteuse en temps. Par conséquent, elle pourrait être utilisée comme une approche simplifiée lorsque les plans structurels ou les informations sur les matériaux ne sont pas facilement disponibles. Cependant, plusieurs limites doivent être prises en compte. Une hypothèse de comportement linéaire du milieu dans lequel les ondes se propagent est adoptée. La non-linéarité dans le chemin de propagation (de la source à la structure), en raison de sols et matériaux de construction, les effets de site et les interactions sol-structure sont négligés. En outre, la source de l'événement simulé possède le même emplacement et le mécanisme focal du tremblement de terre utilisé comme EGF. Par conséquent, cette méthode peut être utilisée pour générer des signaux synthétiques á amplitude modérée dans les bâtiments à des distances épicentrales suffisantes. De plus, dans le cas où les enregistrements proviennent uniquement du toit de la structure, la formule Kanai-Yoshizawa pourrait être utilisée pour estimer les réponses à différents niveaux (ou même le mouvement au sol).

Les limites actuelles de la technique pourraient être réduites par des recherches à venir. La considération de certaines non-linéarités dans les simulations de l'EGF est possible. La tendance est l'utilisation croissante d'instrumentation dans les constructions, en particulier avec les développements de capteurs peu coûteux. L'applications des techniques proposées permet de déterminer la vulnérabilité des bâtiments avant et après des événements sismiques et d'estimer la réponse dynamique pour un événement plus fort choisi comme référence.

Peut-on simuler la réponse sismique d'un bâtiment en utilisant un modèle simplifié et des données de vibrations ambiantes?

Dans le chapitre 6, un modèle de poutre à base fixe d'un bâtiment, avec un comportement dynamique équivalent, est identifié à l'aide de données de vibrations ambiantes. Un modèle de poutre Timoshenko est calibré avec les observations, en faisant correspondre les fréquences naturelles, les vitesses de propagation des ondes et les courbes de dispersion. Tous les paramètres mécaniques nécessaires pour modéliser la structure peuvent être obtenus à partir d'une fenêtre de bruit de temps court, sans avoir besoin d'information sur la disposition, les dimensions ou les matériaux des éléments structuraux. Seulement la hauteur du

bâtiment est supposée. Le coefficient de Poisson, pour le modèle équivalent, est déduit du rapport de la vitesse des ondes de compression et de cisaillement. Celui-ci montre que les ondes de compression sont environ 5 fois plus rapides que celles de cisaillement (pour la construction étudiée). La procédure peut être appliquée à partir de 60 secondes d'enregistrement de vibrations ambiantes. Cela permet de réaliser des campagnes de mesure temporaire dans de nombreux bâtiments afin d'identifier leurs propriétés dynamiques. La reproduction de l'histoire de la déformation en utilisant le modèle de poutre équivalent est excellente pour les modes inférieurs (cinq premièrs modes pour le bâtiment étudié). Cependant, la modélisation du bâtiment comme une poutre homogène ne permet pas de prendre en compte les modes locaux et leur contribution est négligée. Les modes inférieurs sont souvent responsables de la majeure partie du déplacement. Par conséquent, l'approche proposée pourrait être intéressante comme approximation. La méthodologie proposée peut être d'un intérêt particulier pour les simulations numériques à grande échelle avec un grand nombre de bâtiments (comme simulations d'interaction site-ville) où la modélisation et le temps de calcul sont très importants si tous les bâtiments sont modélisés en détail. Le principal avantage d'un modèle de poutre équivalent à un bâtiment est qu'aucun détail structurel n'est nécessaire pour reproduire sa réponse.

La poutre Timoshenko reproduit bien la réponse de la structure, mais l'hypothèse d'une section uniforme ne permet pas de considérer les excentricités de masse et d'adapter plus précisément les modes de torsion. Les résultats obtenus pour le bâtiment de la préfecture de Nice sont satisfaisants, car il est relativement symétrique aux deux directions orthogonales dans le plan horizontal. Les modes de torsion peuvent être mal reproduits dans les bâtiments avec des excentricités fortes. Une reformulation des équations analytiques en considérant un trou excentrique à travers la section homogène serait capable de mieux simuler des effets de torsion plus importants.

Author's publications

International Journals

- Fernández Lorenzo, G.W., Mercerat, D., Santisi D'Avila, M.P., Deschamps, A., Bertrand, E. (2016). Identification of building mechanical parameters from ambient vibration interferometry. Manuscript submitted for publication.
- Fernández Lorenzo, G.W., Mercerat, D., Santisi D'Avila, M.P., Bertrand, E., Deschamps, A., Foundotos, L., Courboulex, F. (2016). Application of empirical Green's function approach to building seismic response prediction. Manuscript submitted for publication.

International Conferences

- Fernández Lorenzo, G.W., Mercerat, D., Santisi D'Avila, M. P., Bertrand, E., Deschamps, A. (2015). Operational Modal Analysis of a high rise RC building and modelling. The 6th International Operational Modal Analysis Conference. Gijón, Spain.
- Fernández Lorenzo, G.W., Santisi D'Avila, M.P., Deschamps, A., Bertrand, E., Mercerat, D. (2015). Étude de la réponse structurelle d'un bâtiment de grande hauteur a partir d'enregistrements accélérométriques et de la modélisation par éléments finis. 9ème Colloque National AFPS.

Abstract

The aim of this thesis is to simulate the time history response of a high rise building under seismic excitation and provide simplified methodologies that properly reproduce such response. Firstly, a detailed three-dimensional finite element model is produced to validate its reliability to simulate the real behavior of the building during ground motions, recorded using accelerometers. It is proposed to improve the accuracy of the numerical model by imposing multiple excitations, considering rocking effect and spatial variability on the input motion. The finite element model provides excellent results when dynamic parameters are calibrated to match the service condition of the structure. The use of empirical Green's functions is proposed to simulate the seismic response directly from past event records, without the need of construction drawings and mechanical parameters calibration. A stochastic summation scheme, already used to predict ground motions, is adopted to generate synthetic signals at different heights of the building, extending the wave propagation path from the ground to the structure. The procedure shows good agreement with numerical signals provided by the finite element model. A simplified representation of the building as a homogeneous Timoshenko beam is proposed to simulate the seismic response directly from ambient vibration records. Equivalent mechanical parameters are identified using deconvolution interferometry in terms of wave dispersion, natural frequencies, and shear to compressional wave velocities in the medium. Response simulation of lower modes, up to the fifth natural frequency, is properly reproduced by the equivalent model. Both proposed techniques provide alternatives to finite element modeling, when in-situ records (either seismic or ambient noise) are available, to avoid difficulties related with the lack of data about structure and materials and computing time.

Résumé

L'objectif de cette thèse est de simuler l'histoire temporelle de la réponse d'un bâtiment de grande hauteur sous sollicitation sismique et de proposer des méthodologies simplifiées qui reproduisent correctement une telle réponse. Initialement, un modèle tridimensionnel par éléments finis est produit afin de valider sa fiabilité pour simuler le comportement réel du bâtiment pendant les mouvements du sol, enregistrés à l'aide d'accéléromètres. Il est proposé d'améliorer la précision du modèle numérique en imposant de multiples excitations, compte-tenu des effets de basculement et de la variabilité spatiale sur la sollicitation d'entrée. Le modèle d'éléments finis fournit d'excellents résultats lorsque les paramètres dynamiques sont calibrés pour correspondre à l'état de service de la structure. L'utilisation de fonctions de Green empiriques est proposée pour simuler la réponse sismique directement à partir d'enregistrements d'événements passés, sans avoir besoin de dessins de construction ni d'étalonnage des paramètres mécaniques. Une méthode de sommation stochastique, déjà utilisée pour prédire les mouvements du sol, est adoptée pour générer des signaux synthétiques à des hauteurs différentes du bâtiment, par extension du chemin de propagation des ondes du sol à la structure. La procédure montre une bonne concordance avec les signaux numériques fournis par le modèle d'éléments finis. Une représentation simplifiée du bâtiment comme une poutre homogène Timoshenko est proposée pour simuler la réponse sismique directement à partir des enregistrements des vibrations ambiantes. Des paramètres mécaniques équivalents sont identifiés à l'aide de l'interférométrie par déconvolution en termes de dispersion des ondes, de fréquences naturelles et de rapport de vitesse des ondes de cisaillement et de compression dans le milieu. La simulation de la réponse des modes inférieurs, jusqu'à la cinquième fréquence naturelle, est bien reproduite par le modèle simplifié. Les deux techniques proposées sont des alternatives à la modélisation par éléments finis, lorsque les enregistrements in situ (soit sismiques, soit bruit ambiant) sont disponibles, afin d'éviter les difficultés liées à l'absence d'informations sur la structure et les matériaux et liées au temps de calcul.